Università degli Studi di Pavia

Facoltà di Ingegneria

Dipartimento di Ingegneria Civile e Architettura

Corso di Laurea Magistrale in Bioingegneria

tesi di laurea

Biomechanical Simulation of Chimney-EVAR technique For Aortic Aneurysm Treatment

Simulazione Biomeccanica Della Tecnica Chimney-EVAR Per il Trattamento Endovascolare Dell'Aneurisma Aortica

Candidato:

Chehab Ali

MAT **431214**

Relatore:

Prof. Michele Conti

Correlatore:

Prof. Enrico Maria Marone

A.A. 2016/17

L'oggi non è che il ricordo di ieri, e il domani il sogno di oggi.

Gibran Khalil Gibran

Abstract

Endovascular Aneurysm Repair (EVAR) is a **minimally invasive** alternative to major open surgery for the repair of **abdominal aortic aneurysms** (AAAs) that results in reduced recovery times and potentially improved survival rates. The challenging anatomy and especially inadequate landing zones create limitations to its application. Stent grafts fenestrated and branched were developed to overcome these anatomic restrictions. However, both fenestrated and branched stent grafts cannot be used in an urgent settings as they require time for manufacturing.

An alternative to fenestrated endovascular grafts is the so-called "**Chimney Graft**" technique, which has been designed to extend the proximal sealing zone and can be used in emergency settings when it is not possible to wait for a custom-made fenestrated stent graft. In such a technique, one or more stents ("chimneys") are implanted inside the visceral arteries in parallel with the main aortic SG. **Inadequate sealing** between chimney graft (CG) and main graft leads to the formation of so-called **gutters** between the grafts and the aortic wall, which could lead to type Ia **endoleaks**.

The purpose of present activity is to perform a structural Finite Element Analysis (**FEA**) of the chimney stenting technique in order to simulate the mechanical response of the device during crimping and deployment phases and to predict the optimal chimney graft configuration to minimize the gutter size by an optimal choice of the main graft **oversizing**. To achieve this goal, various chimney configurations consisting of one main stent and one parallel stent inside an aorta artery model have been built. In each configuration, the geometrical properties (diameter size, stent ring's elementary units number) of the main

stent have been modified and measures such as average of gutter area, main stent compression ratio and Von Mises values have been calculated in order to find the relationship between oversizing degree and gutter size.

From the results obtained, to get the optimal configuration: better endograft stent apposition and low gutter size, an oversizing of 15% is needed. Chimney optimal configuration requires a good compromise between adequate oversizing and a low gutter size, considering also an acceptable stress value in the grafts contact area to avoid potential mechanical damage of the device.

The analysis results show that the deformation of the stent is not uniform, but depends on the stent features such as geometry, material, and stent configuration inside aortic wall. Furthermore, the routine application of the presented numerical models could help clinicians in their intervention strategies, potentially improving the procedural outcomes. Various chimney stenting procedure options could be simulated for patient-specific cases, comparing results in terms of mechanical behavior of the intravascular devices and of the arterial wall.

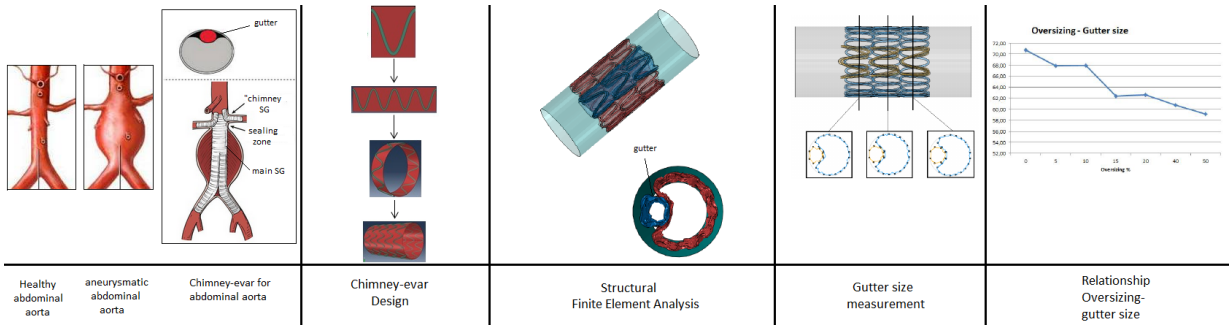

Figure 1: The image shows the workflow followed throughout the thesis. We started from the chimney device reconstruction, which is designed and modelled using 3 tools: Rhinoceros 5.0 (McNeel&Associates), Abaqus 6.14-2 (Simulia, Dassault Systems) and Matlab (MathWorks). After we applied the structural Finite Element Analysis for the gutter size calculation and we finish with the results of simulations to find the relationship between oversizing and gutter size.

Sommario

Il **trattamento endovascolare dell'aneurisma** (EVAR) é un'alternativa **meno invasiva** alla chirurgia tradizionale per la riparazione degli **aneurismi dell'aorta addominale** (AAA) in quanto riduce il tasso di mortalità e morbilità. Tuttavia, fattori anatomici come la lunghezza e la morfologia del colletto e il coinvolgimento delle arterie iliache, influenzano l'idoneità di un paziente all'EVAR. Per ridurre questi limiti, sono stati sviluppati gli stent fenestrati e ramificati, per preservare il flusso arterioso all'interno dei vasi viscerali, ma a causa dei lunghi tempi (4-6 settimane) di progettazione e personalizzazione di questi dispositivi, durante il quale i pazienti sono a rischio di rottura dell'aneurisma, é stata sviluppata una nuova tecnica chiamata "**Chimney graft**" (CG) che si pone come valida alternativa agli stent fenestrati in emergenza.

Il "Chimney graft" (CG) è una tecnica che permette la preservazione delle collaterali aortiche presenti sulla "sealing zone" ovvero la porzione in cui lo stent aderisce al colletto prossimale dell'aneurisma. In questa tecnica, uno e più stent ("chimney graft") sono impiantati all'interno dei vasi viscerali e in parallelo ad un stent principale ("main graft"), ma un **inadeguato sealing** tra questi grafts e la parete aortica porterebbe alla formazione dei cosidetti "**gutters**", che puo' portare a una diretta pressurizzazione del sacco dell'aneurisma (**Endoleak Ia**) considerato il "tallone d'Achille" della tecnica.

L'obiettivo della presente attività é quello di eseguire un'**analisi strutturale ad elementi finiti** (FEA) della tecnica chimney al fine di simulare le risposte meccaniche del dispositivo durante le fasi di crimping e deployment per poter individuare la migliore configurazione chimney e minimzzare la dimensione del gutter **(gutter size**) grazie ad una scelta otti-

male del grado del main graft **oversizing**. Per raggiungere questo obbiettivo, sono state sviluppate diverse configurazioni chimney composte da un main stent e un parallel stent assemblati all'interno del modello dell'aorta. In ogni configurazione, sono state variate le proprietà geometriche dello stent come il diametro e il numero delle unità elementari che formano l'anello del main stent e sono state calcolate delle misure come l'area media del gutter (**gutter size**), la percentuale del **main stent compression** e lo **stress di Von Mises**, al fine di trovare la relazione che lega l'oversizing alla dimensione del gutter.
I risultati suggeriscono che per ottenere la configurazione chimney ottimale in termine di gutter size bisogna utilizzare una configurazione con un grado di oversizing pari al 15%. La configurazione chimney ottimale richiede un compromesso tra un basso gutter size e un grado di main stent oversizing adqeguato, considerando anche un livello di stress accettabile nella zona di contatto dei due stents per evitare dani meccanici del dispositivo.
I risultati delle analisi potrebbero aiutare i medici nelle loro strategie di intervento, migliorando potenzialmente i risultati procedurali. Inoltre, le varie procedure di stenting chimney potrebbero essere simulate per casi patient-specific, confrontando i risultati in termine di comportamento meccanico dei dispositivi intravascolari e della parete arteriosa.

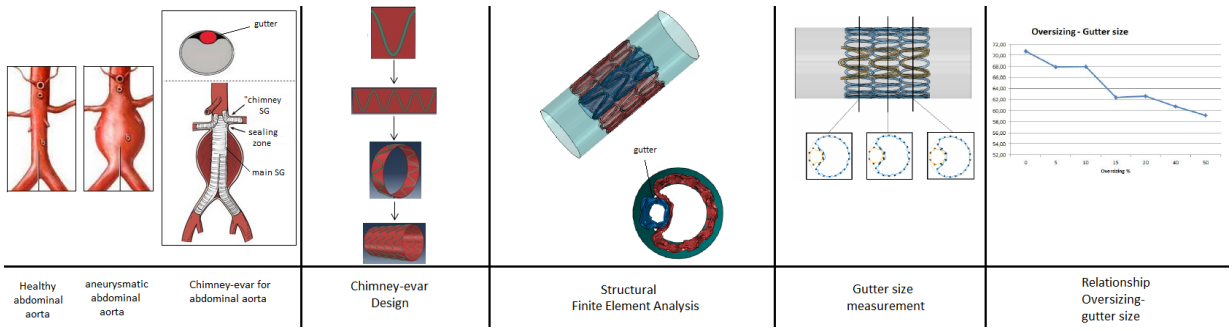

Figure 2: The image shows the workflow followed throughout the thesis. We started from the chimney device reconstruction, which is designed and modelled using 3 tools: Rhinoceros 5.0 (McNeel&Associates), Abaqus 6.14-2 (Simulia, Dassault Systems) and Matlab R2016b (MathWorks). After we applied the structural Finite Element Analysis for the gutter size calculation and we finish with the results of simulations to find the relationship between oversizing and gutter size.

Abbreviations and Nomenclature

3D	Three Dimensions
AAA	Abdominal Aortic Aneurysm
CAD	Computer aided design
CFD	Computational Fluid Dynamics
CG	Chimney Graft
E	Young Modulus
EVAR	Endovascular Aneurysm Repair
FEA	Finite Element Analysis
FEM	Finite Element Method
OS	Oversizing
PET	Polyethylene Terephthalate
PTFE	Polytetrafluoroethylene, or Teflon
ePTFE	expanded Polytetrafluoroethylene
SG	Stent Graft
Ch-EVAR	Chimney endovascular aneurysm repair
JVS	Journal of Vascular Surgery

STL	stereolithography
FDA	U.S. Food and Drug Administration
BC	Boundary Condition
OSR	Open surgery repair

Contents

1 Endovascular aortic aneurysm repair **5**

1.1 Aorta: Anatomical point of view 6

1.2 Aortic diseases 7

1.2.1 Aneurysm 7

1.2.2 Dissection 9

1.3 Medical treatments options 11

1.3.1 Open Surgical Repair(OSR) 11

1.3.2 Endovascular Aneurysm Repair (EVAR) 13

1.3.3 Comparison of Surgical AAA-Treatment Options 14

1.3.4 Limitations and Contraindications to the EVAR 15

1.4 Fenestrated and Branched Endovascular Aneurysm Repair 18

1.5 Chimney Graft Technique 21

1.5.1 Comparison between chimney graft and fenestrated graft 23

1.5.2 Post-op complications 25

1.5.3 How can I prevents type I Endoleak? 26

2 Chimney-Evar Technique: Set-up of Structural FEA Simulations **27**

2.1 Introduction 27

2.1.1 Abaqus (Simulia, Dassault Systems) 28

2.2 Chimney-evar Finite Element Analysis Set-up 31

2.2.1 Part module 31

2.2.2 Property module 39
2.2.3 Mesh module 42
2.2.4 Assembly module 43
2.2.5 Step module 44
2.2.6 Interaction module 46
2.2.7 Load module and Boundary conditions set-up 46
2.2.8 Analysis Finite Element Analysis step by step 47
2.2.9 Visualizzation module: Case-Patient simulation test 50
2.3 Gutter size measurement 52
2.3.1 Oversizing (OS) 53
2.3.2 Measurement procedure 55
2.3.3 Gutter size measurement of 3 rings-stent and 11-rings-stent models 57
2.3.4 Gutter size in literature 59
2.4 Reconstruction of Chimney technique configurations 60

3 Chimney-Evar Technique Simulation: Results 63
3.1 Others simulations tests results 63
3.1.1 Configuration 1: Oversizing=0%, Main stent diameter=20 mm . . . 63
3.1.2 Configuration 2: Oversizing=5%, Main stent diameter=21 mm . . . 66
3.1.3 Configuration 3: Oversizing=10%, Main stent diameter=22 mm . . 66
3.1.4 Configuration 4: Oversizing=15%, Main stent diameter=23 mm . . 66
3.1.5 Configuration 5: Oversizing=20%, Main stent diameter=24 mm . . 67
3.1.6 Configuration 6: Oversizing=35%, Main stent diameter=27 mm . . 67
3.1.7 Configuration 7: Oversizing=40%, Main stent diameter=28 mm . . 67
3.1.8 Configuration 8: Oversizing=50%, Main stent diameter=30 mm . . 68
3.2 General discussion 68

4 Physician Modified Endovascular Graft (PMEG) 73
4.1 PMEG using 3D Printing 75

4.2 Medical imaging analysis and processing 78
4.2.1 Patient-specific case 79
4.2.2 Image segmentation 81
4.2.3 Centerlines extraction and branches clipping 87
4.2.4 From virtual model to physical model: 3D printing 92

5 Conclusion, limitations and future perspectives 93
5.1 Conclusions 93
5.2 Limitations and future development 97
5.2.1 Chimney-EVAR technique 97
5.2.2 Physician Modified Endovascular Graft 98

A Input File Analysis 101
A.1 Format Input File 101
A.1.1 Keyword lines 103
A.1.2 Data lines 103

B Finite Element Method (FEM) 105
B.1 Overview of the method 105
B.2 A simple example of using FEM 106
B.3 A typical FEA workflow 107

List of Tables 111

List of Figures 119

Bibliography 119

Introduction

The present activity aims at achieving a structural finite element model to simulate a patient-specific chimney stenting intervention for the abdominal aortic aneurysm treatment. In particular, an actual chimney stenting procedure performed at Hospital San Matteo (Pavia, Italy) was simulated by creating an idealized chimney model.
The goal of this research activity is to perform a structural Finite Element Analysis (FEA) of various chimney configurations with the aim to calculate the gutter area and predict the best optimal chimney graft configuration with the most adequate stent-graft oversizing.

A brief description of the thesis structure is here presented.

- **Chapter 1:** In the first chapter, the main vascular diseases are shortly overviewed. Subsequently, the medical treatments options and endovascular aortic aneurysm repair are discussed, concentrating on a novel reconstruction technique. Furthermore, the main limitations of the endovascular aneurysm repair (EVAR) techniques are briefly highlighted.

- **Chapter 2:** In the second chapter, the structural model of the chimney evar intervention is described. The steps carried out to achieve a realistic 3D reconstruction of the chimney evar model are explained, as well as the methods used to create CAD geometries of the intravascular devices used in the stenting procedure. Also, the final simulation details are described, as well as the preliminary analyses (crimping and

bending) performed in order to make the final analysis possible.

- **Chapter 3:** The third chapter shows the obtained results and discusses the outcomes in terms of geometrical and mechanical considerations obtained on the stent models and arterial wall. Furthermore, a comparison between gutter size and main graft compression in various chimney configurations with different stent graft oversizing degree is made. Finally, the values of Von Mises stress in the contact zone of the two stent grafts will be discussed.

- **Chapter 4:** The fourth chapter introduces a modified technique to Fenestrated-Evar called Physician Modified Endovascular Graft PMEG. Subsequently, the use of 3D printing to innovate this technique is described in details.

- **Chapter 5:** In the fifth chapter, limitations and some main conclusions are reported, followed by its possible further developments.

Chapter 1

Endovascular aortic aneurysm repair

Endovascular aortic aneurysm repair (EVAR), first described in 1991 and since that time, it has become widely accepted as a safe technique for the treatment of abdominal aortic aneurysm (AAA) and an alternative to traditional open repair [1] because it offers the advantage of lower perioperative morbidity and mortality as well as shorter hospital stay and operative time compared with open repair [2].

Although the method's safety and efficacy have been established, challenging anatomy and especially inadequate landing zones create limitations to its application. In this case, a modification of EVAR may be required in order to successfully exclude aneurysms. One such modification is the use of fenestrated and branched stent grafts, but customization, planning and manufacturing of such stent-grafts requires time, during which the patients remain at risk of rupture which makes this procedure not available for urgent cases.

Greenberg was the first to suggest the "chimney" or "snorkel" graft technique as an alternative method to preserve renal arteries during endovascular aneurysm repair (EVAR) when there is no time to manufacture a fenestrated device [3, 4].

Chimney graft technique (CG), is an EVAR technique in which a stent is deployed parallel and outside of the aortic endograft to preserve flow to a vital aortic branch that was overstented to obtain an adequate seal[5].

1.1 Aorta: Anatomical point of view

The aorta, is the largest artery in the human body, originating from left ventricle of the heart and extending down to the abdomen, where it bifurcates into two smaller arteries (the common iliac arteries). The aorta distributes oxygenated blood to all parts of the body through the systemic circulation. The size of the aorta is directly proportionate to the patients height and weight. Its diameter may range from 1.2 cm (half an inch) to 3 cm (more than an inch). It is typically largest in the aortic root and smallest in the abdominal aorta [6].

As shown in Figure 1.1, the aorta is divided into five sections:

- **Aortic root** connects the heart to the systemic circulation and is a highly sophisticated and complex structure.
- **Ascending aorta** rises up from the heart and is about 2 inches long. The coronary arteries branch off the ascending aorta to supply the heart with blood.
- **The aortic arch** curves over the heart, giving rise to branches that bring blood to the head, neck, and arms.
- **Descending thoracic aorta** travels down through the chest. Its small branches supply blood to the ribs and some chest structures.
- **Abdominal aorta** begins at the diaphragm, splitting to become the paired iliac arteries in the lower abdomen. Most of the major organs receive blood from branches of the abdominal aorta.

Like all arteries, aorta's wall has several layers:

- **Intima**, the innermost layer, provides a smooth surface for blood to flow across.
- **Media**, the middle layer with muscle and elastic fibers, allows the aorta to expand and contract with each heartbeat.
- **Adventitia**, the outer layer, provides additional support and structure to the aorta.

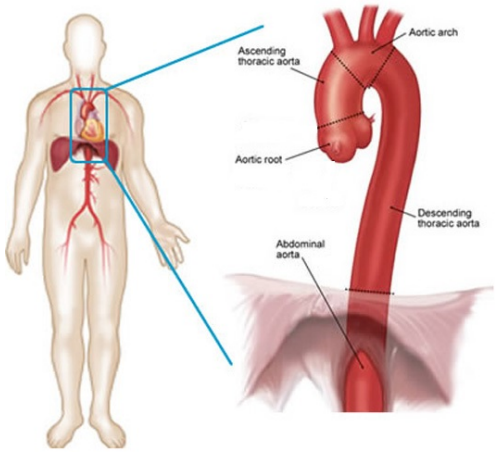

Figure 1.1: (a) Aortic wall layers: Intima, media, adventitia. (b) Aorta's sections: Ascending Aorta, Aortic arch, Descending Aorta and Abdominal Aorta

1.2 Aortic diseases

Diseased aortic tissue is characterized by degeneration of the cells composing the aortic wall. This diseased tissue is weak, and the first indication of this abnormality may be a localized enlargement in the area of weakness. When it reaches a certain size this enlarged area is referred to as an aneurysm [7]. Aortic tissue may also tear, even if the aorta is not enlarged. Tearing of the inner layer of the vessel wall allows blood to leak into the middle layer of the aorta, separating the inner and outer layers, causing so-called dissection.

1.2.1 Aneurysm

As shown in Figure 1.2, an aneurysm is an irreversible localized dilatation of an artery greater than 50% of its original diameter, due to gradual wall weakening. As the aneurysm expands, it may eventually bring to a rupture. They result from weakening of an arterial wall section owing to a variety of genetic, biomechanical, biochemical, and hemodynamic factors such as hereditary conditions, atherosclerosis, inflammation, infection, hypertension, lung disease, smoking and obesity [8]. Although aneurysms can occur in any blood vessel, most are asymptomatic (75%). They are incidentally discovered during routine physical exams or are revealed on radiographic studies performed for unrelated issues [9].

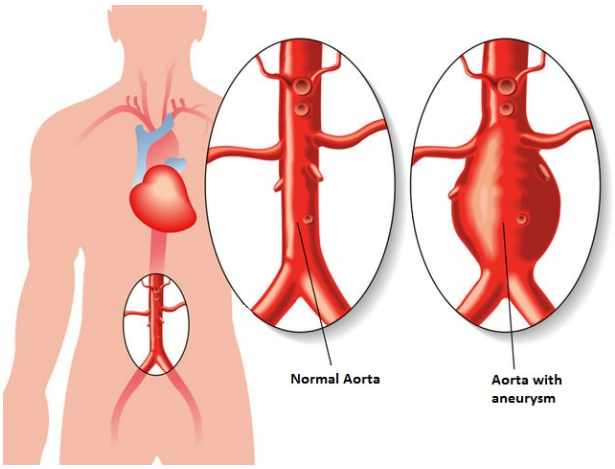

Figure 1.2: Difference between a normal aorta and an aorta with aneurysm.

Usually, it is formed in areas of the vascular system where the pressure is the highest such as the abdominal aorta, thoracic aorta and in the brain[4].

Aortic aneurysm rupture is ranked as the thirteenth most common cause of death in the western world. It has been documented that it leads to about 15,000 deaths each year in the US and about 8,000 deaths per year in England [10]. Aortic aneurysms have been found in both the chest and the abdomen areas of the aorta and may be classified into Abdominal Aortic Aneurysms (AAAs) and Thoracic Aortic Aneurysms (TAAs).

Abdominal aortic aneurysm

Among the two types of aortic aneurysms, Abdominal aortic aneurysms (AAA) is highly prevalent, supported by the fact that 80% of all reported aortic aneurysm are those of AAAs [11]. Abdominal aortic aneurysms, Figure 1.3, are commonly located just below the renal arteries (infrarenal) but above the point in which the descending aorta bifurcates into the two common iliac arteries [6].

The occurrence of AAA varies markedly by ethnicity. In the United Kingdom the rate of AAA in Caucasian men older than 65 years is about 4.7% while in Asian men it is 0.45% [12]. There are 9000 deaths yearly in the United States due to AAA rupture [13]. Other risk factors include hypertension and male sex. The incidence of abdominal aortic aneurysm is higher in the elderly men than in women and young people. A systematic review of a

large number of studies has shown that prevalence of AAA disease is 60-90% among the elderly male population [14]. Furthermore, the frequency is much higher in smokers than

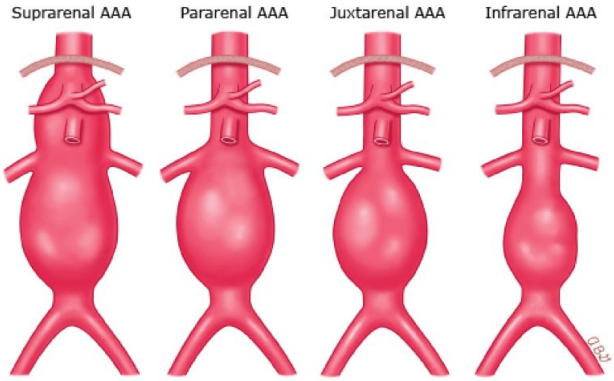

Figure 1.3: Classification of abdominal aorta aneurysm

in non-smokers (8:1), and the risk decreases slowly after smoking cessation [15]. Rupture of the AAA occurs in 1-3% of men aged 65 or more, the mortality is 70-95% [16, 17, 18, 19].

Thoracic and Thoracoabdominal aortic aneurysm

As shown in Figure 1.4, the aneurysms which involve the ascending aorta, aortic arch and descending thoracic aorta are termed "thoracic aortic aneurysms (TAAs)" [6]. Clinically, TAAs are not as common as abdominal aortic aneurysms [9].

Most thoracic aortic aneurysms do not generate any symptoms. However, rupture can cause rapid blood loss and death. Furthermore, surgical repair of a ruptured thoracic aneurysm carries a 25-50% mortality as opposed to a 5-8% mortality when such aneurysms are treated electively [6].

Thoracoabdominal aortic aneurysms, result from continuous dilation of the descending thoracic aorta extending into the abdominal aorta.

1.2.2 Dissection

Aortic dissection as shown in Figure 1.5, is a tear that develops in the inner layer of the aorta, causing blood to flow between the layers. The layers then separate, interrupting the

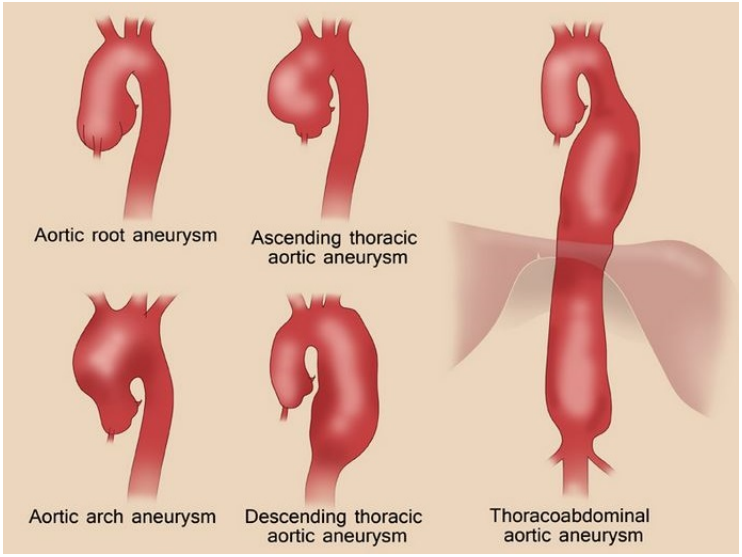

Figure 1.4: Thoracic and Thoracoabdominal aortic aneurysms.

blood flow and possibly causing the arterial wall to burst.

There are two aortic dissection types, as shown in Figure 1.6:

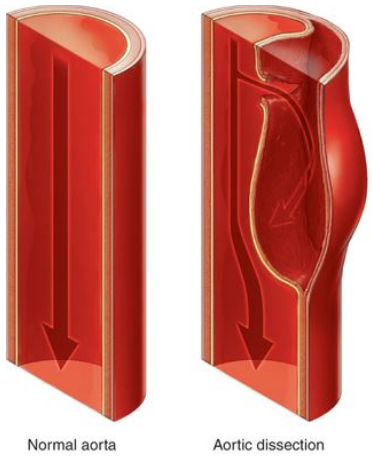

Figure 1.5: Comparison between blood flow in a healthy aorta and aorta with dissection

Type A aortic dissections, are the most common and dangerous type of aortic dissection. These dissections involve a tear in the ascending portion of the aorta just where it exits the heart or a tear extending from the ascending portion down to the descending portion of the aorta, which may extend into the abdomen.

Type B aortic dissections involve a tear in the descending aorta only, which may also

extend into the abdomen.

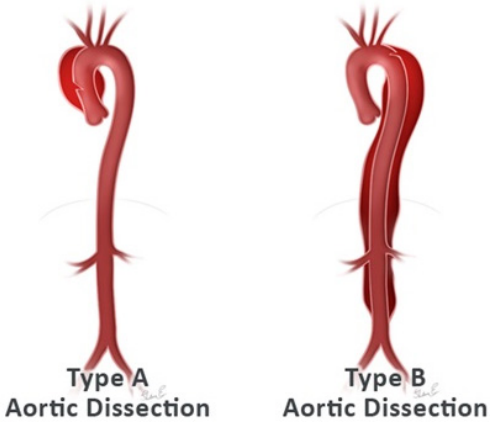

Figure 1.6: Aortic dissection types

1.3 Medical treatments options

Over the last few years, endovascular or minimally invasive techniques have been developed for many types of aneurysms. The treatment options for asymptomatic AAA are conservative management, surveillance with a view to eventual repair, and immediate repair [20]. The risk of aneurysm rupture can be prevented by repairing it with either open surgical repair (OSR) or endovascular aneurysm repair (EVAR) respectively, as shown in Figure 1.7. An intervention is often recommended if the aneurysm grows more than 1 cm per year or it is bigger than 5.5 cm [20].

1.3.1 Open Surgical Repair(OSR)

Traditionally (1951 - current), the available treatment required for patients with high risk of rupture is open surgical repair [8].

For aortic aneurysms, an incision is made in the patient's chest and/or abdomen, the thrombus in the aneurysm is removed, and the weakened portion of the aorta is replaced with a synthetic prosthetic graft made of polyethylene terephthalate (Dacron or PET) or polytetrafluoroethylene (PTFE) as shown in Figure 1.8(a). This graft then acts as a

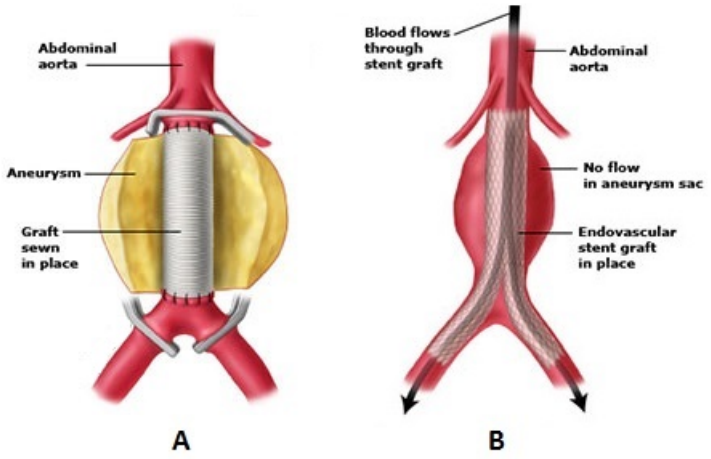

Figure 1.7: Aneurysm repair options. (a) Open surgical repair (OSR); (b) endovascular aneurysm repair (EVAR). Adapted from (shahid et.al., 2013) [14]

synthetic vascular replacement reinforcing the diseased arterial tissue [9].

Open repair is a substantially invasive procedure, which involves a large amount of blood and fluid transfusion and requires increased hospital stay and long recovery time [14]. Overall, mortality rates for electively repaired aneurysms with OSR found in literature are 2-10% [21]. Although open repair is the standard and still performed it may not be the best

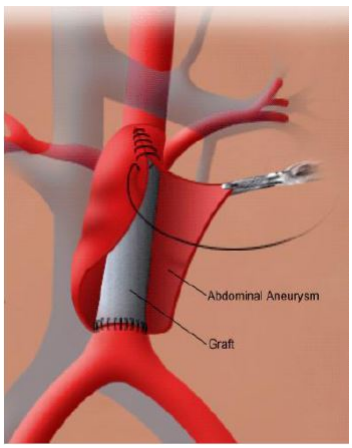

(a) *AAA open surgical repair procedure*

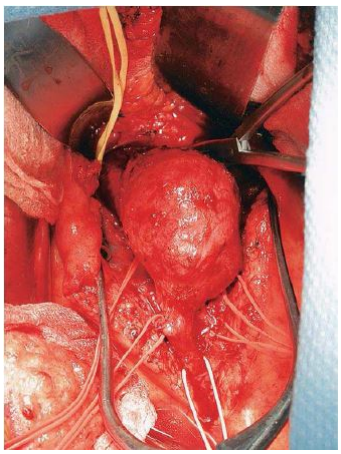

(b) *Open Aortic Aneurysm Repair*

Figure 1.8: Open Surgical Repair(OSR).

choice of procedures depending on patient's age, condition and or medical history. Along

with mortality open repair have possible perioperative and post-operative complications including morbidities such as, myocardial infarction, respiratory complications, excessive bleeding and prolonged reduced blood flow for the lower extremities. The last two decades have brought a new, less invasive alternative endovascular aneurysm repair (EVAR) [4].

1.3.2 Endovascular Aneurysm Repair (EVAR)

Endovascular aneurysm repair (EVAR) represented on Figure 1.9, is a minimally invasive technique to treat aneurysms reported for the first time by Juan Parodi et.al. in 1991 [22]. Endovascular means that surgery is performed inside the aorta using thin, long tubes called catheters guided by X-rays (fluoroscopy), through small incisions into the femoral artery in which the stent graft (SG) goes through the leg artery to the aneurysm site. After it is correctly positioned in the abdominal aorta, the SG is released and restores to its original shape under self-expandable or balloon-expandable mechanisms. The expanded SG then

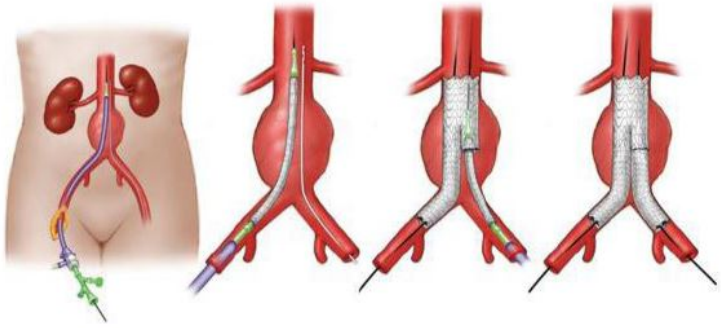

Figure 1.9: Endovascular aneurysm repair. Reproduced from Schwarz, 2012.

forms a new blood vessel excluding the aneurysm cavity. A stent-graft (SG) or endograft is an endoprosthesis classified as a class III medical device both in Europe and in the United States of America. It can be defined as a tubular device composed of a flexible membrane, i.e., a graft, supported by a rigid structure. Endovascular repair of aortic aneurysms is generally less painful and has a lower risk of complications than traditional surgery because it is a minimally invasive procedure, significantly reduces perioperative mortality, decreases hospital stay and prompt recovery [4, 9, 14].

1.3.3 Comparison of Surgical AAA-Treatment Options

Table 1.1 provides a comparison between the traditional surgical intervention and EVAR. Clearly, EVAR is safer than open surgery; however, it is only suitable for patients who have the suitable AAA anatomy. Currently, only 60%-70% of AAAs can be repaired by EVAR [8, 9].

Furthermore, the cost is much higher than that for open surgery, mainly because of

Open Surgery	EVAR
Fits almost any patient	Only for AAA with "right anatomy"
Large abdominal incision	Small incision in groin
Average 6 days in hospital	Average 2 days in hospital
Full recovery –6 weeks	Full recovery –2 weeks
Morbidity: 29%	Morbidity: 18%
Blood transfusion: high	Blood transfusion: low
Mortality rate: 3,8%	Mortality rate: 1,3%
No long-term surveillance	Long-term surveillance
Total cost: $12,500	Total cost: $20,000

Table 1.1: Comparison between open surgery and EVAR. Adapted from (Noll, et.al.,2007) [23].

the need for long-term annual check-ups. However, EVAR is a relatively new technology without long-term follow-up outcome. Despite it has shown outstanding success for patients with abdominal aortic aneurysms (AAAs), it can also cause many problems, such as seepage of blood into the cavity (endoleaks), SG migration, SG failure, and other complications[4]. Numerous studies indicates that, EVAR is a feasible alternative treatment option for the patients with suitable anatomy. However, good results of EVAR do not sustain for the patients with unfavourable anatomical features and those already unfit for OSR [14, 24].

1.3.4 Limitations and Contraindications to the EVAR

AAA geometric parameters should satisfy certain conditions for successful EVAR as seen in Figure 1.10.

The aneurysm is described in terms of the proximal landing zone, the characteristics of

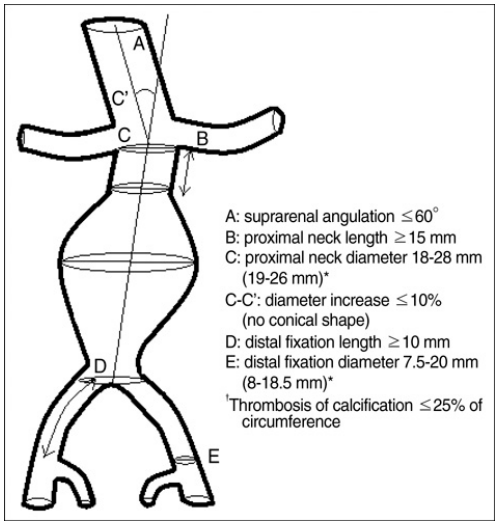

Figure 1.10: Diagram shows example of planning template. Diameters and lengths must be accurately reported for appropriate sizing of endograft components. An example of inclusion criteria of Zenith (Cook Company, Bloomington, IL, U.S.A.)

the aneurysm sac, the distal landing zone, and the vascular access [25]. This unfavorable configuration may lead to an improper seal and higher complication rate. Approximately 20–30% of patients have proximal neck anatomy traditionally considered unfavorable for stent-graft placement. "About half of the 40,000 patients who undergo elective repair of aortic aneurysms do not have a suitable neck to seal the endograft", Dr. Benjamin W. Starnes, Chief of Vascular Surgery at Harborview Medical Center, explained [26]

Among different researchers, it is a well established fact that major complications dictating success of EVAR are those including endoleaks and migration, sac expansion, and even rupture. Since these problems have directly challenged the success of EVAR, they demand special considerations through secondary interventions, which otherwise could lead to the enlargement of an aneurysm and hence rupture [27, 28, 29].

Some of these complications are listed below:

Device migration. SG migration usually means distal movement of the proximal portion of the stent, as shown in Figure 1.11. It may be thought of as a failure of attachment with an unchanged aorta or as a failure related to change in aneurysm morphology.

Generally, migration ≥10 mm or any migration requiring secondary intervention has to

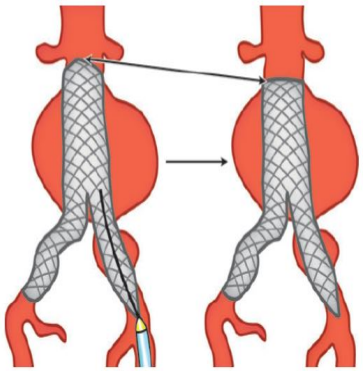

Figure 1.11: Schematic of stent-graft migration. Reproduced from Kleinstreuer et. al, 2007.

be considered clinically significant after EVAR [9].

Zarins et al. [30] reported that with the increase of time after EVAR, the migration rate increases, i.e., 1.4% at 1 year, 6.4% at 2 years, and 18.8% at 3 years. Generally, neck dilation, neck angulation, neck thrombus and calcification, higher blood pressure, short neck length, conic neck shape, large iliac bifurcation angle, and large SG size are the main reasons causing SG migration. Endograft migration, reported at 2.3% to 9.5% [31], is strongly associated with proximal fixation and anatomy of the aneurysm neck. An Aortic neck dilatation >10% and a preoperative aortic diameter >5.5 cm are independent risk factors for stent graft migration [32]. Recently, Pintoux et al. [33] found that the absence of proximal stent graft fixation of the proximal aneurysm neck enhances proximal migration.

Endoleaks. Endoleak is the most common complication associated with the endovascular repair, defined as persistent blood flow in the aneurysm sac, i.e. portion between the

outside wall of the graft and the interior wall of aneurysm as seen in Figure 1.12. In some studies, endoleak has been reported as the principal cause of EVAR failure. As a result, endoleaks may cause elevated intrasac pressure and high stresses in the abdominal aortic aneurysm wall causing AAA rupture and hence the need for a second procedure [9, 14].

Currently, five endoleak types are defined in the literature on the basis of the source of the

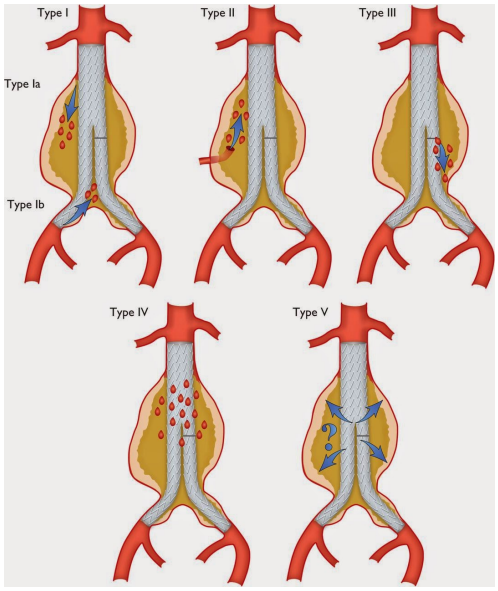

Figure 1.12: Schematics of endoleaks.

leakage and usually named numerically: leakage at the anchor sites (Type I, if proximal Ia, if distal Ib), leakage via collateral arteries (Type II), defective SG (Type III) and leakage owing to porosity of the graft material (Type IV) and endotension (Type V) [9].

Endoleaks have seen to occur at various stages. However, they are more prevalent during the first 30 days after the endvascular procedure and thus classified as the primary endoleaks [34]. Endoleak seen in the early stages may vanish in a follow up due to thrombus formation and similarly, it can appear in the long run due to remodelling and device failure [14]. Infact, Thrombus formation after EVAR is considered responsible for transmission of intra-aneurysm sac pressure. In an experimental study, Chaudhuri et al. [35] have reported, that intrasac pressure waveforms measured post-operatively are reliable indicators of the Type-I endoleaks, but not of Type-II or combined types. Currently, the hemodynamics of

endoleaks is not completely understood. For example, Parodi et al. [36], hypothesized that an endoleak may significantly increase intrasac pressure because of the lack of appropriate outflow from the aneurysm sac, which could increase the risk of rupture unless adequately treated.

Due to the longitudinal migration or radial dilatation of the proximal aneurysm neck in the area of the proximal endograft fixation, endoleak type Ia can occur. The aneurysm neck anatomy >28 mm diameter and >60 angulation and a short landing zone play a major role in the occurrence of endoleak type Ia [31].

Management of endoleak includes balloon dilation of unexpandable stent graft, additional endvascular procedure with extenders and cuffs, embolization, or conversion to open repair [14]. In general, Type-I endoleaks are addressed by additional cuff placement and balloon angioplasty, whereas Type-II endoleaks are treated by embolization [37]. In any case, conversion to open repair is always considered as a last resort.

1.4 Fenestrated and Branched Endovascular Aneurysm Repair

The concept of endovascular aneurysm repair (EVAR) was first reported by Parodi and colleagues in 1991 [38]. Since then, EVAR has become widely accepted as a safe technique for the treatment of abdominal aortic aneurysm (AAA) [39].

Endovascular aortic repair (EVAR) has developed as a less-invasive technique for the treatment of infrarenal abdominal aortic aneurysms (AAAs) [40, 41] as seen in Figure 1.13. Currently, the majority of patients with anatomically suitable infrarenal AAA are treated with EVAR, rather than with open repair [39]. However, 30%–50% of AAA patients are not suitable for elective conventional endovascular repair because of unfavorable anatomy such as a short (<10 mm) proximal landing zone [42, 43]. Furthermore, patients with aortic necks with large diameter (>32 mm), severe angulation (>60°), or an absent infrarenal neck, are not candidates for the currently available devices, and open repair is the best

option for these patients [42, 44].

Good surgical candidates may tolerate open conventional repair of the aneurysm, but patients with large aneurysms and poor cardiac, pulmonary, or renal performance have limited options. Infact, EVAR is ideally suited for older patients and those with medical or surgical contraindications for open surgical repair, especially those who have had prior aortic interventions [45]. However, to address these restrictions, new devices with fenestrated and branched stents have been proposed and successfully used, capable of providing with an option to extend the proximal sealing zone from the infrarenal segment to the juxta and suprarenal aorta, thereby circumventing the limitation of short or absent aortic necks [42, 43, 46].

Park et al described the first fenestrated aortic graft in 1996. A fenestrated endovascular

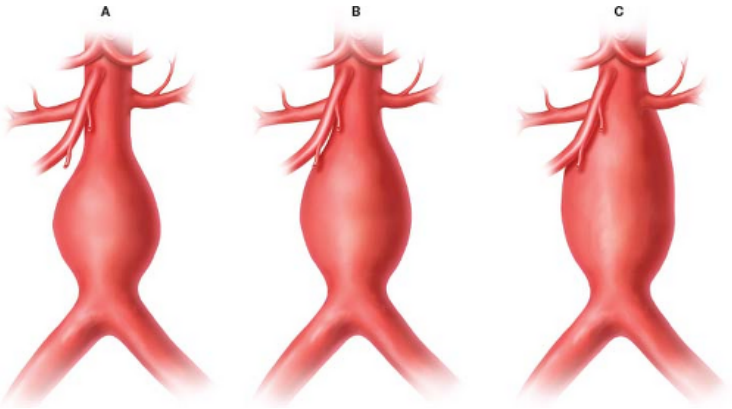

Figure 1.13: Relationship between abdominal aortic aneurysms and renal arteries. A: Infrarenal aortic aneurysm (neck >10 to 15 mm). B: Juxtarenal aortic aneurysm (neck = 4 to 10 mm). C: Suprarenal aortic aneurysm, neck length <4 mm. Reproduced from http://thoracickey.com

repair is used to repair an aneurysm with inadequate neck length, yet the target vessels (e.g, renal arteries, celiac and superior mesenteric arteries) arise from normal aorta and are located within the proximal landing zone [42]. Complex endovascular repairs involving the visceral segment can be divided into 2 broad categories: fenestrated and branched endograft repairs:

Fenestrated stent grafts, as shown in Figure 1.14, have small holes along their body and vary in size depending on the need of a particular patient, and scallops at the edges in

order to accommodate positioning of branch vessels. Scallops are openings cut created at the proximal aspect of the stent graft, allowing additional proximal extension of the repair across the origin of a vessel (eg, superior mesenteric artery) [40, 45, 47]. Although fenestrated stent graft repairs do not typically require branches to ensure a tight seal, most visceral branches are stented open using balloon-expandable stents to ensure proper alignment of the graft and the particular visceral branch vessel.

Branched endovascular repair is currently performed using 1 of 2 main approaches. Branch

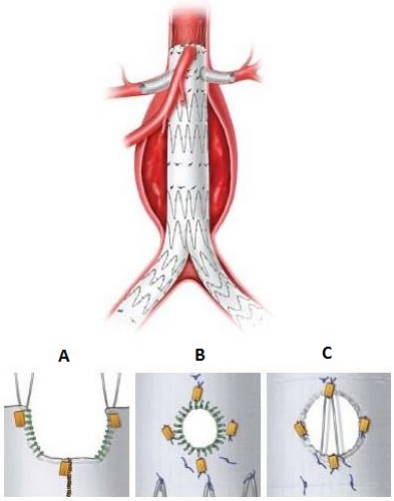

(a) *Fenestration types.*

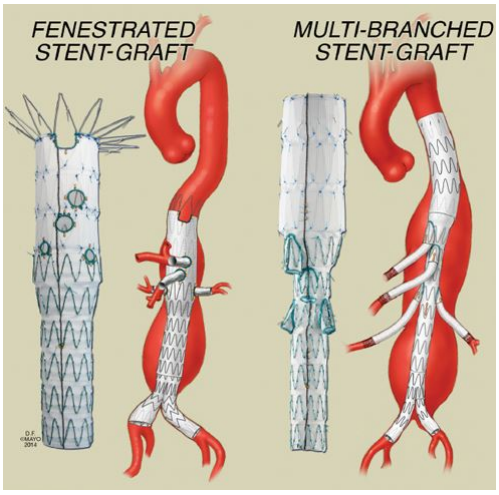

(b) *Fenestrated Stent-Graft and Multi-Branched Stent-Graft.*

Figure 1.14: (a) Cook Zenith Fenestrated Endograft with: **B**:scallop, **C**:small fenestration, and **D**:large fenestration; (b) Endovascular options for branch incorporation include fenestrated branched devices for pararenal aneurysms, multibranched devices for thoracoabdominal aneurysms.

artery stenting can be based on fenestrations reinforced with a nitinol ring (fenestrated-branched stent grafts), or the main device can have cuffs that function as directional branches and serve as attachment sites for each branch artery stent involved in the repair (cuffed-branched stent grafts) [42]. On the other hand, the device may have multiple branches that arise from the aortic graft proximal to the target branch and are completed with a bridging covered stent extending into the target vessel [45].

Fenestrated and branched stent grafts have increased the applicability of EVAR to patients

who would otherwise be subject to highly morbid open repair procedures [48]. The mortality associated with conventional treatment of open pararenal and suprarenal aneurysms ranges from 2.5% to 8%, while the one association with the thoracoabdominal aneurysms ranges from 5% to 34%. In addition, open surgery is associated with significant morbidity rates, ranging from 20% to 40%. Endovascular repairs have been shown to reduce perioperative morbidity, mortality, length of hospital stay, and postprocedure disability [45, 49]. Compared with standard EVAR, a disadvantage of EVAR using fenestrated stent grafts is that these grafts often require a high degree of customization and long manufacturing time (1-2 months), which increases cost and makes the technique prohibitively expensive for emergent cases. In addition, technical considerations such as severely angulated necks, aortic thrombus in the area of target vessels, and small, calcified target vessels might also prohibit the use of fenestrated grafts. Fenestrated devices are very attractive and, when available, will likely have an increasing role in the treatment of anatomically suitable patients, but they are still associated with a higher (>10%) secondary intervention rate [45, 48]. In critical cases where the patient condition does not allow to wait several months for a custom SG system to be manufactured, a novel solution is recently being employed using off-the-shelf SGs. This solution is an endovascular surgical procedure termed the ”chimney” technique [50]. The nomenclature of this technique has varied overtime and various terms have been used: "snorkel", "parallel grafts" or as the majority called it a "chimney graft (CG)" [51].

1.5 Chimney Graft Technique

With the introduction of the chimney procedure, a ready available alternative to a fenestrated stent graft, for the treatment of acute aneurysm in patients with challenging anatomy when there is no time to manufacture a fenestrated device.

Greenberg et al. [3] were the first to describe a CG procedure that was performed in 2001 and it was applied over the last decade for visceral debranching [4]. This technique can be used as a bailout procedure for unintentional coverage of vital side branches or can be

planned as an alternative procedure to extend the aortic neck in patients considered ineligible for fenestrated or branched stent grafts [52, 53, 54]. Recently, several authors have presented their series and two reviews showed excellent results, with a technical success rate of 94.8% and 30-day mortality of 7.1% [4, 55].

In chimney endovascular aneurysm repair (Ch-EVAR), one or more tubular covered stents (chimneys SG) are implanted inside the visceral arteries in parallel with the main aortic SG that excludes the aneurysm sac [50].

These covered stents facilitate proper blood flow to arteries that would otherwise be

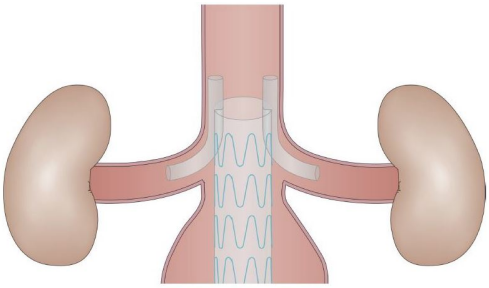

Figure 1.15: A chimney graft tecnique to preserve the renal and/or mesentric perfusion.

blocked by the main aortic SG. A common case of repair with the chimney technique shown in Figure 1.15, involves proximity of the aneurysm to the two renal arteries. In this case, in order to preserve blood flow to the kidneys, a chimney stent graft is inserted into each renal artery.

By implanting a CG parallel to the main aortic SG, side branches could be preserved both in the abdominal and thoracic aorta [3]. Thereafter many groups expanded the application of CG technique beyond juxtarenal aneurysms to suprarenal, thoracoabdominal, and aortic arch aneurysms. The technique has been used in the renal arteries, superior mesenteric artery (SMA), left subclavian artery (LSA), left common carotid artery (CCA), and innominate artery [56]. Chimney graft is deployed into a vital aortic side branch alongside and parallel to the main aortic SG in order to extend the sealing zone and maintain blood flow to the aortic side branches.

The largest collected world experience of snorkel/chimney EVAR was recently published

from the PERICLES registry, which included 898 chimney grafts in 517 patients and noted an early mortality rate of 4.9%, as well as a persistent type Ia endoleak rate of 0.4% and primary patency of 94% during a mean follow-up of 17.1 months [57].

1.5.1 Comparison between chimney graft and fenestrated graft

Compared to fenestrated graft technique, the "chimney graft" technique has the advantage of avoiding the delay in device manufacturing and the high cost. Long-term data and larger series are needed to determine the safety and efficacy of this technique[4]. Table 1.2 presents a resume of the comparison between chimney graft technique and the use of fenestrated grafts.

Urgent cases. One of the primary advantages of the snorkel/chimney technique is the ability to use this approach in the urgent or emergent setting for patients presenting with symptomatic, rapidly expanding, or ruptured abdominal aortic aneurysms (AAAs), compared to the fenestrated approach that require a high degree of customization and long manufacturing time (1-2 months), which increases cost and makes the technique prohibitively expensive for emergent cases [45, 48, 59]. e.g. A patient with an aneurysm that was considered lifethreatening (diameter >60 mm, rapidly expanding or painful aneurysm) and who could not wait for a fenestrated stent graft to be manufactured.

Tortuous visceral aortic segment. There are some anatomical contraindications that are related to the small or tortuous iliac arteries, severe iliac occlusive disease, proximal migration, type Ia EL after previous EVAR, or an angulated aorta [58]. In addition, the rigidity of the larger fenestrated delivery system may also hinder trackability of the device in iliac systems with severe tortuosity and make snorkel/chimney EVAR a better option in cases with challenging access anatomy [23].

A hostile visceral aortic segment with calcium, thrombus, and severe tortuosity can significantly impede complex EVAR, regardless of endovascular strategy. In this case, this technique is disadvantageous; The difficult task of navigating a relatively large, rigid device into a tortuous segment may contribute to misalignment of the fenestrations/ scallops and

Fenestrated grafts	**Chimney grafts**
More anatomic branch revascularization	"Off the shelf"
Needs more planning (Not ideal for urgent cases)	Suitable for urgent AAA cases (rupture and symptomatic aneurysm)
Custom made for each patient	Possibly easier
Long time-manufacturing and expensive procedure	No time to manufacturing and Cheaper procedure
Risk of rupture and need to a second intervention to Re-fixing	Can get guttering effect and compression —> Endoleak type I
Not suitable for small-caliber iliofemoral arteries	better option in cases with challenging access anatomy
Not ideal with challenging access anatomy	Chosen when the use of a fenestrated stent graft is contraindicated due to short main graft length
Not suitable in hostile visceral aortic segments with severe tortuosity	Thanks to its maneuverability,this technique is ideal in cases of visceral aortic segments with severe tortuosity

Table 1.2: Comparison between chimney graft and fenestrated graft [5, 58]

subsequent target vessel occlusion. This could limits maneuverability and predictability of the final endograft position, which may be less detrimental during snorkel/chimney EVAR because the branch vessels are stented independently from the aortic segment, and there is no concern for visceral/ renal misalignment [60].

Therefore, CH-EVAR may be an appealing and efficient alternative, not only in emergent settings but also in elective cases where f-EVAR is predicted to be technically difficult or is contraindicated [58].

1.5.2 Post-op complications

A well-placed and anchored SG forms a new blood vessel, and therefore completely protects the weakened aneurysm wall from the pulsatile blood pressure. However, various postoperative complications may occur, for such as the device migration, but endoleaks are the most frequent and severe. In the "chimney" technique, excess oversizing is needed to facilitate the formation of channels lateral to the graft in order to accommodate the chimney grafts. Chimney grafts, however, induce large "gutters" along the main endograft which may cause a proximal type I endoleak [61], as seen in Figure 1.16.

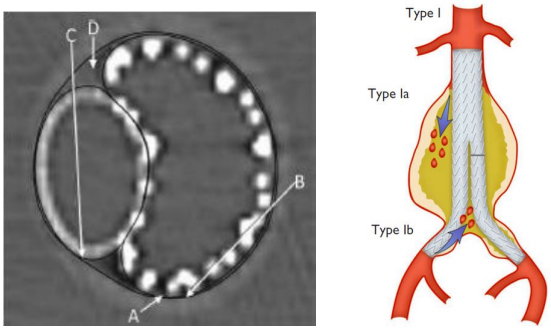

(a) *Cross section view of chimney configuration.* (b) *Endoleak type I.*

Figure 1.16: (a) Different cross-sectional areas: A: outer perimeter of the main graft, B: inner diameter of the aorta, C: outer perimeter of the chimney graft, and D: gutter. Adapted from de Bruin, et al., 2013 [62].
(b) Endoleak type I: persistent filling of the aneurysm sac due to ineffective seal at the proximal (type Ia) or distal (type Ib) end of the stent graft. Adapted from https://www.emaze.com/

1.5.3 How can I prevents type I Endoleak?

Type I endoleak is considered the "Achilles' heel" of the Chimney method. Usually, type I Endoleaks resolve spontaneously in follow-up. Several studies show a high rate of spontaneously resolved type I endoleaks, possibly due to the formation of clot or poor outflow. Viscous, inertial forces and the minimum velocity of the outer layer of blood, added to the interaction of blood with the graft and the elastic deformation of the native aorta can lead to clot formation and eliminated free flow in tight gutters.[4, 63, 62]
But this is not enough. The choice of the optimal CG configuration with an appropriate size and geometry, material and configuration of stent grafts, is important to reduce gutter size and consequently prevents the risk of Endoleak Ia.

Chapter 2

Chimney-Evar Technique: Set-up of Structural FEA Simulations

2.1 Introduction

In order to study the endoleaks type Ia formed in Chimney Graft configurations, by studying the gutter size, and examine how the deformation occur in the endografts, we choose an approach in Finite Elements. So the next step is to develop a finite element analysis (FEA), relying on a multidisciplinary approach aimed at designing and optimizing patient-specific tailored prosthesis and procedure. (All details related to FEA are described in Appendix B).

To perform a simulation of the prosthesis implantation in the native aortic root, the whole study is conducted using the graphical finite element preprocessor ABAQUS/CAE (Dassault Systemes) to simulate the two main stent phases: crimping and deployment.

Starting from its undeployed shape, the stent crimping consists in narrowing the stent graft (SG) to introduce it into the delivery catheter. In order to virtually reproduce this operation, a cylinder has been introduced round the SG for imposing a radial displacement that produces the structure shrinkage. This cylinder is also used in the deployment phase for modeling the catheter, from which the SG is released in the aortic tract of the patient

where the aneurysm is located.

2.1.1 Abaqus (Simulia, Dassault Systems)

Abaqus [64] (Simulia, Dassault Systems, Providence, RI, USA) is a suite of powerful engineering simulation programs, based on the finite element method, that can solve problems ranging from relatively simple linear analyses to the most challenging nonlinear simulations. Abaqus contains an extensive library of elements that can model virtually any geometry. It has an equally extensive list of material models that can simulate the behaviour of most typical engineering materials including metals, rubber, polymers, composites, reinforced concrete, crushable and resilient foams, and geotechnical materials such as soils and rock. Designed as a general-purpose simulation tool, Abaqus (Simulia, Dassault Systems) can be

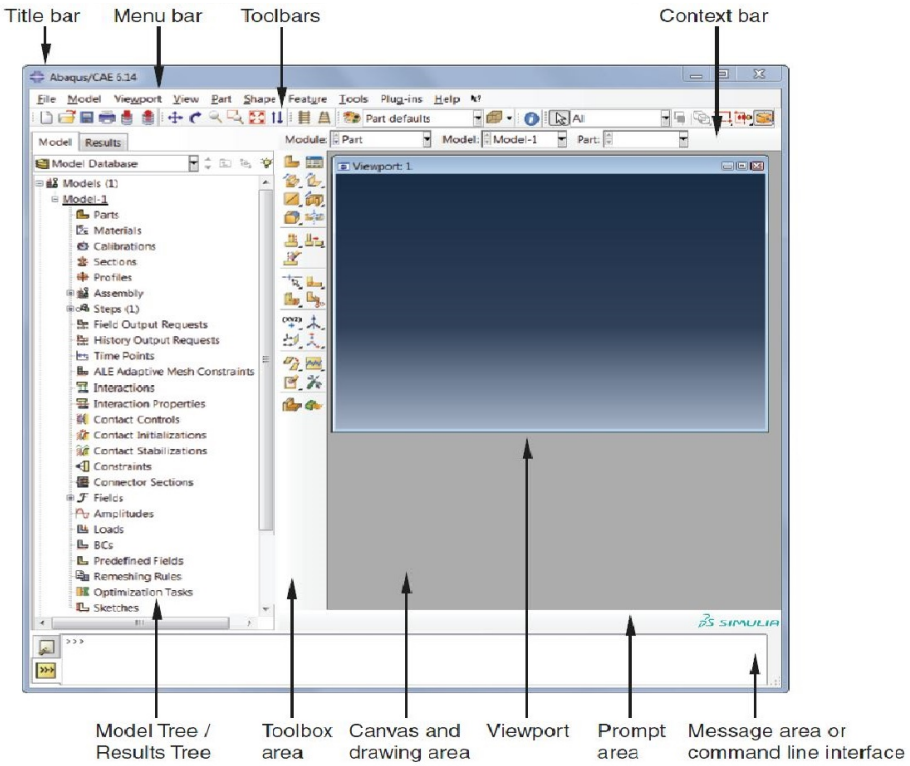

Figure 2.1: Abaqus interface

used to study more than just structural (stress/displacement) problems. It can simulate problems in several areas such as heat transfer, mass diffusion, thermal management of

electrical components (coupled thermal-electrical analyses), acoustics, soil mechanics (coupled pore fluid-stress analyses), piezoelectric analysis, electromagnetic analysis, and fluid dynamics.

Abaqus (Simulia, Dassault Systems) offers a wide range of capabilities for simulation of linear and nonlinear applications. Problems with multiple components are modeled by associating the geometry defining each component with the appropriate material models and specifying component interactions. In a nonlinear analysis Abaqus automatically chooses appropriate load increments and convergence tolerances and continually adjusts them during the analysis to ensure that an accurate solution is obtained efficiently.

As shows in figure 2.2, Abaqus/CAE is a complete Abaqus environment that provides a simple, consistent interface for creating, submitting, monitoring, and evaluating results from Abaqus/Standard and Abaqus/Explicit simulations.

Abaqus/CAE is divided into modules, where each module defines a logical aspect of the

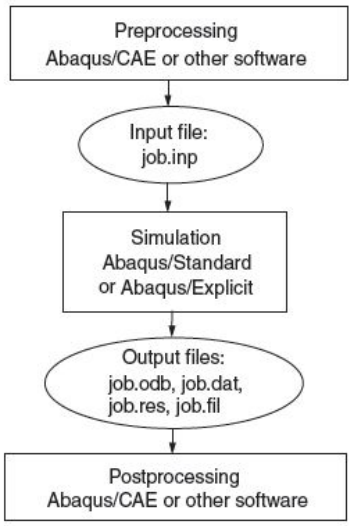

Figure 2.2: Abaqus (Simulia, Dassault Systems) analysis flow

modeling process; Moving from module to module, the model from which Abaqus/CAE generates an input file is built (more details about input file analysis are given in Appendix A), this is submitted to the Abaqus/Standard or Abaqus/Explicit analysis product. The analysis product performs the analysis, sends information to Abaqus/CAE to allow the

monitoring the progress of the job, and generates an output database. Finally, the Visualization module of Abaqus/CAE is used in order to read the output database and view the results of the analysis.

Each module in Abaqus contains only those tools that are relevant to a specific portion of the modeling task. The order of the modules in the menu as shown in Figure 2.3 corresponds to the logical sequence followed to perform a FEM analysis with Abaqus 6.14-2 (Simulia, Dassault Systems). The modules are the following:

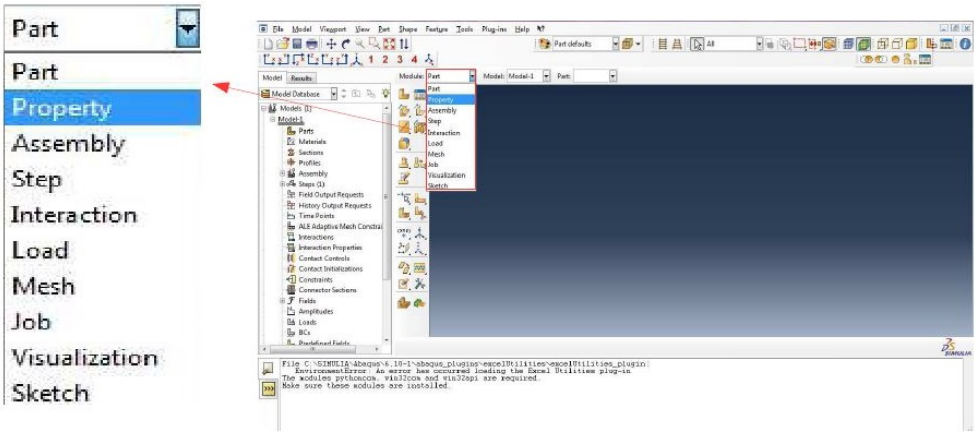

Figure 2.3: Abaqus (Simulia, Dassault Systems) Modules

1. **Part:** create individual parts by sketching or importing their geometry.
2. **Property:** create material definitions and assign them to regions of parts.
3. **Assembly**: create and assemble part instances.
4. **Step:** create and define the analysis steps and associated analysis procedure.
5. **Interaction:** specify the interactions, such as contact, between regions of a model.
6. **Load:** specify loads, boundary conditions, and fields.
7. **Mesh:** create a finite element mesh.
8. **Job:** submit a job for analysis and monitor its progress.

9. **Visualization:** view analysis results.

10. **Sketch:** Create two-dimensional sketches.

Below, the procedure followed to complete each module is described in detail.

2.2 Chimney-evar Finite Element Analysis Set-up

2.2.1 Part module

As the figure 2.4 shows, a CG configuration is composed by a main stent graft and a parallel stent graft, also called "chimney" stent graft, wrapped in a abdominal aortic root. In

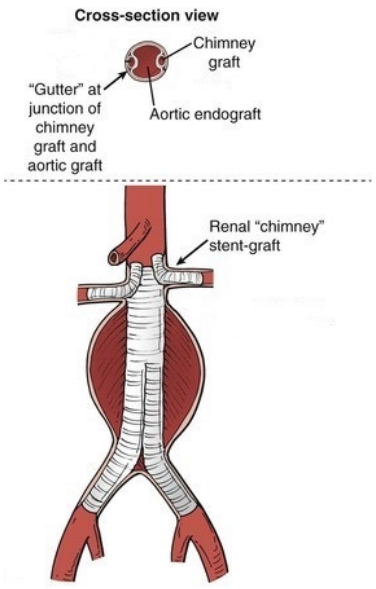

Figure 2.4: Renal artery "chimney" graft configuration. Composed by two stent grafts: Main body SG (Aortic endograft) and Parallel SG (chimney graft)

order to create a CG configuration, specific models are needed which are introduced in the following paragraphs.

Main and Parallel stent grafts: considered the SG's used in the patient-specific case of the Department of Endovascular Surgery of San Matteo Hospital (Pavia). The geometry, size and material related to the both stents come from Gore medical's official website, as

showed in Figure 2.5;

Conformable GORE® TAG® Thoracic, Figure 2.6, is a leading option for the

Stent Type	Company	Stent Name	Graft Marterial	Stent Material	Size (diameter x length)
Main Stent	W. L. Gore and Associates	Conformable GORE TAG	ePTFE/FEP	Nitinol	28x100 mm
Parallel Stent	W. L. Gore and Associates	Viabahn	ePTFE	Nitinol	9x100 mm

Figure 2.5: Stent grafts used in Chimney-EVAR case-specific (Main body and Parallel SG)

endovascular treatment of thoracic aneurysms, transections and all B type dissections. As a proven endovascular treatment for the thoracic aorta, the Conformable GORE®TAG® Thoracic Endoprosthesis provides physicians with several benefits. Conformable GORE TAG (CTAG) composite device consists of an expanded polytetrafluoroethylene- fluorinated ethylene propylene ePTEF/FEP graft supported over its entire length by a nitinol stent [65]. In this case, this endoprosthesis was used as main body stent graft in Chimney

(a) *Main stent graft Conformable GORE® TAG® Thoracic real device*

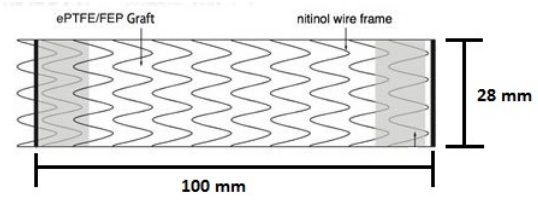

(b) *Main SG "sinusoidal" metallic stent shape*

Figure 2.6: The Conformable GORE TAG Endoprothesis. (Image courtesy of W. L. Gore & Associates Inc).

configuration.

GORE® VIABAHN®, figure 2.7, is made by a durable, reinforced, biocompatible, expanded polytetrafluoroethylene (ePTFE), linearly attached to an external nitinol stent structure. The flexibility of the GORE VIABAHN Endoprosthesis enables it to go through

tortuous areas of the SFA and conform closely to the complex anatomy of the artery.
W. L. Gore & Associates has now added a heparin-bonded surface to the GORE VIABAHN Endoprosthesis. The GORE VIABAHN Endoprosthesis with HeparinBioactive Surface is the only device of its kind accepted by both the SFA and iliac artery. All those information has been taken from the website dedicated to the device (Gore[66]). In this case, this

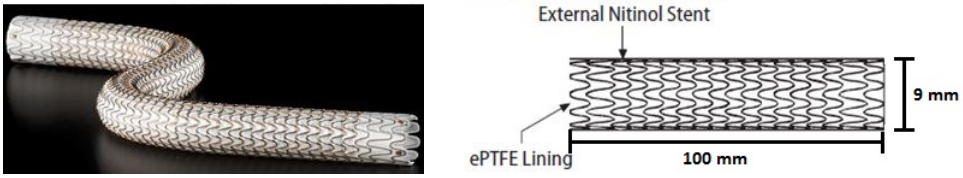

(a) *Parallel stent graft GORE VIABAHN real device*

(b) *Main SG "sinusoidal" metallic stent shape*

Figure 2.7: The GORE VIABAHN Endoprosthesis. (Image courtesy of W. L. Gore & Associates Inc).

endoprosthesis was used as a parallel stent graft in the Chimney configuration.

Delivery catheters: two cylindrical models representing the main and parallel catheters, were created with Abaqus 6.14-2 (Simulia, Dassault Systems) tools. The lenght of both models is 140 mm, the diameter is 30 mm for main SG and 11 mm for parallel SG, 2 mm bigger than endoprosthesis diameters.

Abdominal Aortic root model: this geometrical model represents the arterial wall, created with Abaqus tools. The model is 140 mm in length and 20 mm in diameter.

All models details are presented in Figure 2.8.
The reason why it has been decided to create personal stents along the line of the CTag and Viabahn is because these stents have been implanted with chimney-evar technique into the patient of the San Matteo Hospital, Pavia.
Both stents were created in expanded shape. Through some design parameters, a new model has been generated. During the planning, some rules were established. The first

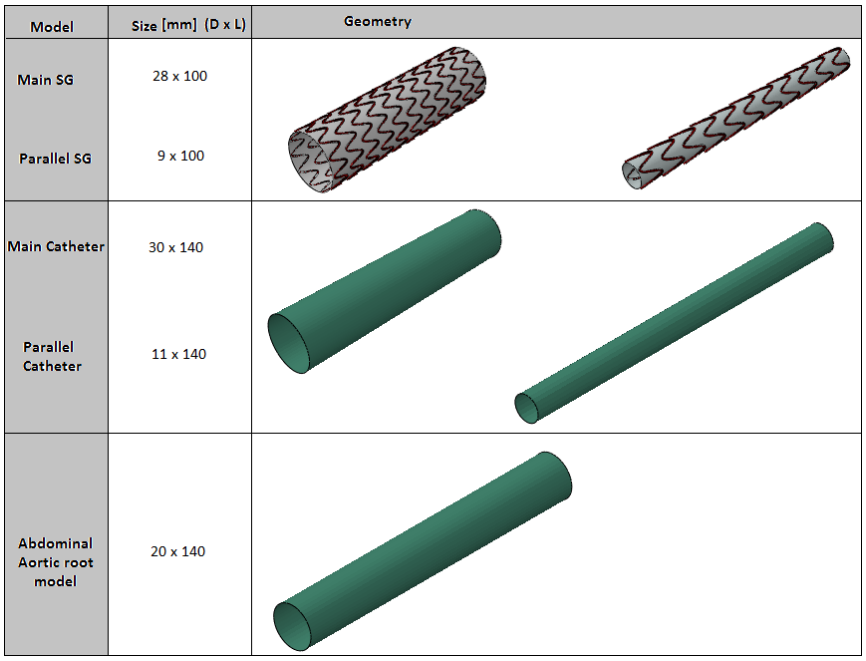

Figure 2.8: Parts models created in Abaqus 6.14-2 (Simulia, Dassault Systems).

important decision to take for the design is the choice of the elementary unit shape. It's a basic characteristic that is going to be repeated several times in the stent mesh. The geometries of both stents were based on dimensions found in open resource and, given that all of these stents have a similar "sinusoidal" shape as shown in Figure 2.7, only two stents with similar metallic shape and different diameters were designed.

Stent graft reconstruction

Stent graft reconstruction follows some rules as shown in Figure 2.9.

Step 1: Design of the elementery unit with Rhinoceros 5.0 (McNeel&Associates)
The stent's shape is based on the sinus function, where the amplitude and the frequency in the unity space of the wave are set by the user. Solid models of the full stent can be generated by knowing the size and the geometry parameters of the stents and by using the repeating unit geometry of each design.
During the design, some rules have been set, such as the initial part of elementary unit, a

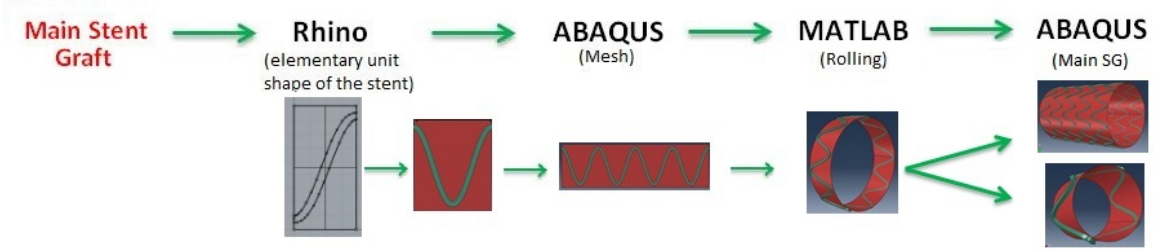

Figure 2.9: Stent graft reconstruction workflow. Strating from Rhinoceros 5.0 (McNeel&Associates) the first part of the elementeray unit geometry of the stent is created. Then it has been imported in Abaqus 6.14-2 (Simulia, Dassault Systems) to create the elementary unit and the planar geometry of the stent composed by multiple copies of elementary units. After that, the planar geometry is wrapped into a cylindrical geometry using Matlab R2016b (MathWorks) and finally, using Abaqus again the final stent graft model is obtained. The same procedure was used to both main and parallel stent grafts reconstruction.

half wave accurately drawn with Rhinoceros 5.0 (from McNeel&Associates, Indianapolis, USA), a NURBS-based 3D modeling tool used for industrial design. This half-wave geometry is made up of two geometries, a sigmoidal geometry for the stent strut with thickness s=0.5 mm and a rectangular geometry (L x l=9.075 x 3.888), for the stent membrane as shown in Figure 2.10. Afterwards, it has been saved as a file with IGES extension and

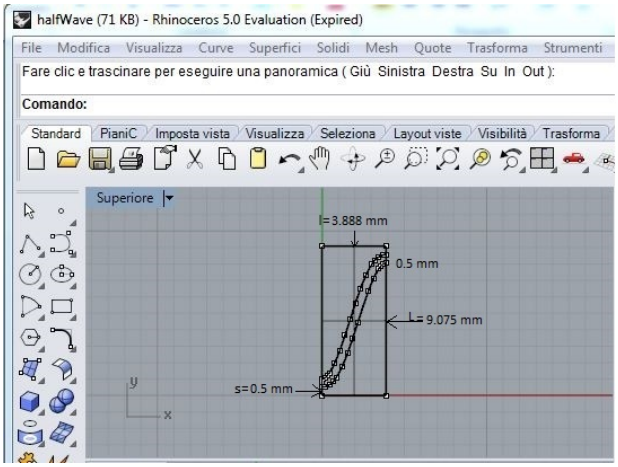

Figure 2.10: 3D elementary unit design with Rhinoceros 5.0 (McNeel&Associates).

imported in Abaqus 6.14-2 (Simulia, Dassault Systems), ready to the next step.

Step 2: Creation of the planar geometry of the unrolled stent using Abaqus 6.14-2 (Simulia, Dassault Systems)

The second step requires the specular copy of the half part of elementary unit to obtain a complete elementary unit model (figure 2.18). In order to create the planar geometry of the unrolled stent, it is needed to create multiple copies of the elementary unit part using the linear pattern tool of Abaqus along horizontal direction. Two planar geometries were

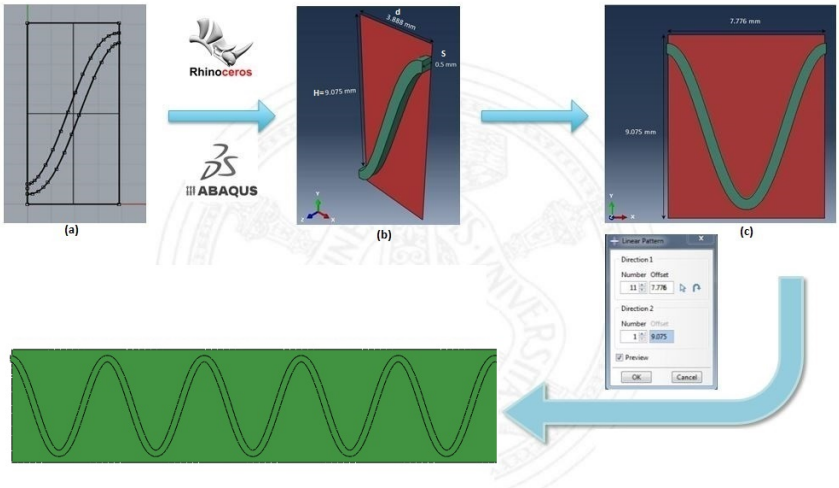

Figure 2.11: Reconstruction of the planar geometry of the unrolled stent. The elementery unit created with Rhinoceros 5.0 (McNeel&Associates) (a). The elementery unit imported in Abaqus as a iges part (b). The elementary unit geometry (c). Creation of planar model with the linear pattern tool of Abaqus along horizontal direction (d).

constructed, one for each stent graft and in order to create two stent grafts of different diameters, the formula (2.1) that correlates the inner radius of the stent R, the width of the elementary unit d and the number N of the elementary units has been applied, as shown in the top view in Figure 2.17:

$$\begin{aligned} d &= \frac{2\pi R}{2N} \\ N &= \frac{\pi R}{d} \end{aligned} \tag{2.1}$$

Having R_1=14 mm as main stent radius, R_2=4.5 mm as parallel stent radius and d=3.888 mm as half elementary unit width, we obtain the main stent unrolled model composed

by N_1=11 waves and the parallel stent unrolled model composed by N_2=4 waves. The overlapping nodes of the junction region belonging to two specular strips are joined in a so called "merging nodes" operation. Finally the mesh information about nodes and elements are saved in a INP file ready to be rolled using Matlab R2016b (MathWorks).

Step 3: Stent rolling using Matalb script

Once the planar stent model has been meshed, it has been wrapped into a cylindrical shape by transferring the nodal coordinates from a cartesian system into a cylindrical system. Therefore a MATLAB script has been implemented to roll the stent. Given the stent radius, the script transforms the input file containing cartesian nodal coordinates into an output file containing cylindrical nodal coordinates, ready to be imported in Abaqus 6.14-2 (Simulia, Dassault Systems).

Step 4: Extension of the ring to obtain the final model with Abaqus

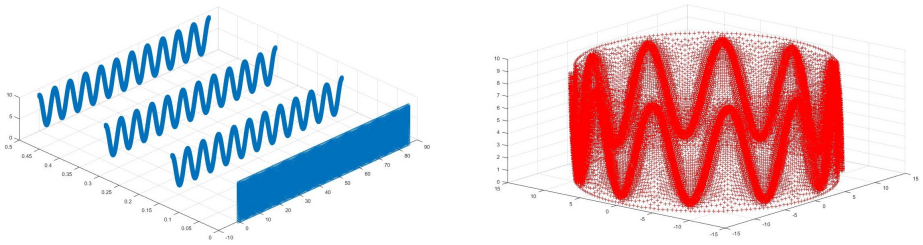

(a) *cartesian coordinate system* (b) *cylindrical coordinate system*

Figure 2.12: Matlab script's output figure. Transferring the nodal coordinates from a cartesian coordinate system (a) into a cylindrical coordinate system (b).

Once obtained the rolled part (one ring element), it is possible to create multiple copies of the selected part using the same linear pattern tools used before in Abaqus (Simulia, Dassault Systems), but this time Abaqus's tools reproduce that ring a certain amount of times along Z-direction. The stent is composed by a series of consecutively rings and the number of rings depends on the stent length, as shown in Figure 2.13

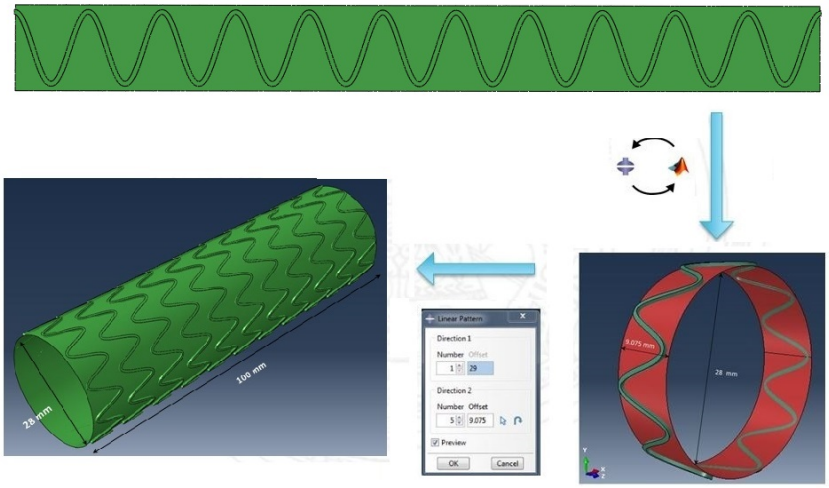

Figure 2.13: Main ring stent rolling and extension.

The delivery system: catheter

The delivery system has to be guided through the small and tortuous arterial tunnels in order to reach the target lesion. As a consequence, its main features have to be the flexibility and the trackability [67]. In this case, the delivery system, also called catheter is a rigid cylindrical surface created with a diameter of 2 mm larger than the endografts as shown in Fig. 2.8. Catheters are placed around the stent model in the crimping and deployment phases of simulation.

Abdominal Aorta segment Design

The abdominal aorta is the largest artery in the abdominal cavity. As part of the aorta, it is a direct continuation of the descending aorta. The average diameter of the aorta is 20-25 mm. Note that, the inner diameter of aorta segment, was calculated in order to fit in each CG configuration. According with this information and considering a straight small segment in abdominal aorta, it was designed a hollow cylinder with 140 mm of length and 20 mm of diameter without wall thickness which represents a simple geometric model of abdominal aorta. The final appearance of the model is presented on Figure 3.8.

2.2.2 Property module

The next step in creating the model involves defining and assigning material and section properties to the part. Each region of a deformable body must refer to a section property, which includes the material definition.
A material model describes the stress-strain relation for a material. In order to properly characterize a material it is necessary to perform mechanical tests to evaluate its properties, such as radial stiffness, flexural rigidity, and shear rigidity [5].
According to the commercial SG's models presented in precedent section, Nitinol and ePTFE are the widely-accepted materials used in stent fabrication by manufacturers.

Nitinol and ePTFE

Nitinol, is a metal alloy which combines Nickel and Titanium (Nickel Titanium Naval Ordnance Laboratory), where the two elements are nearing materials like stainless steel Nitinol alloys exhibit two unique properties that are closely related: shape memory and superelasticity. In fact, they are the most important shape memory alloys from the commercial point of view, thanks to the excellent performance in terms of shape memory and superelasticity of the good mechanical properties. The shape memory is the material ability to undergo deformation at one temperature, then recover its original, unreformed shape upon heating above its transformation temperature. The superelasticity occurs at a narrow temperature range just above its transformation temperature. Under these conditions the material shows an enormous value of elasticity. The behavior of the material is shown below in Figure 2.14. At high temperatures, nitinol assumes an interpenetrating primitive cubic crystal structure, known as austenite. At low temperatures, nitinol spontaneously transforms to a more complicated monoclinic crystal structure, known as martensite (Figure 2.14 part 4).
ePTFE. The superficial layer that covers internally the stent is ePTFE (Expanded Polytetrafluoroethylene), which is a waterproof/breathable fabric membrane (registered trademark of W. L. Gore and Associates (Wikipedia (2014)). Gore-Tex materials are typically

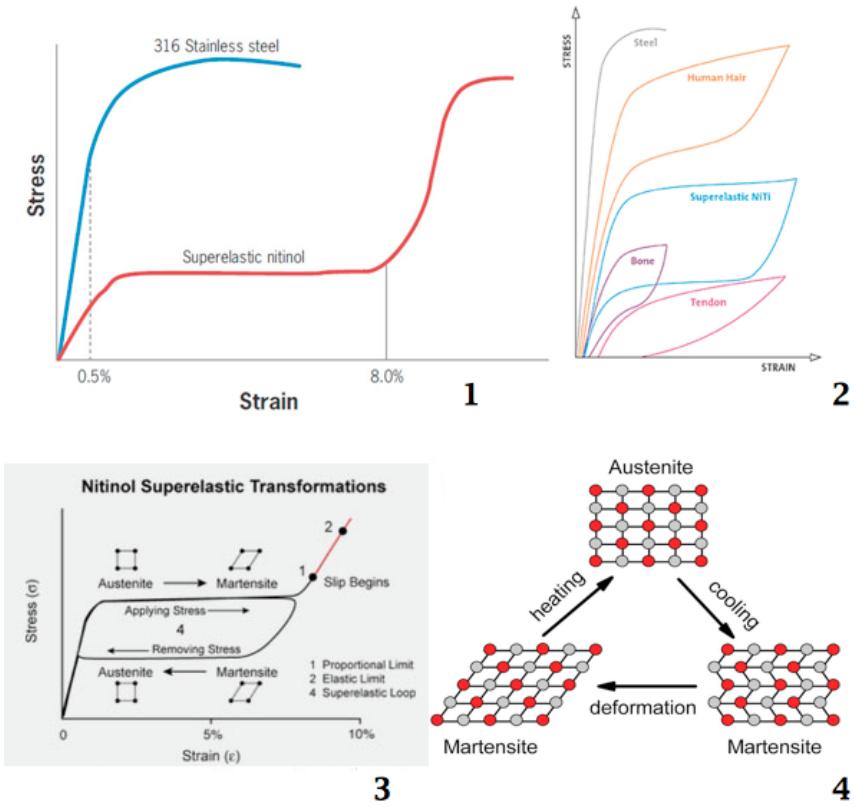

Figure 2.14: Some features of the Nitinol. From the top left (1), a plot of the curve Strain/Stress of the Nitinol compared to the 316 Stainless steel one; (2) the sale curve compared to other materials of the human body, the plot wants to stress the attention on the hysteresis characteristic of the material; (3) Nitinol superelastic trasformations; (4) a schematic explanation of the transition of the material between Martensite and Austenite.

based on thermo-mechanically expanded PTFE and other fluoropolymer products. They are used in a wide variety of applications such as high performance fabrics, filter media, insulation for wires and cables. Because it is nearly inert inside the body, they are also used internally in medical applications.

PTFE and Nitinol, have been defined in Abaqus (Simulia, Dassault Systems). **PTFE** is defined as an isotropic and linear elastic material whose density has been evaluated around 2200 kg/m^3, elastic modulus around 552 MPa and the Poisson's ratio is 0.45 [5].

Nitinol, is defined as superelastic material. The Abaqus user material subroutine of Nitinol proposed by Kleinstreuer et.al., 2008 [68] has been used to reproduce the super-elastic material response for stent model, as shown in table 2.1.

Once defined the material, strut and membrane sections habe been assigned to Nitinol

Abaqus superelasticity UMAT constants	(Kleinstreuer, et al., 2008)
Austenite elasticity (MPa)	51700
Austenite poisson ratio	0.3
Martensite elasticity (MPa)	47800
Martensite poisson ratio	0.3
Transformation strain	0.063
dσ/dT loading (MPa/°C)	6.527
Start transformation loading (MPa)	600
End transformation loading (MPa)	670
Reference temperature (°C)	37
dσ/dT unloading (MPa/°C)	6.527
Start transformation unloading (MPa)	288
End transformation unloading (MPa)	254
Strat transform stress compression (MPa)	900
Volumetric Transformation strain	0.063

Table 2.1: Abaqus (Simulia, Dassault Systems) superelasticity UMAT constants.

and PTFE materials, respectively as seen in Figure 2.15.

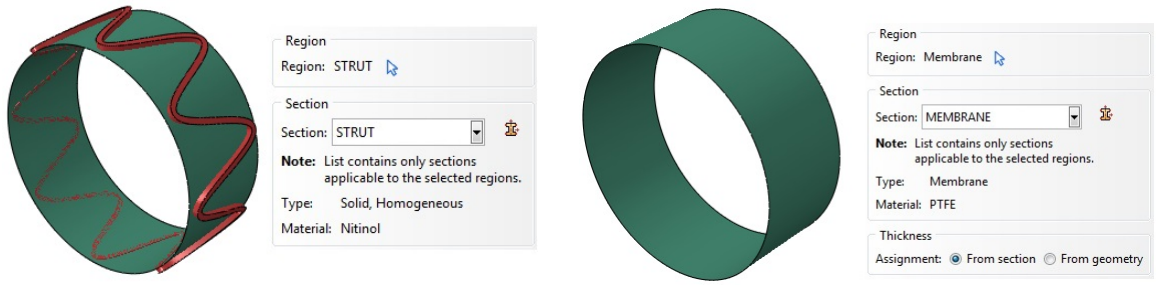

(a) *Strut section (Solid, Homogeneous), assigned to Nitinol material.*

(b) *Membrane section, assigned to PTFE material*

Figure 2.15: Stent graft section assignments

2.2.3 Mesh module

The automatic mesher in the software generates a mesh based on a global element size, tolerance, and local mesh specifications. The software estimates a global element size for the model taking into consideration its volume, surface area, and other geometric details. In order to generate a high-quality mesh, the CAD surface representing the stent graft was firstly partitioned, dividing the strut curved regions from the straight ones which represent the stent membrane. The curved parts, as shown in Figure 2.16, were characterized by a highly dense linear discretization as solid elements, while the straight regions were discretized as membrane elements to represent thin surfaces.

Stent grafts models were meshed using 3 element types: 8-node linear hexahedral elements

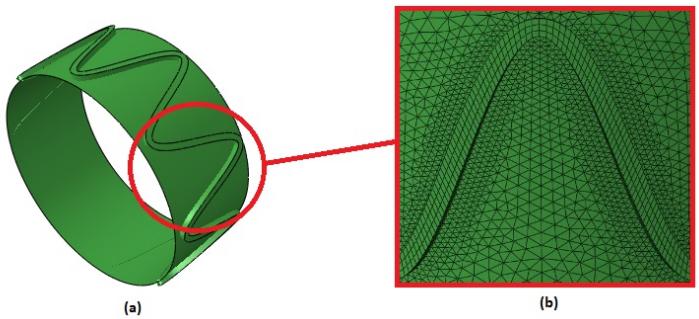

Figure 2.16: (a) Isometric view of a meshed stent ring;(b) Close-up of stent elementary unit composed by strut curved region and membrane straight region.

(C3D8R) for the strut geometry; 4-node quadrilateral membrane elements with reduction

(M3D4R) and 3-node triangular membrane elements (M3D3) for stent graft geometry. Catheters models were meshed using quadrilateral surface element with reduced integration (SFM3D4R). Aorta model was meched using 4-node quadrilateral rigid element (R3D4). Mesh statistics of model parts are presented in table 2.2.

Part Name	Nodes Number	Element Type	Element Shape	Elements
Main SG model	370920	M3D4R	quadrilateral	43318
		M3D3	triangular	296692
		C3D8R	hexahedral	115434
Parallel SG model	134880	M3D4R	quadrilateral	15752
		M3D3	triangular	107888
		C3D8R	hexahedral	41976
Main catheter model	5985	SFM3D4R	quadrilateral	5922
Parallel catheter model	2162	SFM3D4R	quadrilateral	2139
Aorta model	4200	R3D4	quadrilateral	4158

Table 2.2: Mesh statistics in Abaqus (Simulia, Dassault Systems).

2.2.4 Assembly module

The configuration assembly contains all the geometries included in the finite element model. Each Abaqus model contains a single assembly that is initially empty. In the analysis, both main and parallel stent graft have been included, the cylindrical rigid surface catheters and the cylindrical rigid surface aorta root, given that a complete analysis of the model is needed.

The final chimney graft configuration is shown in Figure 2.17. Some translation operations have been made on each part so they are in the correct position for the simulation.

Due to the high number of nodes and elements in the stent graft model, the evaluation of stress and strain values take a lot of time. As a consequence, it is initially necessary to use only a small part of the stent graft model made up by 3 rings, as shown in figure 2.18, while afterwards, the procedure can be extended to the entire model.

By measuring the gutter size in these two models, it has been proved that both 3 rings and 11 rings-stent grafts have roughly equal gutter areas (see subsection 2.4.3 for all mea-

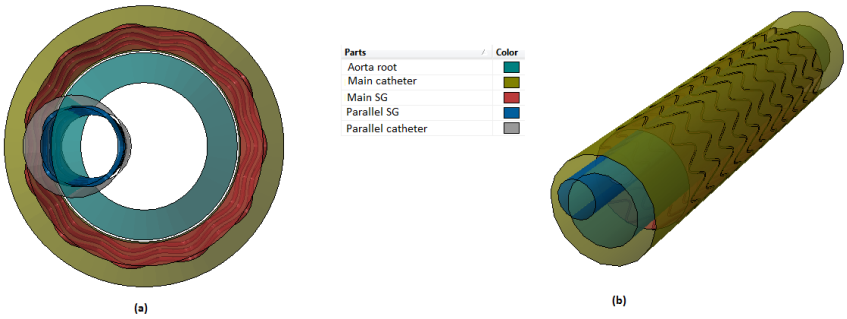

Figure 2.17: Final chimney assembly configuration. (a) front view; (b) Isometric view.

surement details). Thanks to this result, the next FEA simulations in Abaqus can be performed using the 3 rings-stent grafts.

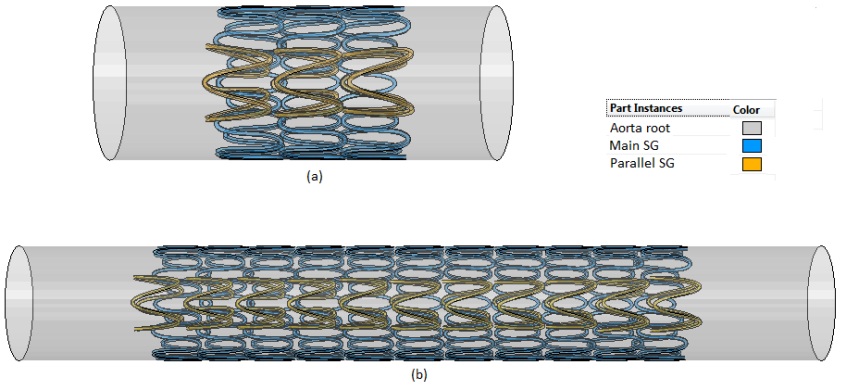

Figure 2.18: Small and entire models configurations created in Abaqus 6.14-2 (Simulia, Dassault Systems). (a) configuration with 3 rings-stent grafts. (b) configuration with 11 rings-stent grafts.

2.2.5 Step module

As already proposed in different studies [69, 70], the endograft deformation is driven by the configuration change of the catheter, imposed by displacement boundary conditions on its nodes and it is determined as the difference between a starting and final catheter configuration for each simulation step. In particular, the simulation consists of two main stages: crimping and deployment.

Stent crimping

In order to simulate the actual crimping process, a rigid cylindrical surface was created and placed around the stent model. By means of a radial displacement control, the catheter decreased its diameter to achieve a final external stent diameter. In the crimping phase the presence of the aortic root is ignored and the parts which interact are only the cylinder and the SG.

Stent deployment

During the deployment, the self-expanding stent is gradually released from the catheter recovering the target diameter thanks to its mechanical properties. This expansion process is due to a nickel-titanium alloy (nitinol), whose main feature is the shape memory. Self-expanding stents are very flexible and have a significant radial force. In the deployment phase the SG interacts with the catheter and the aortic root.

Chimney-EVAR procedure consists of inserting two stent grafts, main SG and chimney (or parallel) SG in a straight abdominal aorta segment; The whole simulation representing the stenting procedure includes four different steps, which have been created in Abaqus 6.14-2 (Simulia, Dassault Systems), as shown in the Figure 2.19.

1. Parallel stent graft crimping
2. Main stent graft crimping
3. Main stent graft deployment
4. Parallel stent graft deployment

Name	Procedure	Time
CrimpingParallel	Dynamic, Explicit	0.01
CrimpingMain	Dynamic, Explicit	0.01
DeploymentMain	Dynamic, Explicit	0.01
DeploymentParallel	Dynamic, Explicit	0.01

Figure 2.19: Abaqus 6.14-2 (Simulia, Dassault Systems) steps.

These four steps follow a Dynamic Explicit analyis procedure. The value of the time-step imposed is $1x10^{-2}$ sec for all four steps. The Mass Scaling technique is used to accelerate

the analysis and the value imposed is $3.5x10^{-8}$. The principle of this method consists in scaling the mass of the model in order to achieve a larger explicit time-step, thus to accelerate the analysis.

Given that the visualization module to post-process the results has been used, it is needed to specify the output data previously added into the output database file. Default history and field output requests are selected automatically by Abaqus 6.14-2 (Simulia, Dassault Systems) for each step. In this case, stress, strain, displacement, velocity, acceleration and contact variables have been selected.

2.2.6 Interaction module

The interaction module to define and manage constraints between regions of a model has been used, specifically to impose stent deformation from crimping to deployment. The interaction type is General contact, used to define contact between many or all regions of the model with a single interaction. A contact interaction property can define tangential behavior (friction and elastic slip) and normal behavior (hard, soft, or damped contact and separation). In addition, a contact property can contain information about damping, thermal conductance, thermal radiation, and heat generation due to friction (adapted from Abaqus (Simulia, Dassault Systems) User's Manual).

The general contact algorithm has been used in order to handle these interactions, the frictional behavior has been described by a Coulomb friction model with a static friction coefficient. These contact specifications allow to avoid numerical instabilities in the simulation of the interactions [71]. The only property that has been set is the tangent behavior of the elements considered as penalty friction formulation.

2.2.7 Load module and Boundary conditions set-up

In Abaqus 6.14-2 (Simulia, Dassault Systems), it is possible to create different types of BC's:

- **Symmetry/antisymmetry/encastre BC**

- **Displacement/rotation BC** to constrain the movement of the selected degrees of freedom to zero or to prescribe the displacement or rotation for each selected degree of freedom.

- **Velocity/angular velocity BC** to prescribe a velocity for the selected degrees of freedom of the selected region's nodes.

- **Acceleration/angular acceleration BC** to prescribe an acceleration for the selected degrees of freedom of the selected region's nodes.

Given that this study only involves the displacements at the top section, in order to calculate the gutter areas and analyze the stent graft oversizing, only displacement/rotation boundary conditions have been selected: (i) the end faces of all parts were bounded in all three directions; (ii) the y- and z- nodal displacements of the stents located on its middle plane were fixed, allowing the radial expansion/compression of the stent but not its rigid motion.

2.2.8 Analysis Finite Element Analysis step by step

In order to replicate the actual chimney stenting intervention, the parallel stent graft was crimped first. In this step, the stent was compressed to simulate the process of stent crimping onto the delivery catheter (Model B in Figure 2.20 (a)). As Boundary condition, a negative displacement in the U1 direction of 3.35 mm is applied, which is a shortening equal to the 74% of the total radius, allowing the shrinkage of the prosthesis. There is no radial displacement for the main catheter. In this step, the only contact was the interaction between the parallel stent and the parallel catheter. The step had a duration of 0.01 s.
The second step simulated the main stent graft crimping (Model A in Figure 2.20 (a)), with a duration of 0.01 s. In this step, a negative displacement of 10.75 mm has been set in the U1 direction, which is a shortening equal to the 77% of the total radius, to allow the shrinkage of the main SG. Contacts were created between the parallel SG and parallel catheter, the main SG and main catheter.

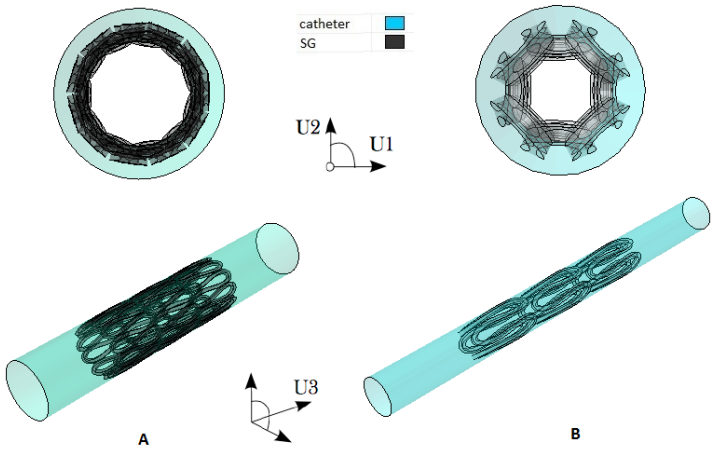

Figure 2.20: Stent grafts crimping. Main SG crimping (model A); Parallel SG crimping (model B).

Subsequently, the main stent was expanded into the artery to simulate the stent deployment; a third step was carried out with duration of 0.01 s, maintaining previous interactions. There were also considered interactions between the two stent models, and between the artery model and the expanded main stent. The catheter model was fully constrained. In this step, the main stent resumes its initial diameter and therefore a positive radial expansion of 10.75 mm at cylinder surface has been set in order to allow the full elastic recovery of the main SG, as shown in the Figure 2.21 (b).

The final step allowed full elastic recovery of parallel stent graft and the reaching of an equilibrium condition as shown in Figure 2.21 (b). Maintaining previous interactions, another

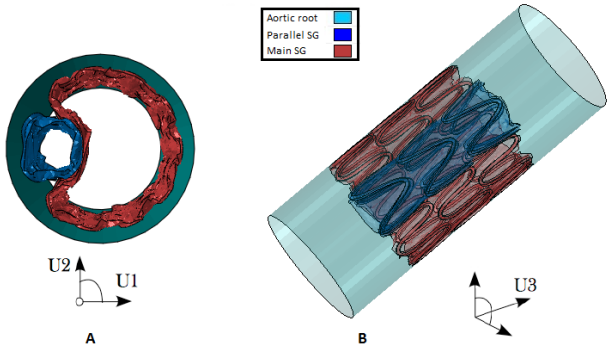

Figure 2.21: Simulation steps in Abaqus 6.14-2 (Simulia, Dassault Systems). Crimping phase (a); Deployment phase (b).

interaction between the artery model and the expanded parallel stent has been considered. The time period was set to 0.01 s.

In every steps, the artery segment model was considered a rigid body having an encastre constraint and all the rotational displacement boundary conditions were removed to allow only spatial displacements. All contacts were modeled using frictional tangential behavior, with the penalty coefficient set to 0.2 to avoid numerical instabilities in the simulation of the interactions and the fraction of characteristic surface dimension is 0.005. All steps are summarized in Table 2.3.

In the next section, simulation performance will be discussed.

Step	Description	BCs	Contacts	Time Step
1	**Parallel SG Crimping**	Parallel Catheter: radial displacement of -3.35 mm	Parallel Catheter - Parallel SG	0.01 sec
2	**Main SG Crimping**	Main Catheter: radial displacement of -10.75 mm	Parallel Catheter - Parallel SG Main Catheter - Main SG	0.01 sec
3	**Main SG Deployment**	Main Catheter: radial displacement of +10.75 mm	Parallel Catheter - Parallel SG Main Catheter - Main SG Aorta - Main SG Main SG - Parallel SG	0.01 sec
4	**Parallel SG Deployment**	Parallel Catheter: radial displacement of +3.35 mm	Parallel Catheter - Parallel SG Main Catheter - Main SG Aorta - Main SG Main SG - Parallel SG Aorta - Parallel SG	0.01 sec

Table 2.3: Steps summary for the chimney stenting intervention simulated.

2.2.9 Visualizzation module: Case-Patient simulation test

This study began with the study of the case-patient chimney configuration, that includes a main stent graft with a diameter of 28 mm and a parallel stent graft with a diameter of 9 mm. In the crimping and deployment stages, as shown in Figure 2.22 and 2.23, the diameters variation had been simulated. In the crimping phase, the stent grafts crossing profile decreased their inner diameter from 28 mm to 7 mm for main SG and from 9 mm to 2.8 mm for parallel SG. While, in the deployment phase the stent grafts resume their initial diameter. The final appearance configuration of chimney evar simulation is showed in Figure 2.24.

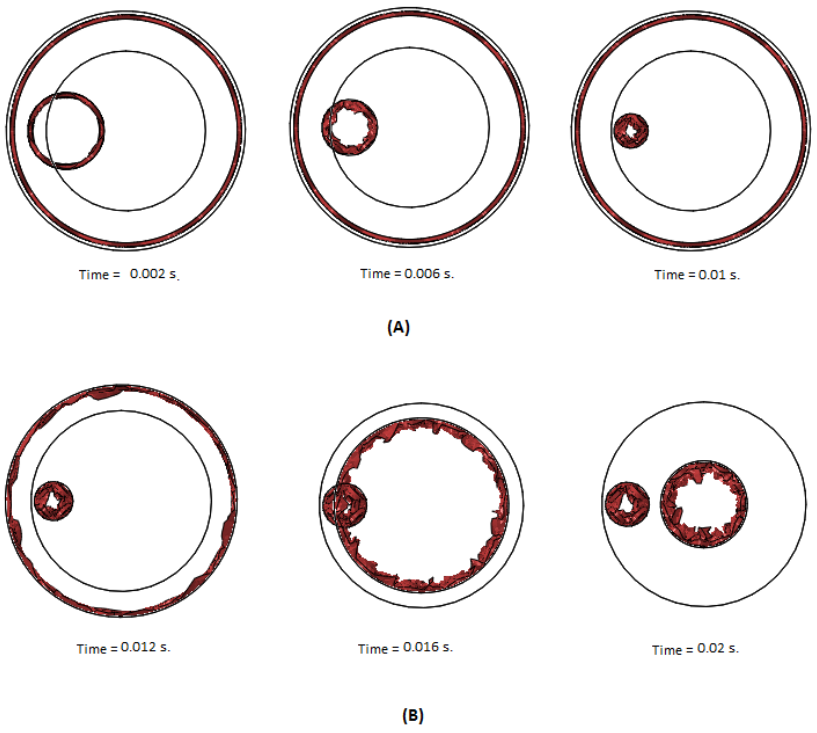

Figure 2.22: Stent grafts crimping in a straight abdominal artery segment. From the left to the right different steps of the stent grafts crimping are illustrated. Parallel stent graft (Model A)and main stent graft (Model B) crimping.

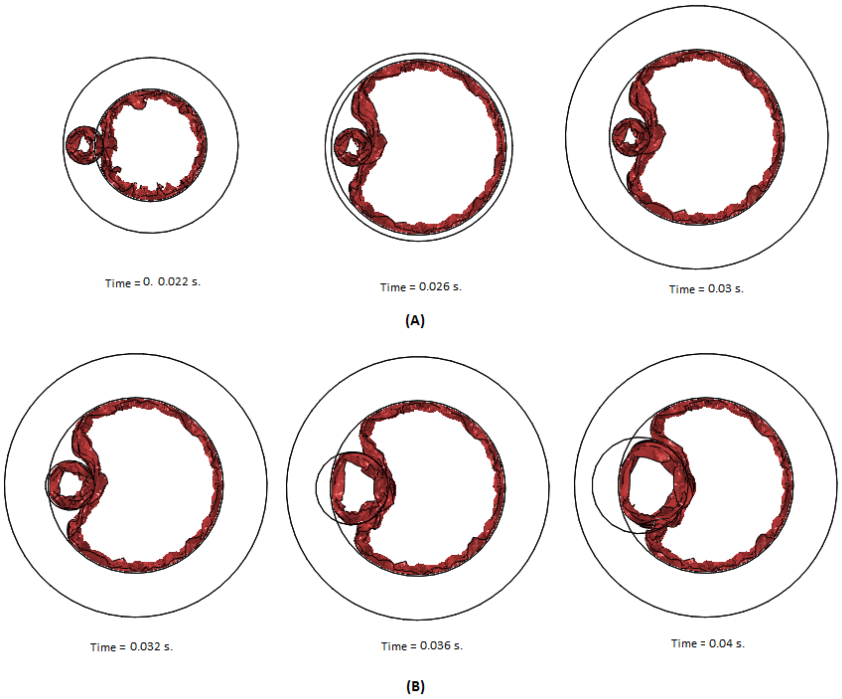

Figure 2.23: Stent grafts deployment in a straight abdominal artery segment. From the left to the right different steps of the stent grafts deployment are illustrated. Parallel stent graft (Model A) and main stent graft (Model B) deployment.

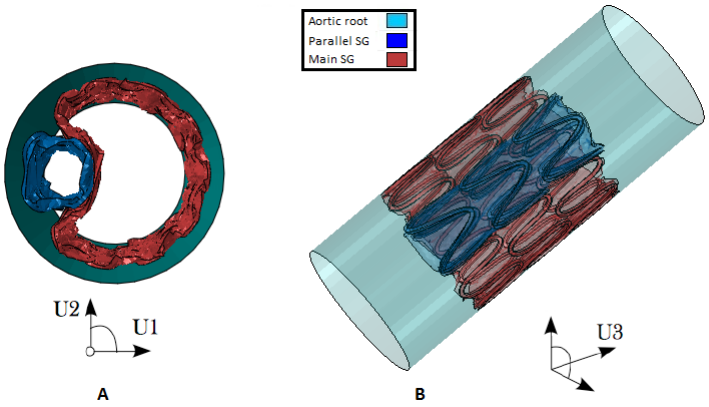

Figure 2.24: Final appearance configuration of the chimney's simulation. Front view (a) and isometric view (b).

Von Mises stress values

Von Mises stress and strain distribution appeared to be greatly symmetrical, having peak local stresses in the curved regions of the stent as shown in Figure 2.25. During crimping

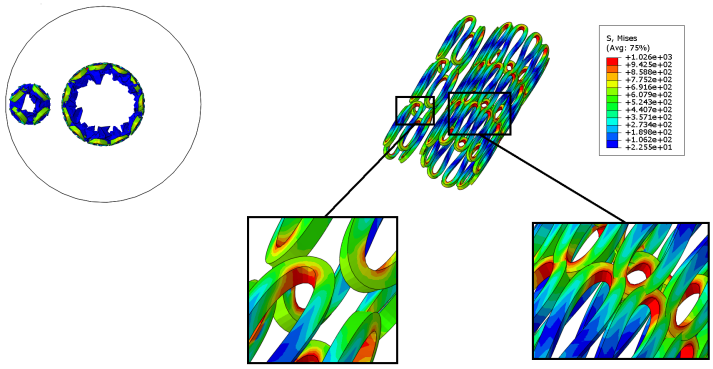

Figure 2.25: Von Mises stress values (MPa) during crimping phase. Stress values are calculated for maximum crimped state. From left to right, a front and a isometric views of the two stent grafts

phase, it is interesting to notice the condition of maximum stress: as a matter of fact, the maximum value can be found in the stent curve regions, where the maximum deformation is visible. On the other hand, the minimum value of "Von Mises" stess can be found in the the minimum stent deformation areas.

A high significantly difference between Vin Moses stress results was observed too during the deployment phase. As shown in Figure 2.26, the highest Von Mises stress value can be found in the contact zone between the two stents.

2.3 Gutter size measurement

Ch-EVAR involves placement of single or multiple stents (Chimney Grafts [CG]) that are parallel to the main aortic stent-graft. In this way, the proximal or distal sealing zones are extended while maintaining the side branch patency. Ch-EVAR appears to work mechanically well with good conformability between the main stent-graft, the chimney-graft, and the aortic wall. However, Endoleaks have occurred as a result of excessive gutter formation caused by inadequate stent-graft oversizing.

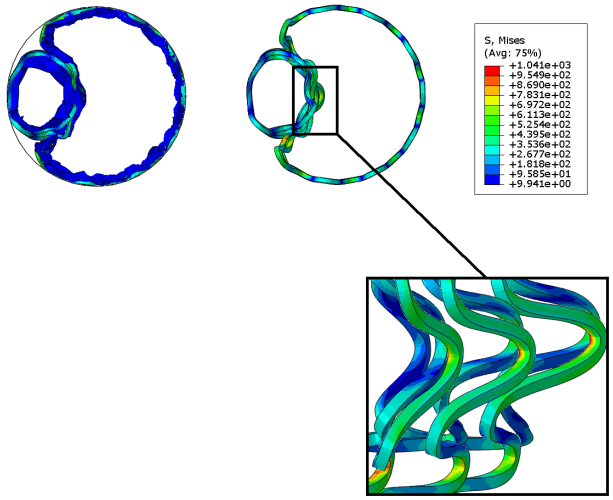

Figure 2.26: Von Mises stress values (MPa) during deployment phase. Stress values are calculated for maximum deployed state

2.3.1 Oversizing (OS)

Oversizing, is a common practice and is perceived to benefit a graft in conforming to tortuous vasculature and reducing the occurrence of migration by increasing the attachment strength thus that is called the "pullout force" [5]. Recent in vitro data showed that increasing oversizing significantly decreased gutter areas [29, 72].

Konstantinos P. et al., 2017 [73], showed in his study that stent-graft oversizing degree, by >30% compared with the diameter of the suprarenal aorta often leads to infolding of the endograft in the neck area and consequent type Ia endoleak. Endograft infolding and the lack of apposition of the endograft to the aortic wall in areas other than parallel stent location, creates new gutters or gaps, as shown in Figure 2.27 (a) . A solution could be the embolization using balloon dilation, with simultaneous inflation of balloons inserted in the main stent-graft and inside the chimney graft. Otherwise, minimal stent-graft oversizing leads to the formation of excessive gutters and endoleaks since the oversizing degree is <20%. This leaves insufficient excess stent-graft material to wrap around the chimney graft especially when placing multiple chimney grafts, as seen in Figure 2.27 (b). Generally, 20% to 30% oversizing degree is recommended for standard chimney grafts to minimize the gutters without excessive infolding.

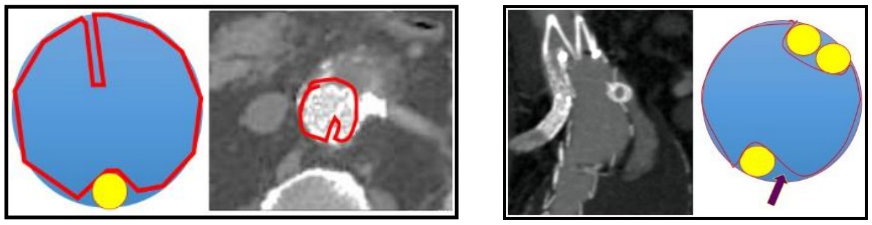

(a) *Infolding of the aortic stent-graft from excessive oversizing.*

(b) *Undersized aortic stent-graft.*

Figure 2.27: Stent-graft oversizing (a); undersizing (b). Image from Donas et al., 2017 [73].

Clinically, OS is calculated from the SG and abdominal aorta diameters using the following equation:

$$Oversizing\% = (\frac{D_{\text{SG}}}{D_{\text{Aorta}}} - 1) \tag{2.2}$$

To analyze oversizing in the chimney evar technique, the parallel SG (9 mm of diameter) is assembled with the main body(ies) inside artery segment (20 mm of diameter)
The purpose of this activity is to find the nonlinear relationship between the area of the gutter (gutter size) and stent graft oversizing degree. To achieve this goal, several chimney configurations have been created, by varying oversizing degree. From the Formula (2.2) and giving OS %, it is possible to calculate the main SG diameter. In all chimney configurations, both parallel stent and aorta models diameters were fixed. The main SG diameter sizes are shown in Table 2.4. This leads to the number N of elementary units in the unrolled

OS%	0%	5%	10%	15%	20%	30%	40%	50%
D_{SG} [mm]	20	21	22	23	24	26	28	30

Table 2.4: Main SG diameters calculated for each oversize value.

main stent, as mentioned in the second step of the stent graft reconstruction in the section 2.2. The results are shown in Table 2.5.

D_{SG} [mm]	20	21	22	23	24	26	28	30
N	8	8	9	9	10	10	11	12

Table 2.5: Elementary unit number in the unrolled main stent.

2.3.2 Measurement procedure

The method to determine gutter areas consists in identifying the countour of the area in the front plane, extrude it and then use the Masuren tool of ImageJ to obtain the precise area of the gutter.

ImageJ

ImageJ, [74] is a public domain Java image processing program inspired by NIH Image. It can display, edit, analyze, process, save and print 8-bit, 16-bit and 32-bit images. It can read many image formats including TIFF, GIF, JPEG, BMP, DICOM, FITS and "raw". It supports "stacks", a series of images that share a single window. It is multithreaded, so time-consuming operations such as image file reading can be performed in parallel with other operations.

It can calculate area and pixel value statistics of user-defined selected ROIs (Region Of

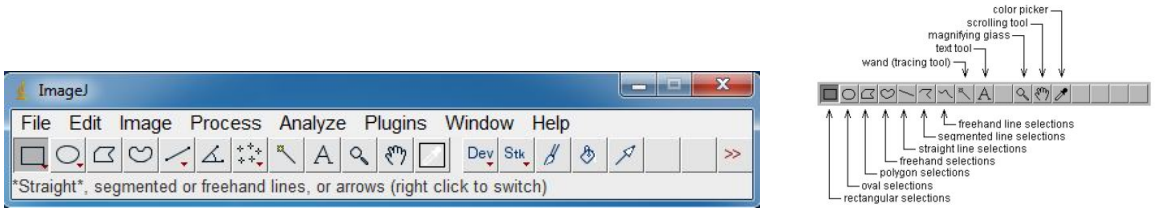

(a) *ImageJ main interface* (b) *ImageJ toolbar*

Figure 2.28: ImageJ

Interest). It can measure distances and angles. It can create density histograms and line profile plots. It supports standard image processing functions such as contrast manipulation, sharpening, smoothing, edge detection and median filtering. ImageJ toolbar, contains the tools to make selections, zooming and scrolling operations on images, changing colors.

Clicking on a particular tool displays its description in the status bar.

Using the view cuts tool of Abaqus 6.14-2 (Simulia, Dassault Systems) that allow to cut planar or deformable sections through a model to see its interior section [74], an "on cut" in the Z-plane has been performed in order to obtain an accurate mean value of gutter area, as shown in Figure 2.29. These cuts are made in the middle of each stent ring, along

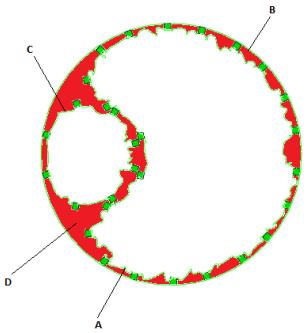

Figure 2.29: Different cross-sectional areas in chimney configuration. A: outer perimeter of the main graft, B: inner diameter of the aorta, C: outer perimeter of the chimney graft, and D: gutter area.

the z axis. The number of cutted sections is equal to the rings number of the stent, as shown in Figure 2.30.

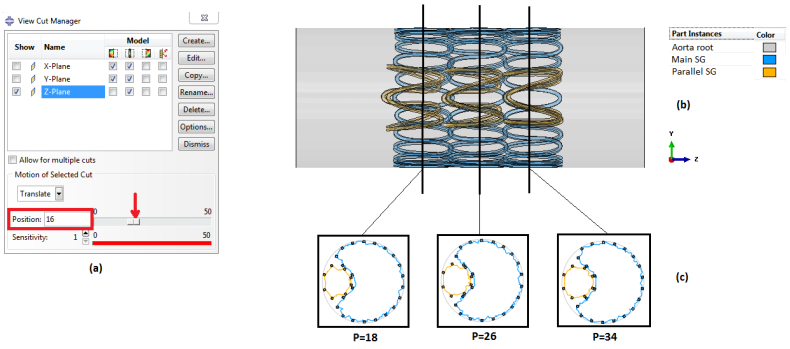

Figure 2.30: (a) View cut manager tool in Abaqus 6.14-2 (Simulia, Dassault Systems). By moving the cursor, we choose the cut section position. (b) Left view of 3 rings-stent model with the position of each section "cut on". (c) Front view of the cutted sections.

ROI identification and gutter area calcolation

Once cutted sections had been identified with Abaqus 6.14-2 (Simulia, Dassault Systems) tool, the screenshots can be imported in ImageJ, the two regions of interest can be selected (areas of main and parallel SG) and added to the ROI list, as shown in Figure 2.31. Measurements of each setup were used to calculate gutter size and main graft compression.

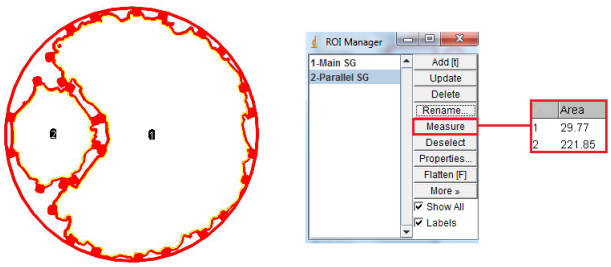

Figure 2.31: Gutter area mean value calculation with ImageJ ROI manager tool.

Absolute gutter size was calculated by subtracting the areas of the CG and main graft from the aortic areas, as shown in the formula (2.3). Main graft compression was calculated by dividing the internal area of the main graft (compressed area, in mm^2) from the internal area of the same main stent without endograft compression (maximum stent area, in mm^2), as shown in the formula (2.4).

$$Gutter\ area = Aorta\ area - (Main\ SG\ area - Parallel\ SG\ area) \tag{2.3}$$

$$Main\ graft\ compression\ \% = \frac{deformed\ Main\ SG\ area}{undeformed\ Main\ SG\ area} \tag{2.4}$$

For each cross section, the gutter area has been calculated and then the final average value of the whole model has been discovered.

2.3.3 Gutter size measurement of 3 rings-stent and 11-rings-stent models

As already mentioned in the previous section, reducing simulation time is important when it is necessary to perform a fairly high number of simulations. It is interesting to evaluate

the chimney configuration gutter size in two different chimney configurations: the first one includes a 3-ring stent grafts, while the other one includes a 11 ring-stent grafts, as we can see in Figure 2.32.

The gutter size in the first configuration is equal to 60.74 mm^2, which corresponds to

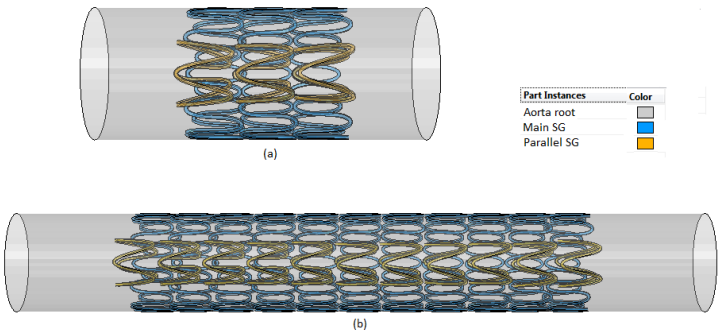

Figure 2.32: Abaqus 6.14-2 (Simulia, Dassault Systems) two chimney configurations. (a) 3-ring stents first configuration; (b) 11-ring stents second configuration.

19% of the total aorta area (311 mm^2), while in the other configuration, the gutter size is equal to 56.08 mm^2, which corresponds to 18% of the total aorta area. The details are presented in Figure 2.33 and 2.34:

Under the same analysis conditions (materials, mesh, interaction and boundary condi-

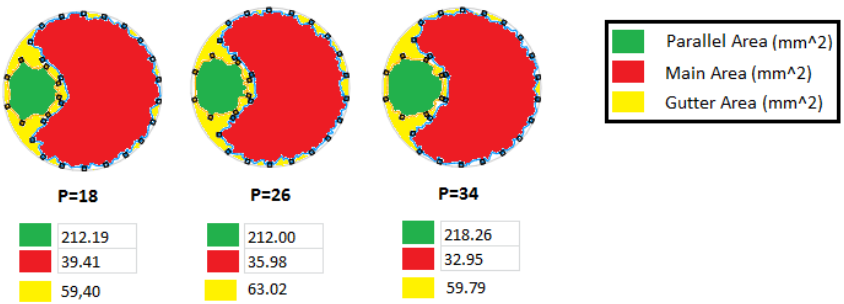

Figure 2.33: Gutter size in the 3 rings-stent configuration.

tions) both configurations can be used in the same way to have the same results. For this reason, it has been decided to use the 3 rings-stent grafts configuration, having fewer nodes and elements, and consequently less simulation time.

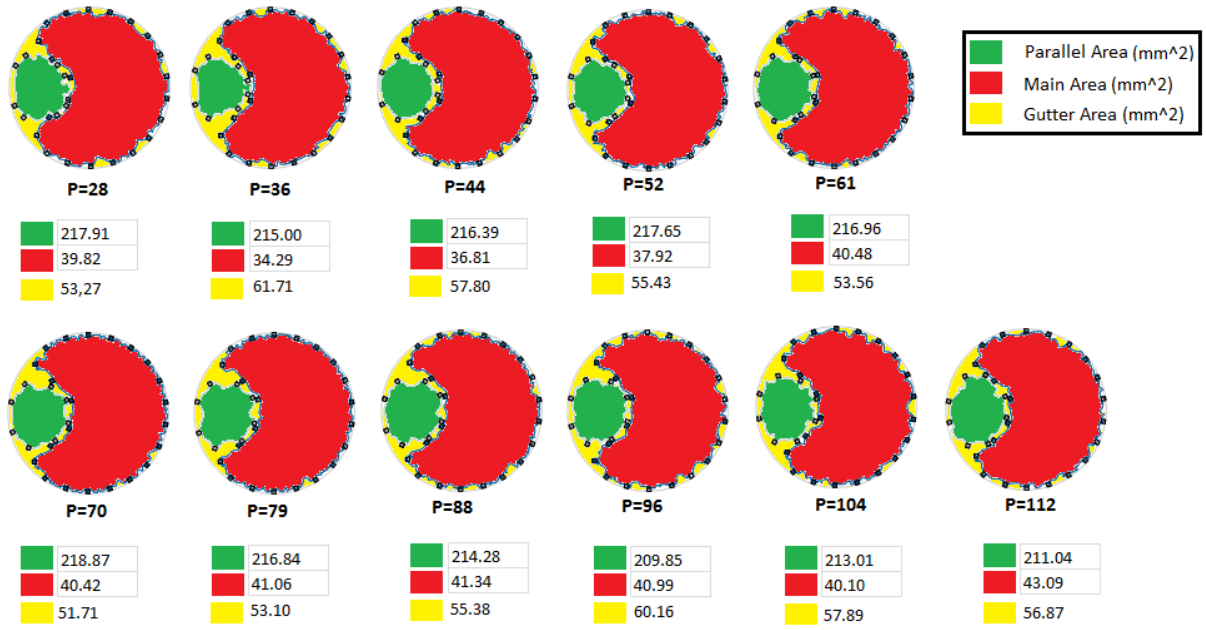

Figure 2.34: Gutter size in the 11 rings-stent configuration.

2.3.4 Gutter size in literature

Several studies in literature analayzed the endoleak type Ia and the relationship between gutter area, stent graft oversizing.

Valério, André Miguel dos Santos Almeida et al. [5], in his thesis work in witch analyzed 15 differents CG configuration with different combinations of main and parallel SG's, found out that the chimney grafts are well conformed in configurations with less then three parallel stents and the configurations in which the disposition of the CG's are closer, have small gutter areas. Furthermore, the configurations with less number of CG's implanted have small gutter areas and a low risk of endoleaks. He concludes his study saying that the CG configuration with the lowest gutter area is the simple one (one main graft and one parallel stent).

Nevertheless, as de Bruin et al.[62] prove in his experimental study, by testing a single CG configuration (one main body and one parallel stent) with many combinations of commercial endograft models such as self-expanding and balloon-expandable chimney grafts and different seal zones and diameters can represent very divergent results.

Moving from such considerations, in the present study, 7 various configurations with a single CG configuration (one main graft and one parallel stent) were tested, applying seven endograft-oversizing degrees (0%, 5%, 10%, 15%, 20%, 35% and 40%) with the aim to calculate the gutter area.

2.4 Reconstruction of Chimney technique configurations

Following the same procedure used in the previous section for the stent graft reconstruction, different configurations for each stent graft oversizing case have been created in Abaqus 6.14-2 (Simulia, Dassault Systems). The details of the reconstruction steps are presented in Figure 2.35. As was done in the previous section, giving FEA set-up (material properties, interactions and contacts between parts, steps and boundary conditions) in every configuration, the simulation can now start.

In the next chapter, the obtained gutter size results of each chimney configuration will be discussed.

OS %	R_SG (mm)	N_Waves	Planar Model	Rolled Ring	Rolled Model	Chimney Configuration
0%	10	8				
5%	10.5	8				
10%	11	9				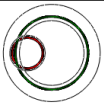
15%	11.5	9			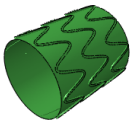	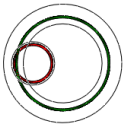
20%	12	10			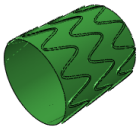	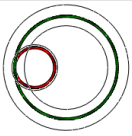
40%	14	11			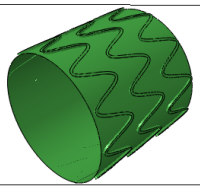	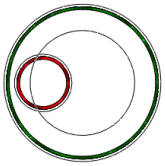

Figure 2.35: Abaqus reconstruction steps. For each SG oversizing case, is illustrated (from left to right) the corresponding radius of the main SG; number of elementary units in the unrolled main stent; planar and cylindrical geometrical model of single ring; cylindrical geometrical model of main 3 ring-stent graft and finally the assembled (main SG in green; parallel SG in red; main and parallel catheters and the aorta segment are modeled as a black circle).

Chapter 3

Chimney-Evar Technique Simulation: Results

3.1 Others simulations tests results

For each chimney configuration constructed, average values of gutter areas and main compression ratio are calculated. Below, measurment tests results are shown in details.

3.1.1 Configuration 1: Oversizing=0%, Main stent diameter=20 mm

Figure 3.1 shows the chimney configuration with oversizing= 0% and it includes 2 SGs: the parallel SG (diameter 9mm) and the main SG, whose diameter size (20mm) is equal to the aortic model in which both stents are assembled. Model A shows the initial no-deformation configuration phase, model B shows the phase in which both SG are completely crimped, while model C shows the deployment phase.

Gutter size and main graft compression measurements

As shown in Figure 3.1 (model C), three areas of interest were measured: total aortic area (outer edge of the aorta including the main device and the chimneys; (1) in the Figure),

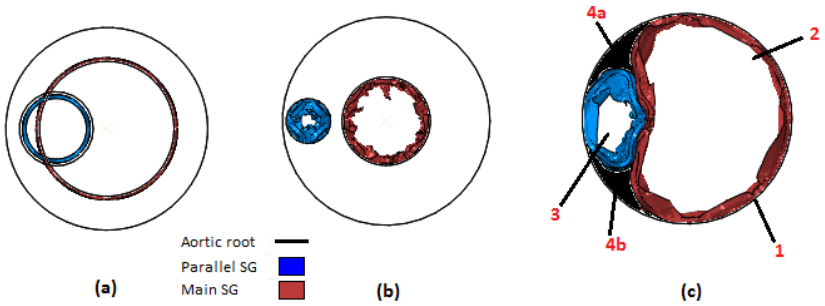

Figure 3.1: 0% endograft oversizing configuration. Undeformed model (Model a); Final apperance of deformed model (Model b). 1, Total aortic area; 2, main graft area; 3, chimney area; 4a and 4b, gutter area.

main device area (outer edge of the main device; (2) in the Figure) and chimney area (outer edge of the chimney device; (3) in the Figure). The residual gutter area was calculated by subtracting the main device and chimney area from the total aortic area (4a e 4b in the Figure). The areas of interest were measured at the level of each ring in the stents as shown in Figure 3.2 and for each section, gutter area was calcluated. The final gutter size value of the chimney configuration was calcolated as the mean of the three values. The final outcome of interest was the gutter area percentage of the total aortic area (proportional gutter area).

The mean gutter area in this configuration is equal to 70.74 mm^2 and the proportional gutter area is 22.74 % of the total aortic area.

Furthermore, it has been possible to calculate the value of the main graft compression, by dividing the main graft's deformed area by the no-deformed stent's area. In order to find the value of the deformed stent area, the main SG's deformed area average value showed in figure 3.2 has been calculated, which is 212.68 mm^2, while the main SG's undeformed area value is equal to 314.16 mm^2. The final result of main graft compression is 67.70%.

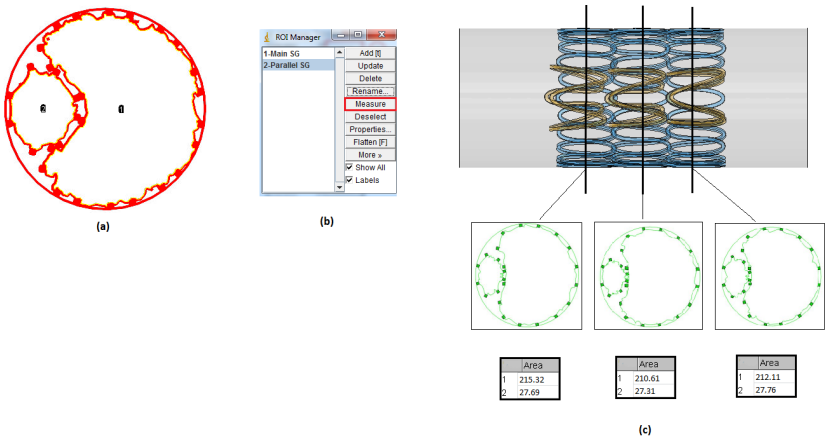

Figure 3.2: 0% endograft oversizing measurments. The two ROI of the cross section (Model a); The ROI manager tool of ImageJ(Model b). A Z-plane view of the chimney configuration; The cross sections relative for every ring and the respective areas measured with ImageJ.

Von Mises stress

Figure 3.3 shows the Von Mises stress value (MPa) when deployment phase is completed. As shown in Figure, the maximum stress value is equal to 959.3 MPa and is observed in the stent's curved regions with a high degree of deformation, precisely in the contact region between the two stents. The minimum Von Mises stress value is equal to $2.766e^{-}02$ MPa

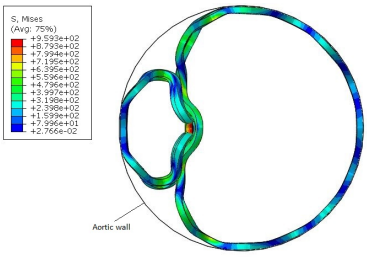

Figure 3.3: Von Mises Stress value (MPa) in the 0% endograft oversizing configuration.

and is located in the regions of contact between stent grafts and arotic wall, where the deformation is minimal.

3.1.2 Configuration 2: Oversizing=5%, Main stent diameter=21 mm

In this case, the main SG diameter is one millimeter larger than the aortic diameter. The areas of interest were measured at the level of each ring in the stents. The mean gutter area in this configuration is equal to 67.86 mm^2 and the proportional gutter area is 21.82 % of the total aortic area.
The deformed stent area value is equal to 219.53 mm^2, while the maximum value of the area is equal to 346.36 mm^2. The final graft compression value is equal to 63.38%.

3.1.3 Configuration 3: Oversizing=10%, Main stent diameter=22 mm

In this case, the main SG diameter is two millimeter larger than the aortic diameter. The areas of interest were measured at the level of each ring in the stents. The mean gutter area in this configuration is equal to 67.98 mm^2 and the proportional gutter area is 21.85 % of the total aortic area.
The deformed stent area value is equal to 208.68 mm^2, while the maximum value of the area is equal to 380.13 mm^2. The final graft compression value is equal to 54.90%.

3.1.4 Configuration 4: Oversizing=15%, Main stent diameter=23 mm

In this case, the main SG diameter is three millimeters larger than the aortic diameter. The areas of interest were measured at the level of each ring in the stents. The mean gutter area in this configuration is equal to 62.39 mm^2 and the proportional gutter area is 20.06 % of the total aortic area.
The deformed stent area value is equal to 211.60 mm^2, while the maximum value of the area is equal to 415.47 mm^2. The final graft compression value is equal to 50.93%.

3.1.5 Configuration 5: Oversizing=20%, Main stent diameter=24 mm

In this case, the main SG diameter is four millimeters larger than the aortic diameter. The areas of interest were measured at the level of each ring in the stents. The mean gutter area in this configuration is equal to 62.64 mm^2 and the proportional gutter area is 20.14 % of the total aortic area.
The deformed stent area value is equal to 205.50 mm^2, while the maximum value of the area is equal to 452.39 mm^2. The final graft compression value is equal to 45.42%.

3.1.6 Configuration 6: Oversizing=35%, Main stent diameter=27 mm

In this case, the main SG diameter is seven millimeters larger than the aortic diameter. The areas of interest were measured at the level of each ring in the stents. The mean gutter area in this configuration is equal to 63.21 mm^2 and the proportional gutter area is 20.33 % of the total aortic area.
The deformed stent area value is equal to 208 mm^2, while the maximum value of the area is equal to 572.55 mm^2. The final graft compression value is equal to 36.32%.

3.1.7 Configuration 7: Oversizing=40%, Main stent diameter=28 mm

In this case, the main SG diameter is eight millimeters larger than the aortic diameter. The areas of interest were measured at the level of each ring in the stents. The mean gutter area in this configuration is equal to 60.74 mm^2 and the proportional gutter area is 19.53 % of the total aortic area.
The deformed stent area value is equal to 214.15 mm^2, while the maximum value of the area is equal to 615.75 mm^2. The final graft compression value is equal to 34.77%.

3.1.8 Configuration 8: Oversizing=50%, Main stent diameter=30 mm

In this case, the main SG diameter is ten millimeters larger than the aortic diameter. The areas of interest were measured at the level of each ring in the stents. The mean gutter area in this configuration is equal to 59.12 mm^2 and the proportional gutter area is 19 % of the total aortic area.
The deformed stent area value is equal to 207.72 mm^2, while the maximum value of the area is equal to 706.86 mm^2. The final graft compression value is equal to 29.38%.

3.2 General discussion

The results of the simulation tests are grouped in the table 3.1.

As it can be noticed, the highest gutter size is present when no oversize is applied or

Oversizing %	**Main SG diameter** (mm)	**Gutter area** (mm^2)	**Proportional gutter size** %	**Main SG compression** %
0	20	70.74	22.74	67.70
5	21	67.86	21.82	63.38
10	22	67.98	21.85	54.90
15	23	62.39	20.06	50.93
20	24	62.64	20.14	45.42
35	27	63.21	20.33	36.32
40	28	60.74	19.53	34.77
50	30	59.12	19.00	29.38

Table 3.1: Main SG diameters calculated for each oversize value.

when the inner diameter of the main stent graft is equal to the inner diameter of the aortic vessel. As the inner diameter of the main stent graft increases, the oversizing consequently increases and the area of the gutter inside the aortic segment decreases. As shown in the Figure 3.4, the gutter size decreases rapidly (around 13%) when oversizing degree increases from 0% to 15%, which is equivalent to an increase of only 3mm in main SG diameter size.

Increasing the oversizing from 15% to 50% (which correspond to an increase of 7mm of the

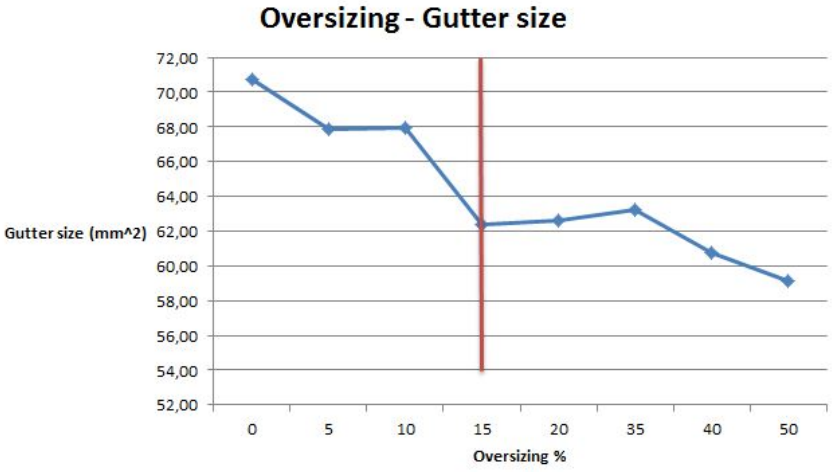

Figure 3.4: Line Graph that plots changes in gutter size (mm^2) over oversizing value (%)

main SG diameter size), the Gutter size decrease only by 5%.

Furthermore, the level of stress increases when the oversizing increase. As shown in figure 3.5, the deformation in the stent bend zone with an oversizing of 50% (B) is much bigger compared to an oversizing of 15% (A). Nevertheless, a high level of stress, especially in the

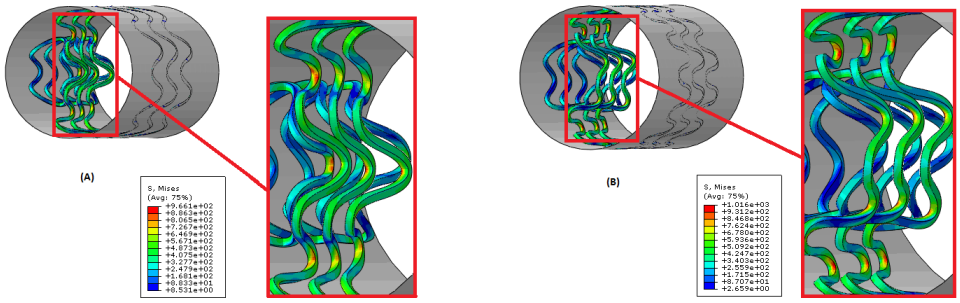

Figure 3.5: Von Mises Stress distribution (MPa) in chimney configuration during deployment phase. 15% oversizing degree configuration (A); 50% oversizing degree configuration (B)

stent folding area, could lead to a break of the device, this is why a compromise had to be made between the oversizing and Gutter size: from this first analysis, the best oversize rate for an optimal chimney configuration is 15%.

The second analysis deals with the variation of the main compression with respect to the oversizing. The figure 3.6 shows the variation of the main graft compression in comparison to oversizing. A linear behavior is noticed in this case, where the main compression decreases when the oversizing increase. The minimum value can be found in the main SG

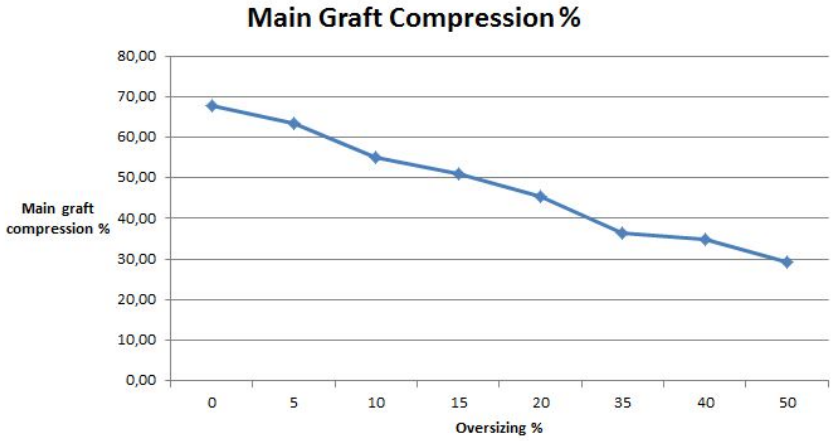

Figure 3.6: Line Graph that plots changes in main stent compression (%) over oversizing value (%)

having oversizing degree 50%, which corresponds to the configuration with the minimum gutter size. Furthermore, all configurations with oversizing $\leq$15% have main graft compression above 50% witch is an acceptable value. This second study confirms that 15% of oversizing is the best rate.

While analyzing the values of von Mises stress (MPa) in the deformed Configuration, it has been noticed that the points of highest stress are those in which the stents are in contact, and, in particular, where it has reached the highest deformation. The results show that the deformation of the stent is not uniform but depends on the stent features as its geometry, model and configuration inside aortic wall.

The table 3.2 shows a summary of the maximum and the minimum Von Mises stress value for different oversizing.

As shown in Figure 3.28, the maximum stress value is obtained with oversizing degree of

Oversizing %	**Maximum Von Mises stress value** (MPa)	**Minimum Von Mises stress value** (MPa)
0	$9.593e^{+}02$	$2.766e^{-}02$
5	$9.539e^{+}02$	$3.350e^{-}02$
10	$9.585e^{+}02$	$3.348e^{-}02$
15	$9.661e^{+}02$	$2.979e^{-}02$
20	$1.001e^{+}03$	$1.930e^{-}02$
35	$1.024e^{+}03$	$4.269e^{+}00$
40	$1.041e^{+}03$	$1.747e^{-}02$
50	$1.016e^{+}03$	$2.659e^{+}00$

Table 3.2: Maximum and minimum Von Mises stress value of the various configurations.

40% (1.041 GPa), and this confirm again the reason of choosing 15% of oversizing as the best rate of an optimal chimney configuration.

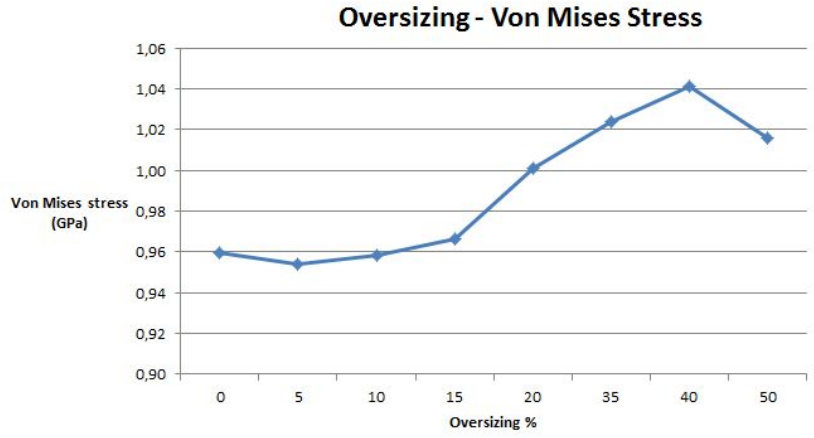

Figure 3.7: Line Graph that plots changes in Von Mises stress (GPa) over oversizing value (%)

Chapter 4

Physician Modified Endovascular Graft (PMEG)

Endovascular treatment of aortic pathology has become standard practice for the treatment of patients with infrarenal aortic aneurysms who are anatomically suitable for repair. But due to short proximal necks and juxtarenal aneurysms, the majority of patients who are not eligible for endovascular repair. Fenestrated technology (Figure 4.1) has been used to extend the applicability of endovascular techniques to more patients who would be deemed ineligible for standard infrarenal bifurcated repair [75, 26]. In some centres, this treatment [76] is considered one of the first options. It is expensive and it takes precise planning: it requires from four to six weeks for it to be made and delivered and it has very specific limitations in terms of what it be made or not. Dr. Benjamin W. Starnes, stated [26] strict anatomic requirements, high costs, and long manufacturing delays limit the applicability of the technique.

This is PMEG, as Starnes stated, holding an endovascular stent graft, a tube of fabric supported by a metal mesh that is close to the width of a garden hose. PMEG is an acronym for Physician Modified Endovascular Graft, a procedure that Starnes created it first and himself by tinkering with expired commercially devices [77]. The physician modification of a currently FDA-approved off-the-shelf aortic stent graft, as seen in Figure 2.1 (Model

C), a ready available alternative to a fenestrated stent graft when there is no time to manufacture a fenestrated device. This technique helps to preserve branch vessels when used in the treatment of patients with asymptomatic, symptomatic, or ruptured juxtarenal aortic aneurysms with no other options for repair and when [75, 26, 76, 78, 79, 80].

Device preparation. The device was chosen according to standard instructions for use

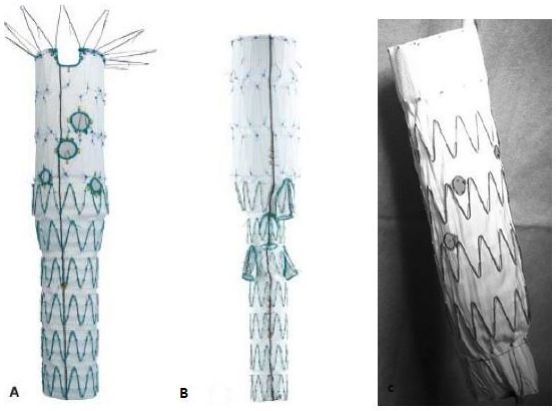

Figure 4.1: **A**, Fenestrated stent graft. **B**, Multi-branched stent graft. **C**, Physician Modified Endovascular Graft.

sizing guidelines, and a routine aortic oversizing of 10% to 15% for the main body graft was utilized. A sterile marking pen was used to mark the location of the fenestrations based on both length and clock face measurements that had been previously determined with reconstruction imaging software [76, 78, 79]. Fenestrations position, has been used as a standardized method. The middle of the SMA was used as the "O" point (reference point, clock position: 12 o'clock). Distances from the middle of the SMA to the middle of each target vessel, to the start of aneurysm and to the intended proximal position of the modified TX2 device were determined on centerline reconstructions [80].

By modifying a standard aortic stent graft as shown in Figure 4.2, the physician creates two to three holes (fenestrations) in the upper portion of the graft based on measurements made from the patient's CT scan. This allows the graft to be located above the renal arteries without blocking blood flow and enables an adequate sealing zone. The obtained MEG device is ready to be implanted in emerging cases. It takes about 2-3 hours to plan it and one hour to make the fenestrations but it depends on the skills of the physician,

who must obtain precise measurements and design the graft [26].

Technical success is defined as successful delivery and deployment of the PMEG with

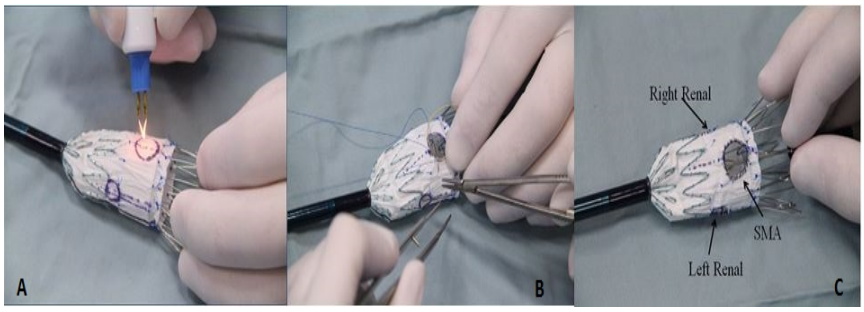

Figure 4.2: **A**, Starnes use of an ophthalmic Bovie cautery device to create the fenestrations. **B**, Gold, 15-mm Amplatz Gooseneck Snares were then used to reinforce all fenestrations. **C**, A typical physician-modified endovascular graft (PMEG). Fenestrations for the superior mesenteric artery (SMA) (struts present) and left and right renal arteries (strut-free) were created for this particular patient. Reproduced from Starnes et.al J Vasc Surg 2012[26]

preservation of those branch vessels intended to be preserved, freedom from type I and III endoleaks at 12 months, freedom from stent graft migration >10 mm at 12 months, freedom from aortic aneurysm sac enlargement >5 mm at 12 months, and freedom from aortic aneurysm rupture and conversion to open repair through 12 months [81].
Physicians who modified the endovascular grafts are largely dependent on the skills of the physician, who must obtain precise measurements and design the graft [26]. To Remove the possibility for human errors, Starnes found the solution by creating grafts with precise fenestrations using 3D printed replicas of each patient's aortic anatomy that is going to fit like a glove, as shown in Figure 4.3.

4.1 PMEG using 3D Printing

Three-dimensional (3D) printing is a manufacturing process in which an object is created by specialist printers designed to print in additive layers to create a 3D object. An object is created by sequentially printing layer upon layer guided by a computer file [83]. Manufacture of anatomically accurate, patient-specific, small-caliber arterial models was

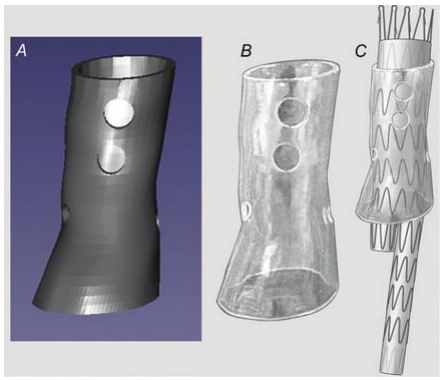

Figure 4.3: Three-dimensional (3D)-printed fenestration template. **A**, Computer model of the template. **B**, Solid printed model of the template created using a stereolithography 3D printer with clear resin. **C**, An endovascular graft inserted in the template. A printed from [82]

attempted using data from a patient's CT scan (Figure 4.4), free open-source software, and low-cost Internet 3D printing services [66].

The first step in creating an anatomical model for general and vascular surgery requires an important preliminary part in the processing of medical images. The phisician provides the patient's TAC or Magnetic Resonance imaging, along with information about the anatomical parts of his interest; the images are then processed to rebuild a virtual anatomical model, then sent to the 3D printer [68].

The final 3D model comes out through a series of steps that will be described in the following paragraphs: from the tac image in DICOM format, to the segmentation via ITK SNAP software, to the extraction of branches via VMTK software, which carries a virtual model in STL format, further processed before it arrives to true 3D printing.

Three-dimensional (3D) printed vascular models have been manufactured for the heart and aorta and used preoperatively for planning and testing prior to surgery, using of rapid prototyping to print a 3D replica of an aneurysm with complex neck morphology as an aid to decision making and device delivery [65].

Physician-modified endovascular grafts, with fenestrations added to accommodate major branch vessels, provide a useful means for endovascular treatment of abdominal aortic aneurysms that are adjacent to the renal arteries [82].

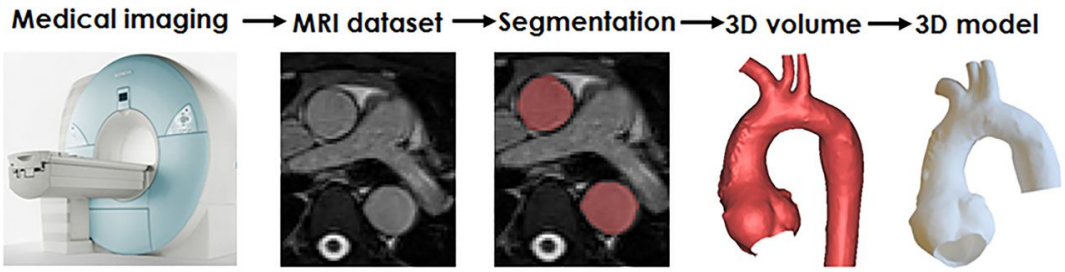

Figure 4.4: Illustrating the steps for manufacturing a three-dimensional (3D) patient-specific model, the example showing a patient with an enlarged Marfan-like aortic root [84].

Leotta, Daniel F., and Benjamin W. Starnes, in their study "Custom Fenestration Templates for Endovascular Repair of Juxtarenal Aortic Aneurysms" used a three-dimensional printer instead of manual measurements of vessel origin locations from computed tomography images, which requires time and can lead to errors in the positions of the fenestrations. This 3D method, helps to create a template (a clear rigid sleeve), that replicates the patient's aorta and includes holes placed precisely at the locations of the branch vessels. The sleeve is slipped over the graft, the locations of the openings are marked with a pen, and the fenestrations are created after the sleeve is removed [82], as shown in Figure 4.5. Without the template, fenestration planning time to modify grafts varies with experience and case complexity [85].

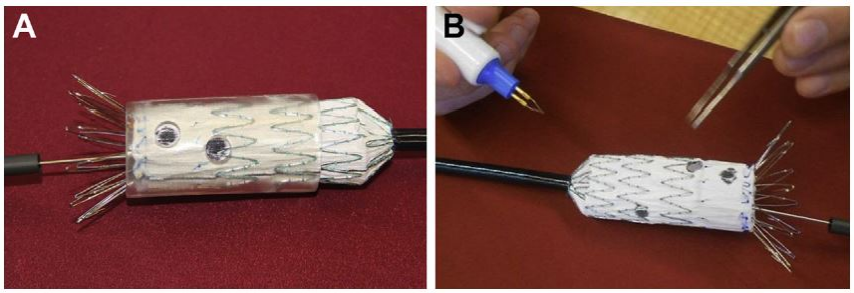

Figure 4.5: Graft fenestration and deployment for validation. **A**, An unsheathed graft is inserted in the fenestration template and the branch vessel origins are marked with a pen. **B**, Fenestrations are cut with an electrocautery device after removal of the template.

4.2 Medical imaging analysis and processing

In the following paragraph, the adopted work flow is shown, highlighting the process which generated the computational domain from medial images regarding the specific clinical case under investigations.

The process from images to computational domain to represent realistic vascular geometries involves several separate steps shows in the figure 4.6. Sets of images are first acquired using one of the clinically available imaging techniques as like CT(Computer Tomography) or MRI(Magnetic Resonance Image).

Computed Tomography(CT), is based on computer-processed combination of many X-

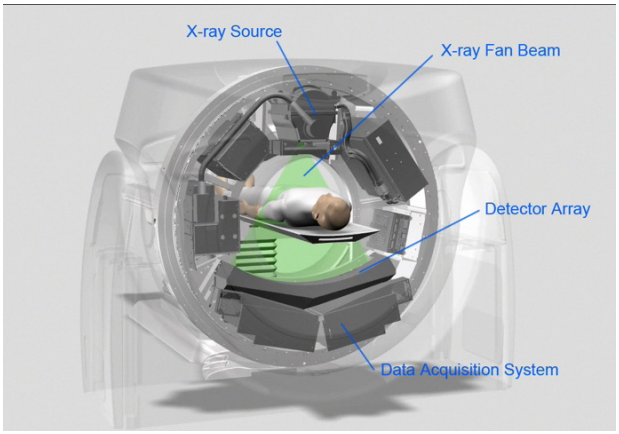

Figure 4.6: Computerized Tomography (CT) Scan

ray images taken from different angles to produce cross-sectional images of specific areas of a scanned object. The CT captures images by detecting the attenuation that ionizing radiation undergo when they pass through body tissues. The level of attenuation depends on the absorption capacity of the tissues. Thus we get the image that represents the information of attenuation expressed in HU (Hounseld unit), according to which the darker values characterize tissues and areas of low density, as the air and soft tissues, while lighter values characterize high density tissues such as bone or areas with the presence of calcium. In this case, a real clinical case has been investigated. Computational fluid dynamics (CFD) analysis has been performed on patient-specific vasular model derived from medical image, which has been captured by CT witouth contrast.

4.2.1 Patient-specific case

This study is based on a patient specific simulation. The patient studied is a 42-year-old male, presented with a 5.2 mm toraco abdominal aortic aneurysm at the level of the chest.

Images set-up

Post-operative CT images have been collected for research purposes as shown in Figure 4.7, thanks to the Fondazione IRCCS Policlinico San Matteo-DEA (Pavia) and especially to the vascular surgery department. The images were acquired with equipment CT with TOSHIBA Definition, with bolus of contrast agent iomeron. DICOM CT images had been used from patient with the following characteristics:

- Dimensions: 512 x 512 x 600;
- Number of images: 600;
- Voxel spacing: 0.77 x 0.77 x 0.799927mm;
- Orientation: RAI;
- Modality: CT;
- Scan option: HELICAL CT;
- Slice Thickness: 1.0mm;

The goal is to create a threedimensional (3D) printed rigid template, by using a patient's CT image data. This model based on patient's aortic anatomy provides fenestrations in place of each branch vessel in the abdominal aortic aneurysm (AAA), Celiac artery; Superior mesenteric artery; Left renal artery and Right renal artery. The openings has been obtained through a procedure of Centerlines identification and branches clipping by using vmtk 3D Slicer, a geometric analysis software and surface data processing of 3D blood vessel models. To get to the final 3D model, it's essential to go through a series of steps that

will be described in the following paragraphs: from the CT images in DICOM format, to segmentation via ITK-Snap, a special software to allow isolation of the anatomical regions of interest, to clipping via vmtk software which carries a STL format virtual model, further processed with paraview before coming to the actual 3D printing. The workflow of the whole process is described in Figure 4.7.

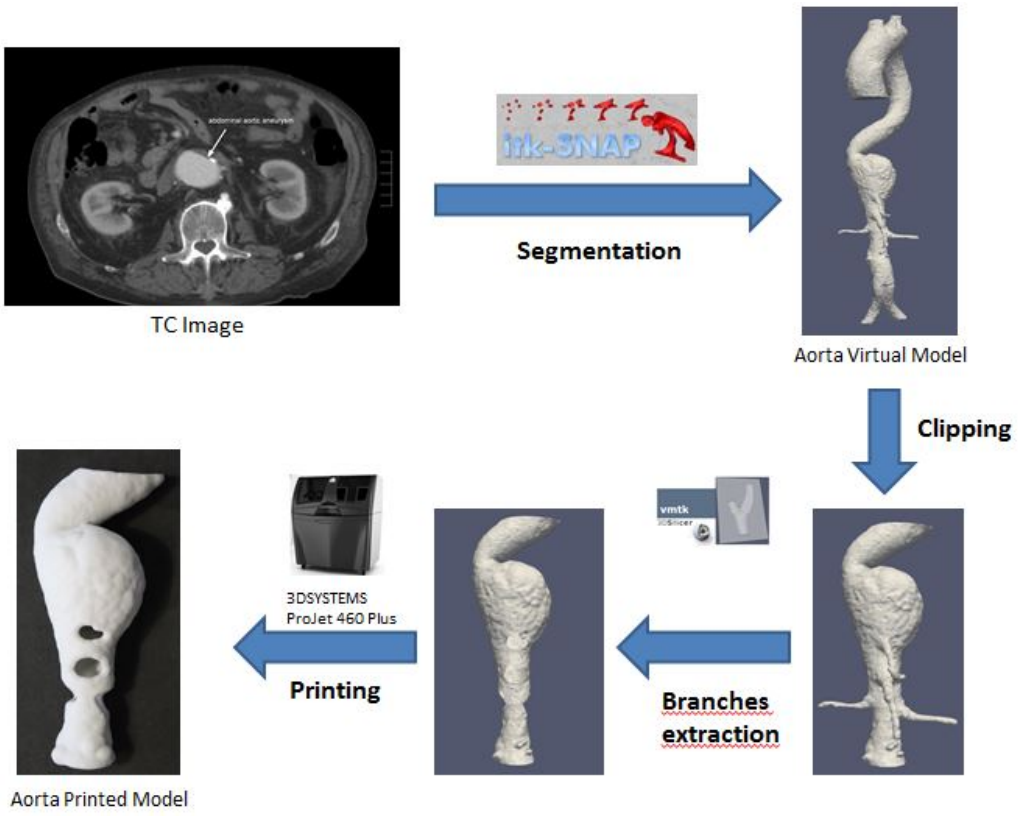

Figure 4.7: Workflow used in this chapter. From images acquisition to Aorta Printed Model using various softwares and techniques.

DICOM image format

Digital Imaging and Communications in Medicine (DICOM) is a standard developed by ACR (American College of Radiology) and NEMA (National Electrical Manufacturer's Association) for handling, storing, printing, and transmitting information in medical imaging. DICOM format (an example shown in Figure 4.8)combines visual information of medical exams, such as CT or MRI scans, to other technical information about the patient, the exam, the employed machine and its settings. This format allows hospitals to communicate

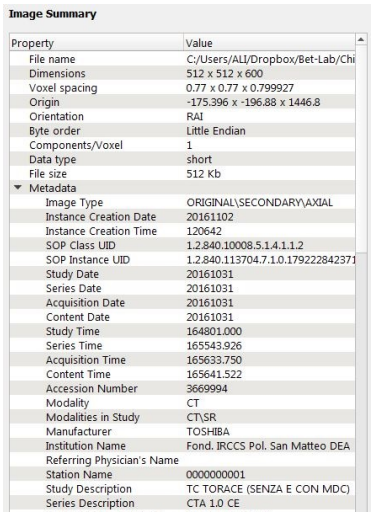

Figure 4.8: DICOM CT images characteristics

easily among each other, exchanging exams performed on a patient and other information. The Dicom files contain both alphanumeric information (the name of the patient, date of birth, diagnosis, the name of the doctor) and one or more images compressed or in raw format.

4.2.2 Image segmentation

Segmentation [86] is the extraction of an area of interest from an image volume. The segmentation result is the computational domain of numerical simulations, it plays a vital role in many biomedical imaging applications: the quantifications of tissue volumes, diagnosis, localization of pathology, study of anatomical structure, treatment planning, partial vol-

ume correction of functional imaging data, and computer-integrated surgery. The goal of segmentation is to simplify and/or change the representation of an image into something more meaningful and easier to analyse. The segmentation procedures can be divided in the following categories:

- **Manual segmentation:** plan to manually draw the outline of the image portion to assign a specific label.
- **Automatic segmentation:** automatically divide the image into regions that show similar characteristics to them and differ from each other for the same characteristics.
- **Semi-automatic segmentation:** represent a compromise between the two previous techniques. This approach requires a modest interaction with the user, which is required to set some parameters of the algorithm. In this case, it is necessary to use an automatic segmentation for preliminary steps, to extract the vessel part in which the stent is. After that, by using the manual segmentation, it is possible to separate and segment the endograft, without vessel.

In this work, for the semi-automatic segmentation, ITK-Snap software, described below has been used:[87].

ITK-Snap software

ITK-Snap (http://www.itksnap.org) is an open source software, used to segment structures in 3D medical images with three-dimensional content such as TAC or RM. It can be used in two different modes: manual segmentation and semi-automatic segmentation. It is possible to perform manual segmentation of images by a contours tracking tool of the regions to be segmented. The input of this program is a DICOM series, which are organized into cross-sections according to the three anatomical planes: Sagittal, Frontal and Axial; and it is visualized in gray scale, slice by slice. Once the data is loaded, the image of the whole volume that represents the information of attenuation expressed in HU (Hounsfield units) is visible; since the soft tissues have low attenuation, for the reconstruction of the

vessel geometry, a fundamental role is played by the blood. Blood is a low attenuation tissue, therefore the CT technique, see before, are performed by injecting, within blood flow, a contrast medium, i.e a substance with an high absorption index, in this way blood attenuation will be as high as the bone tissue. This allows to recognize and to close off (during the segmentation) the vessel to the other soft tissue.

The main interface, shown in Figure 4.9, is intuitive and easy to use. The interface allows the visualization of axial images and sagittal and coronal reconstructions: a fourth window allows to visualize the 3D reconstruction at the end of the segmentation; on the left side of the interface, a series of toolboxes allows to interact with images and perform segmentation. In this phase, it is needed to select the region of interest. In this case, the 3D segmentation

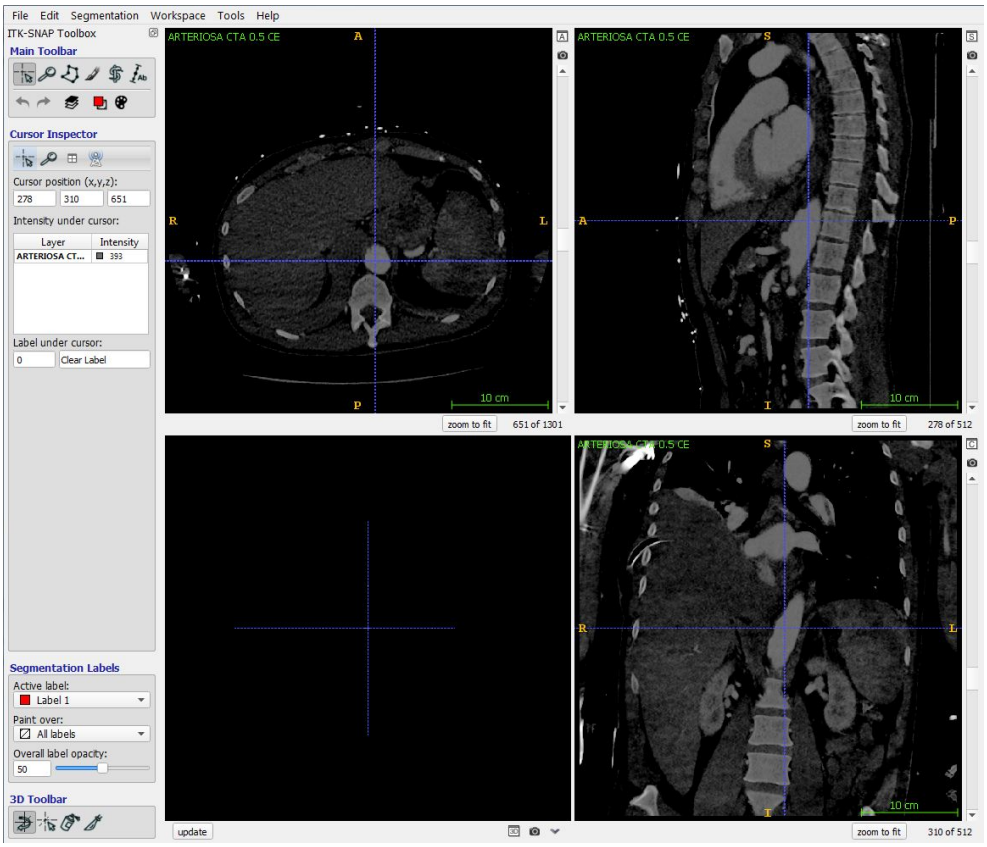

Figure 4.9: ITK-Snap software interface. Viewing DICOM images

algorithm used a threshold technique to determine the edges of the vessels. Once an adequate threshold is set, 3D bubbles approximately as big as the diameter of the vessel

are placed throughout the vessel to be segmented. Bubbles placed within the axially reconstructed images produced the models that most accurately replicated the anatomy of the vessel. Once the vessel is sufficiently filled with bubbles, expansion and contraction forces are set to limit the expansion of the bubbles and ensure they remain mostly within the vessel. These regions can be selected and eliminated in ITK-snap. The resulted model is stored in stereolithography representation (STL format).

Segmentation process

The stages of the segmentation process will be explained below; in particular, the patient's pre-operative case will be illustrated.

1. First, it is needed to proceed with the image acquisition:
   File → Open Main Image (→ Browse...)

2. In the second step the pre-proccessing phase takes place; this improves the contrast of the image to make the structures of interest more visible. To improve the contrast, it is needed to work on the histogram of the gray scale.
   Tools → Image Contrast

3. After the first two phases of preparing the image of interest, the segmentation phase takes place with the algorithm called Snake Evolution. Snake is a closed curve or 3D surface representing segmentation (Snake roi tool, symbol S). Firstly, select the region of interest (ROI) with the dotted line and the label color (Label). Secondly, the actual segmentation process begins right afer the click on Segment 3D.

Segmentation is divided into three steps, described below:
Step 1: Presegmentation- choose between two different modes of realizing an image feature:
Intensity regions: based on the relative intensity of the pixels. In this case, the feature image assigns a positive value for all pixels belonging to the structure to be segmented, and a negative for all others.

Image edges: based on the definition of the contours of the image. In this case, the feature image assigns values close to 0 to intensity pixels similar to that of the edges of the structure, and values close to 1 to pixels in uniform intensity regions.

Once the method of realizing the image feature based on intensity regions has been chosen; the software allows, through a graphic window, to set the optimal threshold values to select the region of interest to proceed with the segmentation.

Step 2: Initialization of the segmentation- One or more Bubble (spherical areas with the color of the label) are located. These Bubble represent the starting point of the Snake.

Step 3: Evolution- Calibrate the development of the snake, giving informations on where to expand; in particular, there are two parameters to be adjusted:

Baloon Force (propagation velocity): proportional to intensity values, where the intensity is high an expansion of the development area of the snake will take place, while, on the other hand, where the intensity values are negative it is visible a contraction. The higher this value is, the more the algorithm proceeds quickly where it sees high image feature values.

Curvature Force: It is used to control the maximum permissible curvature of the snake surface during evolution. The higher this value is, the more the surface will have to keep it spherical: this prevents the invasion of adjacent structures, connected to those of interest from small portions. For segmenting less regular structures, this value must be low to capture details that are highly curved.

Once the various parameters have been set, segmentation is started with the "PLAY" key; to display the 3D mesh, it is needed to stop the segmentation and click on Update, and then click Finish to finish the segmentation; In this way, the final segmentation is ready, Figure 4.10 (a).

Both aortic reconstructions of the aorta of the patient were considered, reconstruction before surgery, and reconstruction after surgery; in fact, in the first case, the 3D model serves to help the surgeon to explore the patient's anatomy and plan more precisely the intervention. The second case, however, is needed to check if the intervention has been successful (Figure 4.10(b)).

In addition to the case outlined above, another patient-case has been considered, Figure

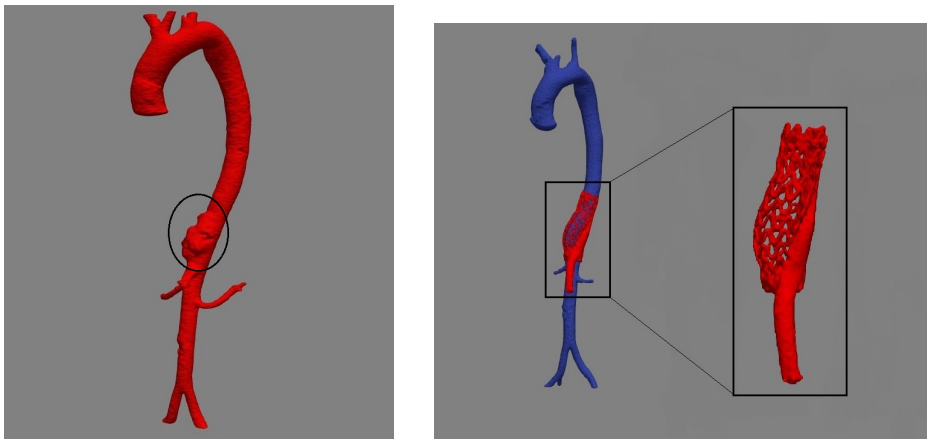

(a) *Pre-intervention case. 3D aorta volume obtained by segmentation with ITK-Snap. Abdominal aorta aneurysm is highlighted the black circle.*

(b) *Post-intervention case. 3D aorta volume obtained by segmentation with ITK-Snap; in red the lumen and in blue violet the stent*

Figure 4.10: Pre and post intervention 3D aorta volume of the first patient-case

4.11. The segmented model was already ready and the segmentation was carried out by Dr. Stefania Marconi and used in a previous study. In fact, in this case the segmented model was used to apply the branches clipping procedure.

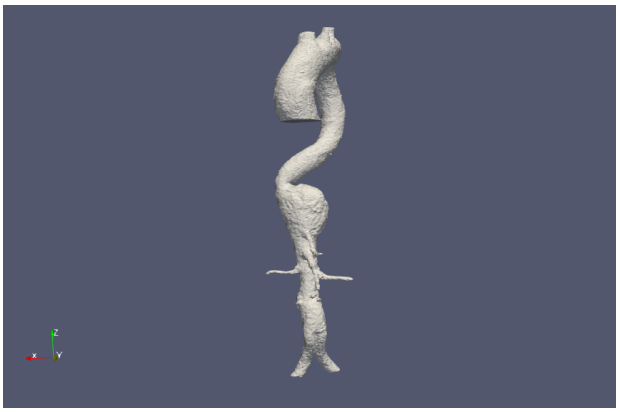

Figure 4.11: 3D aorta volume of the second patient-case.

4.2.3 Centerlines extraction and branches clipping

Once the 3D volume has been obtained from the segmentation, the various steps to obtain the final physical 3D model without branches will be shown, which will be printed and delivered to the physician ready to use during the intervention. The work process comprises two main phases: branches clipping and 3D printing model. The first phase can be accomplished through the use of a software called **VMTK**.

VMTK - The Vascular Modeling Toolkit

VMTK (www.hpfem.jku.at/netgen/), is a collection of libraries and tools for 3D reconstruction, geometric analysis, mesh generation and surface data analysis, from biomedical images. It is based on two libraries: VTK (the Visualization Toolkit) and ITK (the Insight Toolkit). This software was created by Luca Antiga (Unit of Medical Imaging, Department of Biomedical Engineering, Mario Negri Institute) and David Steinman (Biomedical Simulation Laboratory, Mechanical and Industrial Engineering, University of Toronto, Canada) on the basis of other open-source libraries: VTK, which provides tools for processing surfaces allowing for example operations of "cutting" and smoothing the surface; and ITK library, which provides the basic tools needed to perform the segmentation of images.
Vmtk operates in a text based environment but there is a version known as Pypepad which operates in a GUI environment. Pypepad allows to interactively edit the pypes and it is organized in three main frames. The first on the top, referred as the **Input frame**, is dedicated to the pype writing and editing; the second in the middle, referred as the **Output frame**, is where the output text is displayed and the third on the bottom, as the **Entry frame**, is where the values are inserted whenever prompted by a script.
For the visualization of three-dimensional geometries after surface data analysis with vmtk, another software has been used, **Paraview**.

Paraview

ParaView (www.paraview.org) is an open source multiple-platform application for interactive, scientific visualization. It is an application built on top of the Visualization Tool Kit (VTK) libraries. Paraview allows the visualization of three-dimensional geometries and the execution of a large number of analysis through the use of filters, some already present in the software and executable by the tools bar, others imported from the outside, and still others created manually within the software.

Smoothing

Image segmentation can result in bumpy surfaces, especially if the image quality is not high and one didn't use any curvature term in level sets evolution. Since bumps in the surface can result in spurious flow features and affect wall shear stress distributions, one may want to increase surface smoothness prior to building the mesh. The instruction that allows it is **vmtksurfacesmoothing** by writing:
vmtksurfacesmoothing -ifile model.stl -passband 0.1 -iterations 30 -ofile model_ sm.vtp; where *model.stl* is the stl file name obtained from the segmentation.
To compare the smoothed and original versions and to make sure that no shrinking occured and the main surface features were preserved, the following command can be written:
vmtksurfacereader -ifile model.stl –pipe vmtksurfacesmoothing -iterations 30 -passband 0.1 –pipe vmtkrenderer –pipe vmtksurfaceviewer -display 0 –pipe vmtksurfaceviewer -i @vmtksurfacereader.o -color 1 0 0 -display 1
By executing this command, the vmtk display window appears, which allows to compare both models: the original and the smoothed models, as shown in figure 4.12.

Opening the surface

If a surface using a deformable model is generated, the surface could be closed at inlets and outlets. The surface can now be opened by interactive command vmtksurfaceclipper.
vmtksurfaceclipper -ifile model_ sm.vtp -ofile model_ cl.vtp

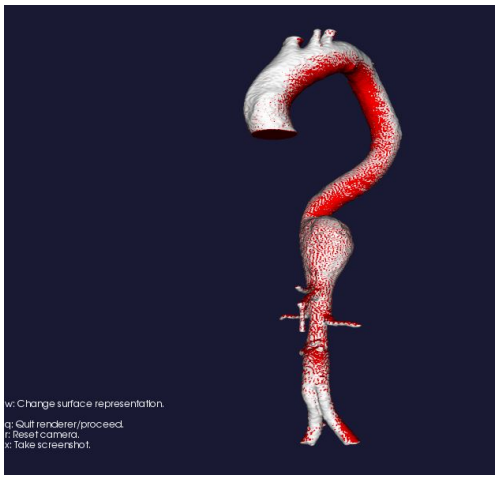

Figure 4.12: Compare original surface with the smoothed one. The original surface in red and the smoothed surface in white.

It allows to choose manually the parts to be cut. Since the part studied is the visceral area, cutting both ends brings the following pattern, figure 4.13

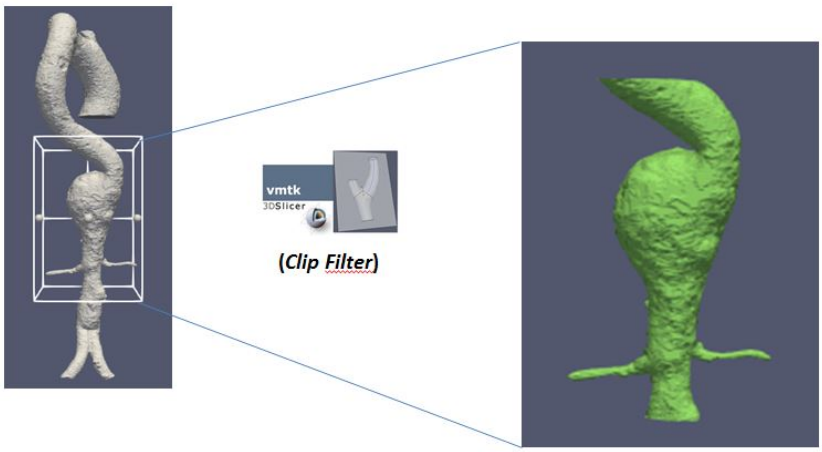

Figure 4.13: VMTK clipping unnecessary parts.

Centerlines extraction

Centerlines are powerful descriptors of the shape of vessels. The algorithm implemented in vmtk deals with the computation of centerlines starting from surface models, and has the

advantage that it is well characterized mathematically and quite stable to perturbations on the surface. Briefly, centerlines are determined as weighted shortest paths traced between two extremal points. In order to ensure that the final lines are in fact central, the paths cannot lie anywhere in space, but are bound to run on the Voronoi diagram of the vessel model. As a first approximation, it can be considered as the place where the centres of maximal inscribed spheres are defined. A sphere inscribed in an object is said to be maximal when there is no other inscribed sphere that contains it. So, for every point belonging to the Voronoi diagram, there is a sphere centred in that point that is a maximal inscribed sphere (the information relative to the radius is therefore defined everywhere on the Voronoi diagram). Centerlines are determined as the paths defined on Voronoi diagram sheets that minimize the integral of the radius of maximal inscribed spheres along the path, which is equivalent to finding the shortest paths in the radius metric.
The script that allows to compute centerlines in vmtk is:**vmtkcenterlines**. It takes in input a surface and spits out centerlines.
vmtkcenterlines -ifile model_ cl.vtp -endpoints 1 -resampling 1 -resamplingstep 0.5 –pipe vmtkbranchextractor -ofile centerlines.vtp
A render window will pop up, asking to specify points on the surface that will act as source points. In the end, the centerlines will pop up, as shown in figure 4.14 (a). It is possible to see the 3D geometric centerlines opening centerlines.vtp with paraview, as shown in figure 4.14 (b).

Branches extraction and clipping

The script that allows to extract and clip branches in vmtk is: **vmtkbranchclipper**. It takes in input a surface and the relative centerline and spits a surface without branches, as it can be seen in figure 4.15.
vmtkbranchclipper -centerlinesfile centerlines.vtp -ifile model_ cl.vtp -ofile vessel_ no_ branches.vtp -groupids 6 8 9 10 -groupidsarray GroupIds -blankingarray Blanking -radiusarray MaximumInscribedSphereRadius -insideout 1

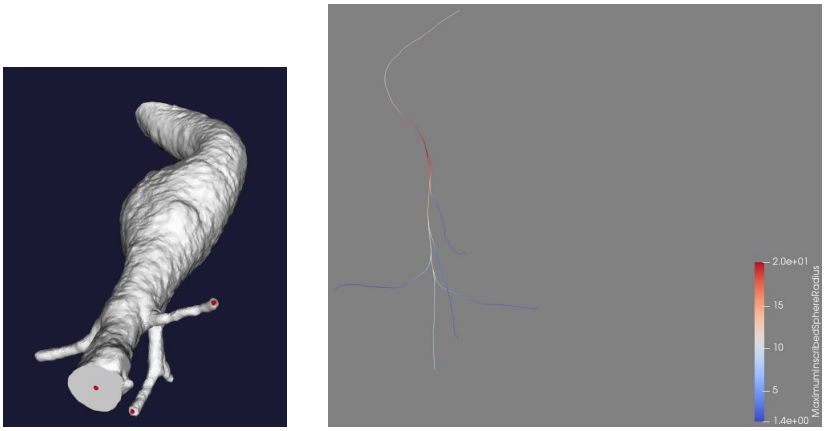

(a) *Spheres located at the ends of the visceral branches*

(b) *Centerlines extraction*

Figure 4.14: VMTK centerline reconstruction.

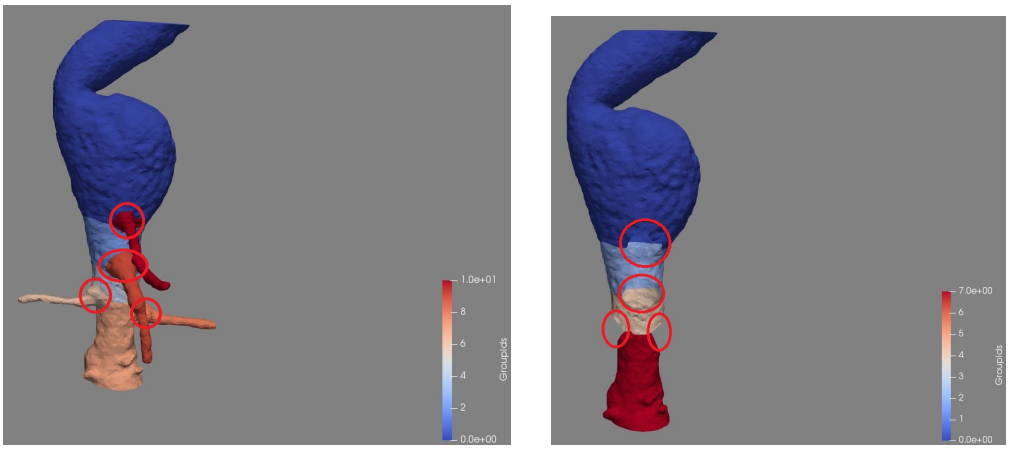

(a) *Branches extraction*

(b) *Branches clipping*

Figure 4.15: VMTK Branches extraction and clipping.

4.2.4 From virtual model to physical model: 3D printing

Once the 3D model is obtained after branches clipping, the 3D printing can start. The 3D printing process was carried out by Dr. Stefania Marconi at our Protolab lab [88] in the Department of Civil Engineering and Architecture of the University of Pavia. The printer used in this case, is the 3D SYSTEMS ProJet 460 Plus; a professional Binder Jetting type printer, in color, that prints using visijet PXL-pastel material. All printing details are showed below in the Figure 4.16 and the printed model is shown in Figure 4.17.

```
Date: Tuesday, July 04, 2017

Build Name: model.stl

Printer Type: ProJet 460 Plus
Material Type: VisiJet PXL - Pastel
Build Height: 72.86 mm
Layer Thickness: 0.1016 mm
Number of Layers: 717

Estimated build time in monochrome mode:: 3 hours and 17 minutes
Estimated binder usage in monochrome mode:  59.0 ml

Estimated build time in color mode:: 3 hours and 33 minutes
Estimated   Clear Binder usage in color mode:  58.6 ml
Estimated color ink usage: Yellow =  0.1202 ml;
                           Magenta =  0.1202 ml;
                           Cyan =  0.1202 ml

Total volume of parts: 79.53 cubic centimeters.
Total surface area: 409.14 square centimeters.
Surface to volume ratio: 13.07.

Number of Models:       1
Number of Vertices:     31085 (0 textured)
Number of Facets:       62186 (0 textured)
Number of Textures:     0

Part Name: model.stl
Width: 166.42 mm
Depth: 77.97 mm
Height: 72.86 mm
Volume: 79530.13 Cu. mm
Area: 40914.30 Sq. mm
```

Figure 4.16: 3D model printing caracteristics.

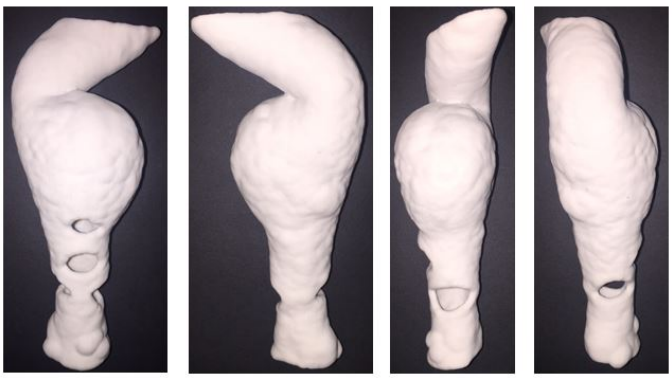

Figure 4.17: 3D printed model.

Chapter 5

Conclusion, limitations and future perspectives

5.1 Conclusions

"**Chimney Graft (CG)**" technique has been designed to extend the proximal sealing zone and can be used in emergency settings when it is not possible to wait for a custom-made fenestrated stent graft. Chimney grafts, however, induce large "gutters" between the main device and the chimney graft which may cause a proximal I endoleak type. For type I endoleak prevention, it is necessary to have an optimal CG configuration characterized by low gutter size and it is need to choose an appropriate size, geometry, material and configuration of stent grafts. This can be achieved by grossly oversizing the aortic endograft to force it to wrap around the smaller endograft.

Throughout, in this activity we presented the analysis of the kinematics of the chimney stenting technique. To search for an optimal chimney stent graft, finite structural element analysis (FEA) are needed to analyse the performances of the implanted stents. Starting from medical investigations obtained from the medical partners, a finite Element method of a chimney evar model has been built. In this FEA, the model can include various chimney configurations with single Chimney graft configuration (one main stent and one parallel

stent). In each configuration, the geometrical properties of the main stent has been modified in order to evaluate which one would influence the most the results.
Taking into account all the simulation made, as first conclusion, for oversizing degree less then 15% and a main stent diameter less than 23 mm, there is a conceptual problem due to the high percentage of the main stent compression ($> 50\%$) and the high value of the gutter size ($> 20\%$ of the aorta area) making the configuration unusable. The most significant result allowed to get better endograft stent apposition was achieved using 15% endograft oversizing degree resulting in the best optimal configuration due to the low values of gutter size and Von Mises stress obtained with this configuration. The results analysis show that the deformation of the stent is not uniform, but depends on the stent features such as geometry, model and stent configuration inside aortic wall.

In the Table 5.1, Recently published papers show other technical results to minimize gutter size and consequently Endoleak Ia.
In de Beaufort et al., 2017 [90], the gutter size has been reduced by using from 20 to 30% of oversizing. Moreover, to decrease the less radial force, a Viabahn stent graft has been used.
In Valério, André Miguel dos Santos Almeida et al., 2014 [5], no significant differences in gutter size were observed between configurations with the same number of CG's. All the configurations with more than 2 CG's have main graft compression above 50%. Configurations with less number of CG's, have small gutter areas. Furthermore, Configuration with one main graft (28 mm) and one parallel graft (6 mm) has gutter area equal to 44.1 mm2 and main compression equal to 14.6%.
Tolenaar et al., 2013 [55] deduced that, oversizing of 20%-30% reduces the gutter. Tendency to oversize closer to 30% when more than one chimney is needed. Covered stents are beneficial because pressurization of the peri-graft channels is reduced, lowering the chance of type I endoleaks, especially in the absence of any aortic neck.
Minion, 2012 [89] presents a technique to mold a parallel endograft into an oblong or 'eye' shape. The molding helps facilitate the apposition of the two parallel endografts to seal

Author	*Indications*
de Beaufort et al., 2017 [90]	• 20% to 30% proximal oversizing. • Viabahn stent grafts.
Valério, André Miguel dos Santos Almeida et al.,2014[5]	• 1 main graft of 28 mm + 1 parallel graft of 6 mm • Gutter area = 44.1 mm^2 • Main compression = 14.6%.
Tolenaar et al., 2013 [55]	• Oversize closer to 30% when more than one tendency to oversize closer to 30% in cases when more than one chimney is needed. • Covered stents are beneficial.
Minion, 2012 [89]	• Mold a parallel endograft into an oblong or 'eye' shape.
R. P. Patel et al., 2013 [29]	• Oversizing the main stent-graft by 20% to 30% • Self-expanding stent grafts. • 5 cm overlap between the layers of the aortic stent graft and CG.
G. Mestres et al., 2012 [72]	• Excessive endograft oversizing of 30%. • Use of Excluder compared to Endurant stent grafts, and Atrium- V12.
This activity	• Configuration used: 1 main graft of 28 mm + 1 parallel graft of 9 mm. • Material used: Nitinol for stent strut and ePTFE for stent graft. • Oversizing the main stent-graft by 15%. • Gutter size equal to 62.3 mm^2. • Main stent diameter equal to 23 mm. • Main compression equal to 51%

Table 5.1: literature review

the aortic endoleak lumen and obliterate the gutters that could lead to in these cases.
R. P. Patel et al., 2013 [29], observed that the oversizing of the main aortic stent-graft by at least 20% to a maximum of 30% minimize the risk of gutters. Self-expanding stent grafts are characterized by increased flexibility and kink resistance, which may adapt better and avoid gutter leaks. Furthermore, the authors propose an overlap of at least 5 cm between the overlapping layers of the aortic stent graft and CG to avoid gutter endoleak.
G. Mestres et al., 2012 [72] shows that there is a better endograft parallel stent apposition and lower gutter area while using excessive endograft oversizing (30%). Wider gutters are seen when using 15% stentgraft oversizing, and stent-graft infoldings occurs when 40% super-oversizing is used, and should be avoided. Therefore, 30% endograft oversizing should be recommended, using Excluder compared to Endurant stent grafts, and Atrium-V12 compared to Viabahn parallel stents with a maximum stent compression in combination of Endurante Viabahn.
This activity shows that wider gutters are seen when using 0% to 10% stentgraft oversizing, and should be avoided. The oversizing of the main aortic stent-graft by at least 20% to a maximum of 50% minimize the risk of gutters but in this range the Von Mises stress values are high. Therefore, 15% of endograft oversizing represents the trade-off between the gutter size and stress value and this chimney configuration is recommended.

The routine application of the presented numerical models could help clinicians in their intervention strategies, well predicting in-vivo outcomes. Various stenting procedure options could be simulated for patient-specific cases, comparing results in terms of mechanical behavior of the intravascular devices and of the arterial wall.

5.2 Limitations and future development

The study analysed in this thesis is an experimental approach to evaluate real medical and biomedical situations. Despite the preliminary results, some limitations should be taken into account in order to improve these analysis. These limitations exist in both Chimney-Evar technique and the Physician Modified Endovascular Graft and they are followed by some future development.

5.2.1 Chimney-EVAR technique

1. The SG design does not have the same geometry and size of the commercial models used in the patient-case intervention. In the design phase, only the sinusoidal ring stent shape and the mechanical properties of the stent strut have been respected.
   A possible future work is to develop the analysis with the complete model device and monitor the mechanical behaviour. Below are some list of action could be taken:

   (a) Study the influence of the materials and the design by testing different shapes and dimensions of the structure of stent wires can help to understand the range of the following values: Young Modulus, Poisson's Ratio, Tensile Strength, Yield Strength, Mass Density and Compressive Strength.

   (b) Use different commercial models with more radial force. This could effect the geometry of the CG configurations and therefore the gutter size.

   (c) Test different stent (diameters, models, materials, chimney grafts number) and maximise the combination of all its variables in order to have larger sample and collect more data.

2. The forces carried by the stent wire control how the deformation of the endografts happens. The use a metallic wire instead of a graft fabric can simplify the design and the computational time.

3. An isotropic and homogeneous artery has been considered in this study. To take into account the collagen fibers orientation, anisotropic arterial wall modelling can be used so three different layers can be characterized.

4. The computational simulations do not consider the arterial blood pressure (averaged 100 mmHg) inside the vessels. To Take into account the characteristics of the aorta behavior (the mechanical interaction between the various stents and the vessel wall and blood flow dynamics), An investigation on the blood flow after the stenting procedure can carry out a fluid dynamics simulations.

5. In this work, only a biomechanical simulation with Abaqus tools has been considered. The results found are based on the design and the features of reconstruction. To compare the simulation with a post-operative reality, a medical imaging analysis and processing of the implanted device in a patient-specific case can be used.

5.2.2 Physician Modified Endovascular Graft

The model printing in this activity is limited to the 3D printing using plaster material. Since the molded model is used at surgical level and it's directly in contact with the implantable device, a PLA sterile material could be used. Due to its particular characteristics, the contamination of the device can be avoided and consequently the probability to be rejected by the body is lower.
Moreover, the PLA is a totally biodegradable, biocompatible, absorbable and non-toxic material but it has a low thermal resistance (it deforms already at 60° C). The sterilization of a material occurs in two ways:

1. By subjecting the PLA into high temperature (120-135°C) for 20-30 min. Therefore this procedure is not suitable for the sterilization due to the deformation and the loss of both mechanical and functional characteristic at these temperatures.

2. Radiosterilization: or making the material free of microorganisms using ionize radiation such as X-rays or gamma irridiation.

Since sterilization takes place in a closed and sterile environment where the model is subjected to very accurate procedures and since our laboratory is not yet provided with such technology, work has been interrupted.
An alternative is to send the printed template to a radiosterilization company. The sterilized model is shipped in an envelope that will then be opened only within the operating room during the preoperative preparation phase.

Appendix A

Input File Analysis

A.1 Format Input File

The explanation here below is taken from DassaultSystèmes (2010). The input file is the means of communication between the preprocessor, usually Abaqus/CAE, and the analysis product, Abaqus/Standard or Abaqus/Explicit. It contains a complete description of the numerical model.
The input file is a text file that has an intuitive, keyword based format, so it is easy to modify using a text editor if necessary; if a preprocessor such as Abaqus/CAE is used, modifications should be made using it.
Why do I go with input files?
Advantage:

- User can change model directly without GUI;
- FASTER than analysis using GUI;
- Useful for minor modification;

Disadvantage:

- No visual information (should use GUI to check model layout);

- User has to discretize model;

The example of an overhead hoist, shown in Figure A.2, is used to illustrate the basic format of the Abaqus input file, The hoist is a simple, pin jointed truss model that is constrained at the lefthand end and mounted on rollers at the righthand end. The members can rotate

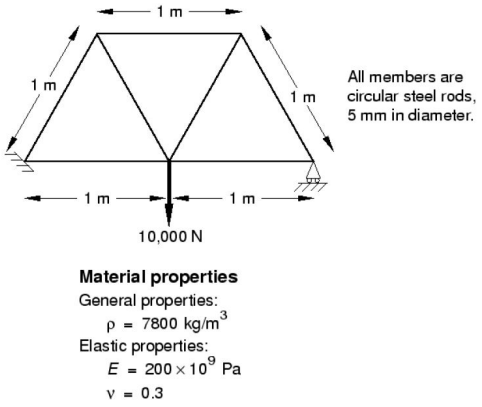

Figure A.1: Schematic of an overhead hoist. (DassaultSystèmes, 2010).

freely at the joints. The frame is prevented from moving out of plane. A simulation is performed to determine the structure's deflection and the peak stress in its members when a 10 kN load is applied as shown in figure.

In the Figure A.3 below we present the input file format related to the figure of the hoist. It is divided in two parts; the first section contains Model Data and includes all the information required to define the structure being analyzed. The second section contains History Data that define what happens to the model: the sequence of loading or events for which the response of the structure is required. This history is divided into a sequence of steps, each defining a separate part of the simulation.

The input file is composed of a number of option blocks that contain data describing a part of the model. Each option block begins with a keyword line, which is usually followed by one or more data lines.

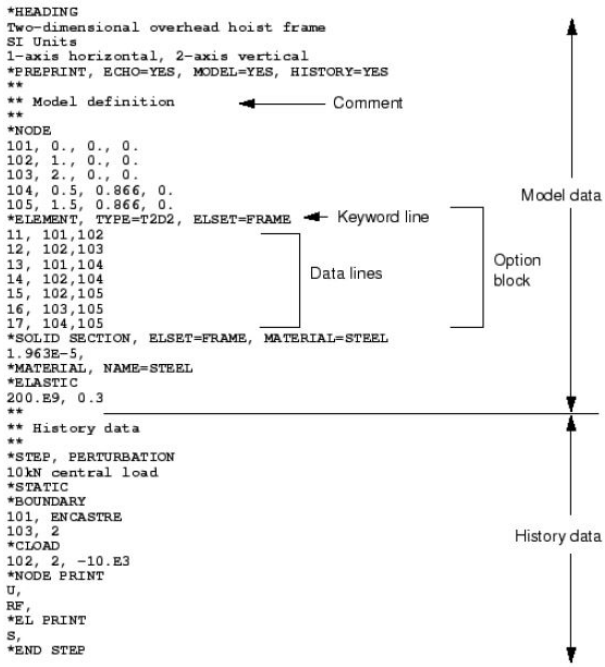

Figure A.2: Format of Abaqus input file for overhead hoist model. (DassaultSystèmes, 2010).

A.1.1 Keyword lines

Keywords (or options) always begin with a star or asterisk (*). For example, *NODE is the keyword for specifying the nodal coordinates, and *ELEMENT is the keyword for specifying the element connectivity. Keywords are often followed by parameters, some of which may be required. The parameter TYPE is required with the *ELEMENT option because the element type must always be given when defining elements.
*ELEMENT, TYPE=T2D2

A.1.2 Data lines

Keyword lines are usually followed by data lines, which provide data that are more easily specified as lists than as parameters on the keyword line. Examples of such data include nodal coordinates, element connectivities, or tables of material properties, such as stress-strain curves.
For example, the option block defining the nodes for the overhead hoist model is:

```
*NODE
101, 0., 0., 0.
102, 1., 0., 0.
103, 2., 0., 0.
104, 0.5, 0.866, 0.
105, 1.5, 0.866, 0.
```

Appendix B

Finite Element Method (FEM)

B.1 Overview of the method

The Finite Element Method (FEM) is a numerical technique to obtain an approximate solution to a class of problems governed by partial differential equations known as boundary value problems as they consist of a partial differential equation and the boundary conditions. This method converts the partial differential equation into a set of algebraic equations which are easy to solve[91].

FEM subdivides the geometrical physical domain into smaller, simpler parts that are called finite elements. The equations that model these finite elements are then assembled into a larger system of equations that models the entire problem, replacing a complex problem by many simple problems that need to be solved simultaneously. Elements share common points called nodes and the process of dividing the model into small pieces is called meshing (Figure C.1)[92].

Usually, the displacements of the nodes are taken as the fundamental unknown variables that a Finite Element solver, like Abaqus, calculates. Once the nodal displacements are known, the stresses and strains in each finite element can be determined easily. The response at any point in an element is interpolated from the response at the element nodes. The response of a node is described, in general, by three translations and three rotations.

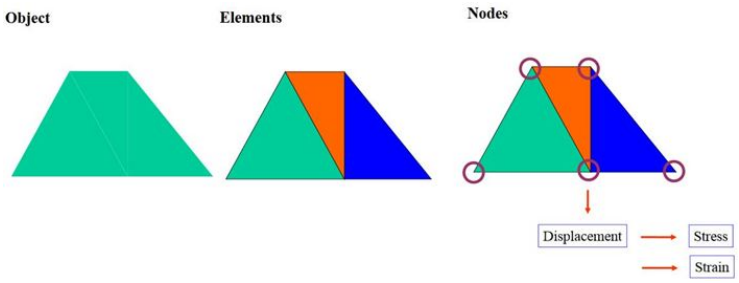

Figure B.1: Finite Element Method.

These are called degrees of freedom (DOFs). Analysis using FEM is called Finite Element Analysis (FEA).

B.2 A simple example of using FEM

An example might be the typical mechanical problem of a beam, Figure C.2, with an extremity fixed, with all degrees of freedom locked by the Boundary Conditions(BCs) imposed. When a constant force is applied on the opposite side of the beam, deformations on beam's structure are expected, according to the specified load. Considering a large set

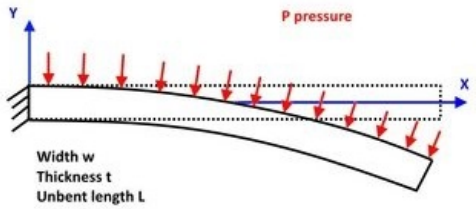

Figure B.2: A classical problem

of parameters, such as material composition of the beam, BCs, loads and temperature, it's possible to create a model of this experiment to explain this phenomenon. Solving this problem by handmade calculus procedures can be possible only in case of simple geometry and when in presence of a small number of degree of freedom, and characterized by low dimensionality. Computer's ability to handle a large set of variables and to solve numerical problems in few seconds leads to the creation of computer aided analysis of mechanical problems. Since computers only operate in discrete logic, to overcome the problem of

the solutions of a continuous problem, FEM and Finite Elements Analysis(FEA) were developed.

B.3 A typical FEA workflow

Many FEM solvers, such as commercial codes as Abaqus or Ansys, usually follow these principal steps for the solution of a mechanical problem:

1. **Definition of geometry**: in this step the user must provide the FEM solver with the geometry of interest, i.e. the beam in figure C.3. In this step only geometrical information are considered;

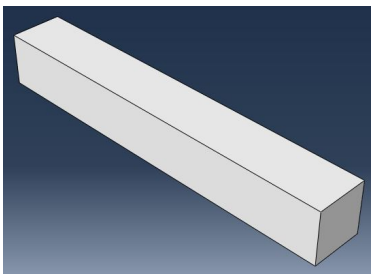

Figure B.3: Input geometry

2. **Definition of material properties**: it's mandatory to define at least one material composing the geometry by providing its mechanical properties such as, in the simplest case, Young module (E) and Poisson ratio (υ).

3. **Interaction and contacts**: if the object considered for analysis is composed by 2 or more entities it's possible to define contact points or surface interactions between parts during simulation. This option usually leads to high and realistic details in solution, since it's possible to simulate frictions. This improvement in solution quality always comes along with an increment in calculations times and complexity;

4. **Loads and BCs**: definition of the type of load (concentrated force, pressure, tractions), BCs (partial blocks on degrees of freedom, encastre), where loads and BCs are applied and in which time interval.

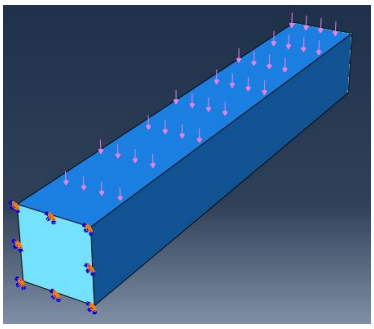

Figure B.4: Loads and BCs applied

5. **Creation of a mesh**: probably the most important step of a FEA. Since it's not possible to directly obtain a solution, the whole geometry must be considered as composed by many small units (elements). Thus, a solution can be found for each

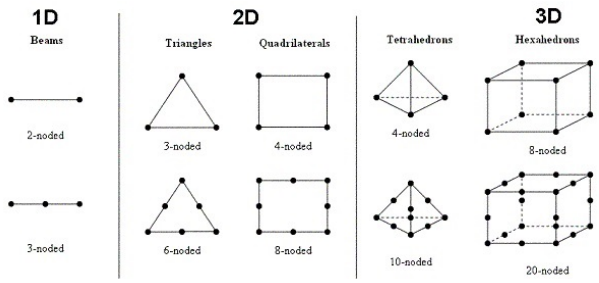

Figure B.5: Some of the most common element types

element composing the geometry of interest, and an overall solution can be obtained. In 2D simulations it's possible to use triangular or squared elements as shown in Figure C.5. In 3D simulation it's possible to use tetrahedral or cubic elements.

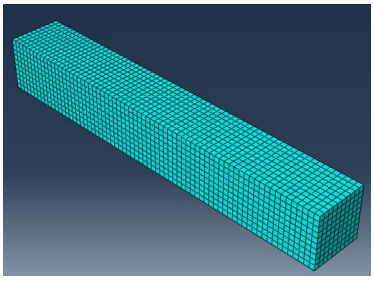

Figure B.6: Meshed geometry

6. **Solution**: in this phase, all remaining variables and settings are defined and the

solver can elaborate the input tasks. Errors and warnings may also be produced during solution procedure. Solution time is proportional to the number of the degree of freedom of the discretized model, and consequently, strictly related to mesh definition and the number of elements of the model. High detailed models are usually composed by millions of elements, and high computational times are usually required to obtain a solution.

7. **Results evaluation**: once a solution is obtained, visual and numerical results can be investigated. The solutions obtained can also be used for future inputs, especially in iterative simulations.

   The beam structural response to BC and loads is in fact a deformation field related to the force direction and intensity, Figure C.7.

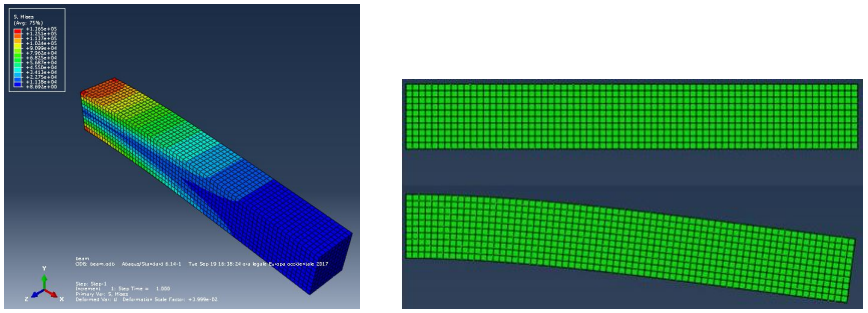

(a) *von Mises stress calculated by applying a deformation analysis*

(b) *(a) Unloaded beam. (b) Loaded beam*

Figure B.7: Results visualization

List of Tables

1.1 Comparison between open surgery and EVAR. Adapted from (Noll, et.al.,2007) [23]. 14

1.2 Comparison between chimney graft and fenestrated graft [5, 58] 24

2.1 Abaqus (Simulia, Dassault Systems) superelasticity UMAT constants. . . . 41

2.2 Mesh statistics in Abaqus (Simulia, Dassault Systems). 43

2.3 Steps summary for the chimney stenting intervention simulated. 49

2.4 Main SG diameters calculated for each oversize value. 54

2.5 Elementary unit number in the unrolled main stent. 55

3.1 Main SG diameters calculated for each oversize value. 68

3.2 Maximum and minimum Von Mises stress value of the various configurations. 71

5.1 literature review 95

List of Figures

1 The image shows the workflow followed throughout the thesis. We started from the chimney device reconstruction, which is designed and modelled using 3 tools: Rhinoceros 5.0 (McNeel&Associates), Abaqus 6.14-2 (Simulia, Dassault Systems) and Matlab (MathWorks). After we applied the structural Finite Element Analysis for the gutter size calculation and we finish with the results of simulations to find the relationship between oversizing and gutter size. II

2 The image shows the workflow followed throughout the thesis. We started from the chimney device reconstruction, which is designed and modelled using 3 tools: Rhinoceros 5.0 (McNeel&Associates), Abaqus 6.14-2 (Simulia, Dassault Systems) and Matlab R2016b (MathWorks). After we applied the structural Finite Element Analysis for the gutter size calculation and we finish with the results of simulations to find the relationship between oversizing and gutter size. IV

1.1 (a) Aortic wall layers: Intima, media, adventitia. (b) Aorta's sections: Ascending Aorta, Aortic arch, Descending Aorta and Abdominal Aorta 7

1.2 Difference between a normal aorta and an aorta with aneurysm. 8

1.3 Classification of abdominal aorta aneurysm 9

1.4 Thoracic and Thoracoabdominal aortic aneurysms. 10

1.5 Comparison between blood flow in a healthy aorta and aorta with dissection 10

1.6 Aortic dissection types 11

1.7 Aneurysm repair options. (a) Open surgical repair (OSR); (b) endovascular aneurysm repair (EVAR). Adapted from (shahid et.al., 2013) [14] 12
1.8 Open Surgical Repair(OSR). 12
1.9 Endovascular aneurysm repair. Reproduced from Schwarz, 2012. 13
1.10 Diagram shows example of planning template. Diameters and lengths must be accurately reported for appropriate sizing of endograft components. An example of inclusion criteria of Zenith (Cook Company, Bloomington, IL, U.S.A.) 15
1.11 Schematic of stent-graft migration. Reproduced from Kleinstreuer et. al, 2007. 16
1.12 Schematics of endoleaks. 17
1.13 Relationship between abdominal aortic aneurysms and renal arteries. A: Infrarenal aortic aneurysm (neck >10 to 15 mm). B: Juxtarenal aortic aneurysm (neck = 4 to 10 mm). C: Suprarenal aortic aneurysm, neck length <4 mm. Reproduced from http://thoracickey.com 19
1.14 (a) Cook Zenith Fenestrated Endograft with: **B**:scallop, **C**:small fenestration, and **D**:large fenestration; (b) Endovascular options for branch incorporation include fenestrated branched devices for pararenal aneurysms, multibranched devices for thoracoabdominal aneurysms. 20
1.15 A chimney graft tecnique to preserve the renal and/or mesentric perfusion. 22
1.16 (a) Different cross-sectional areas: A: outer perimeter of the main graft, B: inner diameter of the aorta, C: outer perimeter of the chimney graft, and D: gutter. Adapted from de Bruin, et al., 2013 [62]. (b) Endoleak type I: persistent filling of the aneurysm sac due to ineffective seal at the proximal (type Ia) or distal (type Ib) end of the stent graft. Adapted from https://www.emaze.com/ 25

2.1 Abaqus interface 28
2.2 Abaqus (Simulia, Dassault Systems) analysis flow 29

2.3 Abaqus (Simulia, Dassault Systems) Modules 30

2.4 Renal artery "chimney" graft configuration. Composed by two stent grafts: Main body SG (Aortic endograft) and Parallel SG (chimney graft) 31

2.5 Stent grafts used in Chimney-EVAR case-specific (Main body and Parallel SG) 32

2.6 The Conformable GORE TAG Endoprothesis. (Image courtesy of W. L. Gore & Associates Inc). 32

2.7 The GORE VIABAHN Endoprosthesis. (Image courtesy of W. L. Gore & Associates Inc). 33

2.8 Parts models created in Abaqus 6.14-2 (Simulia, Dassault Systems). 34

2.9 Stent graft reconstruction workflow. Strating from Rhinoceros 5.0 (McNeel&Associates) the first part of the elementeray unit geometry of the stent is created. Then it has been imported in Abaqus 6.14-2 (Simulia, Dassault Systems) to create the elementary unit and the planar geometry of the stent composed by multiple copies of elementary units. After that, the planar geometry is wrapped into a cylindrical geometry using Matlab R2016b (MathWorks) and finally, using Abaqus again the final stent graft model is obtained. The same procedure was used to both main and parallel stent grafts reconstruction. 35

2.10 3D elementary unit design with Rhinoceros 5.0 (McNeel&Associates). . . . 35

2.11 Reconstruction of the planar geometry of the unrolled stent. The elementery unit created with Rhinoceros 5.0 (McNeel&Associates) (a). The elementery unit imported in Abaqus as a iges part (b). The elementary unit geometry (c). Creation of planar model with the linear pattern tool of Abaqus along horizontal direction (d). 36

2.12 Matlab script's output figure. Transferring the nodal coordinates from a cartesian coordinate system (a) into a cylindrical coordinate system (b). . . 37

2.13 Main ring stent rolling and extension. 38

2.14 Some features of the Nitinol. From the top left (1), a plot of the curve Strain/Stress of the Nitinol compared to the 316 Stainless steel one; (2) the sale curve compared to other materials of the human body, the plot wants to stress the attention on the hysteresis characteristic of the material; (3) Nitinol superelastic trasformations; (4) a schematic explanation of the transition of the material between Martensite and Austenite. 40
2.15 Stent graft section assignments 42
2.16 (a) Isometric view of a meshed stent ring;(b) Close-up of stent elementary unit composed by strut curved region and membrane straight region. . . . 42
2.17 Final chimney assembly configuration. (a) front view; (b) Isometric view. . 44
2.18 Small and entire models configurations created in Abaqus 6.14-2 (Simulia, Dassault Systems). (a) configuration with 3 rings-stent grafts. (b) configuration with 11 rings-stent grafts. 44
2.19 Abaqus 6.14-2 (Simulia, Dassault Systems) steps. 45
2.20 Stent grafts crimping. Main SG crimping (model A); Parallel SG crimping (model B). 48
2.21 Simulation steps in Abaqus 6.14-2 (Simulia, Dassault Systems). Crimping phase (a); Deployment phase (b). 48
2.22 Stent grafts crimping in a straight abdominal artery segment. From the left to the right different steps of the stent grafts crimping are illustrated. Parallel stent graft (Model A)and main stent graft (Model B) crimping. . . 50
2.23 Stent grafts deployment in a straight abdominal artery segment. From the left to the right different steps of the stent grafts deployment are illustrated. Parallel stent graft (Model A) and main stent graft (Model B) deployment. 51
2.24 Final appearance configuration of the chimney's simulation. Front view (a) and isometric view (b). 51
2.25 Von Mises stress values (MPa) during crimping phase. Stress values are calculated for maximum crimped state. From left to right, a front and a isometric views of the two stent grafts 52

2.26 Von Mises stress values (MPa) during deployment phase. Stress values are calculated for maximum deployed state 53

2.27 Stent-graft oversizing (a); undersizing (b). Image from Donas et al., 2017 [73]. 54

2.28 ImageJ 55

2.29 Different cross-sectional areas in chimney configuration. A: outer perimeter of the main graft, B: inner diameter of the aorta, C: outer perimeter of the chimney graft, and D: gutter area. 56

2.30 (a) View cut manager tool in Abaqus 6.14-2 (Simulia, Dassault Systems). By moving the cursor, we choose the cut section position. (b) Left view of 3 rings-stent model with the position of each section "cut on". (c) Front view of the cutted sections. 56

2.31 Gutter area mean value calculation with ImageJ ROI manager tool. 57

2.32 Abaqus 6.14-2 (Simulia, Dassault Systems) two chimney configurations. (a) 3-ring stents first configuration; (b) 11-ring stents second configuration. . . 58

2.33 Gutter size in the 3 rings-stent configuration. 58

2.34 Gutter size in the 11 rings-stent configuration. 59

2.35 Abaqus reconstruction steps. For each SG oversizing case, is illustrated (from left to right) the corresponding radius of the main SG; number of elementary units in the unrolled main stent; planar and cylindrical geometrical model of single ring; cylindrical geometrical model of main 3 ring-stent graft and finally the assembled (main SG in green; parallel SG in red; main and parallel catheters and the aorta segment are modeled as a black circle). . . 61

3.1 0% endograft oversizing configuration. Undeformed model (Model a); Final apperance of deformed model (Model b). 1, Total aortic area; 2, main graft area; 3, chimney area; 4a and 4b, gutter area. 64

3.2 0% endograft oversizing measurments. The two ROI of the cross section (Model a); The ROI manager tool of ImageJ(Model b). A Z-plane view of the chimney configuration; The cross sections relative for every ring and the respective areas measured with ImageJ. 65
3.3 Von Mises Stress value (MPa) in the 0% endograft oversizing configuration. 65
3.4 Line Graph that plots changes in gutter size (mm^2) over oversizing value (%) 69
3.5 Von Mises Stress distribution (MPa) in chimney configuration during deployment phase. 15% oversizing degree configuration (A); 50% oversizing degree configuration (B) 69
3.6 Line Graph that plots changes in main stent compression (%) over oversizing value (%) 70
3.7 Line Graph that plots changes in Von Mises stress (GPa) over oversizing value (%) 71

4.1 **A**, Fenestrated stent graft. **B**, Multi-branched stent graft. **C**, Physician Modified Endovascular Graft. 74
4.2 **A**, Starnes use of an ophthalmic Bovie cautery device to create the fenestrations. **B**, Gold, 15-mm Amplatz Gooseneck Snares were then used to reinforce all fenestrations. **C**, A typical physician-modified endovascular graft (PMEG). Fenestrations for the superior mesenteric artery (SMA) (struts present) and left and right renal arteries (strut-free) were created for this particular patient. Reproduced from Starnes et.al J Vasc Surg 2012[26] 75
4.3 Three-dimensional (3D)-printed fenestration template. **A**, Computer model of the template. **B**, Solid printed model of the template created using a stereolithography 3D printer with clear resin. **C**, An endovascular graft inserted in the template. A printed from [82] 76
4.4 Illustrating the steps for manufacturing a three-dimensional (3D) patient-specific model, the example showing a patient with an enlarged Marfan-like aortic root [84]. 77

4.5 Graft fenestration and deployment for validation. **A**, An unsheathed graft is inserted in the fenestration template and the branch vessel origins are marked with a pen. **B**, Fenestrations are cut with an electrocautery device after removal of the template. 77
4.6 Computerized Tomography (CT) Scan 78
4.7 Workflow used in this chapter. From images acquisition to Aorta Printed Model using various softwares and techniques. 80
4.8 DICOM CT images characteristics 81
4.9 ITK-Snap software interface. Viewing DICOM images 83
4.10 Pre and post intervention 3D aorta volume of the first patient-case 86
4.11 3D aorta volume of the second patient-case. 86
4.12 Compare original surface with the smoothed one. The original surface in red and the smoothed surface in white. 89
4.13 VMTK clipping unnecessary parts. 89
4.14 VMTK centerline reconstruction. 91
4.15 VMTK Branches extraction and clipping. 91
4.16 3D model printing caracteristics. 92
4.17 3D printed model. 92

A.1 Schematic of an overhead hoist. (DassaultSystèmes, 2010). 102
A.2 Format of Abaqus input file for overhead hoist model. (DassaultSystèmes, 2010). 103

B.1 Finite Element Method. 106
B.2 A classical problem 106
B.3 Input geometry 107
B.4 Loads and BCs applied 108
B.5 Some of the most common element types 108
B.6 Meshed geometry 108
B.7 Results visualization 109

Bibliography

[1] Andrew C Picel and Nikhil Kansal. Essentials of endovascular abdominal aortic aneurysm repair imaging: preprocedural assessment. *American Journal of Roentgenology*, 203(4):W347–W357, 2014.

[2] Robert E Noll, Britt H Tonnessen, Krishna Mannava, Samuel R Money, and W Charles Sternbergh. Long-term postplacement cost after endovascular aneurysm repair. *Journal of vascular surgery*, 46(1):9–15, 2007.

[3] Roy K Greenberg, Daniel Clair, Sunita Srivastava, Guru Bhandari, Adrian Turc, Jennifer Hampton, Matt Popa, Richard Green, and Kenneth Ouriel. Should patients with challenging anatomy be offered endovascular aneurysm repair? *Journal of vascular surgery*, 38(5):990–996, 2003.

[4] Konstantinos G Moulakakis, Spyridon N Mylonas, Efthimios Avgerinos, Anastasios Papapetrou, John D Kakisis, Elias N Brountzos, and Christos D Liapis. The chimney graft technique for preserving visceral vessels during endovascular treatment of aortic pathologies. *Journal of vascular surgery*, 55(5):1497–1503, 2012.

[5] André Miguel dos Santos Almeida Valério et al. *Optimal chimney graft configuration in an abdominal aortic aneurysm: a finite element analysis*. PhD thesis, 2014.

[6] Giuseppe C. Balboni. Anatomia umana. Edi. Ermes s.r.l.

[7] Aortic Disease. https://www.cedars-sinai.edu/patients/programs-and-services/heart-institute/conditions/aortic-disease/aortic-disease.aspx.

[8] P Schneider. Endovascular skills: Guidewire and catheter skills for endovascular surgery, informa healthcare, 2008.

[9] C Kleinstreuer, Zhonghua Li, and MA Farber. Fluid-structure interaction analyses of stented abdominal aortic aneurysms. *Annu. Rev. Biomed. Eng.*, 9:169–204, 2007.

[10] E Choke, G Cockerill, WRW Wilson, S Sayed, J Dawson, I Loftus, and MM Thompson. A review of biological factors implicated in abdominal aortic aneurysm rupture. *European Journal of Vascular and Endovascular Surgery*, 30(3):227–244, 2005.

[11] Jonathan L Eliason and Gilbert R Upchurch. Endovascular treatment of aortic aneurysms: state of the art. *Current treatment options in cardiovascular medicine*, 11(2):136–145, 2009.

[12] MK Salem, HS Rayt, G Hussey, S Rafelt, CP Nelson, RD Sayers, AR Naylor, and A Nasim. Should asian men be included in abdominal aortic aneurysm screening programmes? *European Journal of Vascular and Endovascular Surgery*, 38(6):748–749, 2009.

[13] MA Creager, JL Halperin, AD Whittemore, et al. Aneurysmal disease of the aorta and its branches. *Vascular medicine. Little, Brown, New York, S*, 901, 1996.

[14] Shahid Manzoor Toor, Igor Sazonov, Heyman Luckraz, and Perumal Nithiarasu. Aortic aneurysms: Osr, evar, stent-grafts, migration and endoleak—current state of the art and analysis. In *Cardiovascular and Cardiac Therapeutic Devices*, pages 63–92. Springer, 2013.

[15] Teun BM Wilmink, Clive RG Quick, and Nicholas E Day. The association between cigarette smoking and abdominal aortic aneurysms. *Journal of vascular surgery*, 30(6):1099–1105, 1999.

[16] Jes S Lindholt, Svend Juul, Helge Fasting, and Eskild W Henneberg. Screening for abdominal aortic aneurysms: single centre randomised controlled trial. *Bmj*, 330(7494):750, 2005.

[17] Jacques Cornuz, Claudio Sidoti Pinto, Heindrik Tevaearai, and Matthias Egger. Risk factors for asymptomatic abdominal aortic aneurysm: systematic review and meta-analysis of population-based screening studies. *The European Journal of Public Health*, 14(4):343–349, 2004.

[18] Ruby C Lo, Rodney P Bensley, Allen D Hamdan, Mark Wyers, Julie E Adams, Marc L Schermerhorn, Vascular Study Group of New England, et al. Gender differences in abdominal aortic aneurysm presentation, repair, and mortality in the vascular study group of new england. *Journal of vascular surgery*, 57(5):1261–1268, 2013.

[19] R Mofidi, VJ Goldie, J Kelman, ARW Dawson, JA Murie, and RTA Chalmers. Influence of sex on expansion rate of abdominal aortic aneurysms. *British journal of surgery*, 94(3):310–314, 2007.

[20] Roger M Greenhalgh and Janet T Powell. Endovascular repair of abdominal aortic aneurysm. *New England Journal of Medicine*, 358(5):494–501, 2008.

[21] Raghunandan Kamineni and Richard R Heuser. Abdominal aortic aneurysm. *Journal of interventional cardiology*, 17(6):437–445, 2004.

[22] Juan C Parodi, JC Palmaz, and HD Barone. Transfemoral intraluminal graft implantation for abdominal aortic aneurysms. *Annals of vascular surgery*, 5(6):491–499, 1991.

[23] Robert E Noll, Britt H Tonnessen, Krishna Mannava, Samuel R Money, and W Charles Sternbergh. Long-term postplacement cost after endovascular aneurysm repair. *Journal of vascular surgery*, 46(1):9–15, 2007.

[24] United Kingdom EVAR Trial Investigators et al. Endovascular versus open repair of abdominal aortic aneurysm. *N Engl J Med*, 2010(362):1863–1871, 2010.

[25] Thomas A Abbruzzese, Christopher J Kwolek, David C Brewster, Thomas K Chung, Jeanwan Kang, Mark F Conrad, Glenn M LaMuraglia, and Richard P Cambria. Out-

comes following endovascular abdominal aortic aneurysm repair (evar): an anatomic and device-specific analysis. *Journal of vascular surgery*, 48(1):19–28, 2008.

[26] Benjamin W Starnes. Physician-modified endovascular grafts for the treatment of elective, symptomatic, or ruptured juxtarenal aortic aneurysms. *Journal of vascular surgery*, 56(3):601–607, 2012.

[27] R Iezzi and AR Cotroneo. Endovascular repair of abdominal aortic aneurysms: Cta evaluation of contraindications. *Abdominal imaging*, 31(6):722–731, 2006.

[28] George A Antoniou, George S Georgiadis, Stavros A Antoniou, Ganesh Kuhan, and David Murray. A meta-analysis of outcomes of endovascular abdominal aortic aneurysm repair in patients with hostile and friendly neck anatomy. *Journal of vascular surgery*, 57(2):527–538, 2013.

[29] Rakesh P Patel, Athanasios Katsargyris, Eric LG Verhoeven, Donald J Adam, and John A Hardman. Endovascular aortic aneurysm repair with chimney and snorkel grafts: indications, techniques and results. *Cardiovascular and interventional radiology*, 36(6):1443–1451, 2013.

[30] Christopher K Zarins, Daniel A Bloch, Tami Crabtree, Alan H Matsumoto, Rodney A White, and Thomas J Fogarty. Stent graft migration after endovascular aneurysm repair: importance of proximal fixation. *Journal of vascular surgery*, 38(6):1264–1272, 2003.

[31] Dorothee HL Bail, Tobias Walker, and Johannes Giehl. Vascular endostapling systems for vascular endografts (t) evar—systematic review—current state. *Vascular and endovascular surgery*, 47(4):261–266, 2013.

[32] Piergiorgio Cao, Fabio Verzini, Simona Zannetti, Paola De Rango, Gianbattista Parlani, Luciano Lupattelli, and Agostino Maselli. Device migration after endoluminal abdominal aortic aneurysm repair: analysis of 113 cases with a minimum follow-up period of 2 years. *Journal of vascular surgery*, 35(2):229–235, 2002.

[33] David Pintoux, Philippe Chaillou, Laure Azema, Philippe Bizouarn, Alain Costargent, Philippe Patra, and Yann Gouëffic. Long-term influence of suprarenal or infrarenal fixation on proximal neck dilatation and stentgraft migration after evar. *Annals of vascular surgery*, 25(8):1012–1019, 2011.

[34] Marcus J Dill-Macky, Stephanie R Wilson, Yarron Sternbach, John Kachura, and Thomas Lindsay. Detecting endoleaks in aortic endografts using contrast-enhanced sonography. *American Journal of Roentgenology*, 188(3):W262–W268, 2007.

[35] A Chaudhuri, LE Ansdell, AJ Grass, and M Adiseshiah. Intrasac pressure waveforms after endovascular aneurysm repair (evar) are a reliable marker of type i endoleaks, but not type ii or combined types: an experimental study. *European journal of vascular and endovascular surgery*, 28(4):373–378, 2004.

[36] Juan Carlos Parodi, Ramón Berguer, Luis Mariano Ferreira, Ricardo La Mura, and Mark L Schermerhorn. Intra-aneurysmal pressure after incomplete endovascular exclusion. *Journal of vascular surgery*, 34(5):909–914, 2001.

[37] Grace J Wang, Jeffrey P Carpenter, Endologix Investigators, et al. The powerlink system for endovascular abdominal aortic aneurysm repair: six-year results. *Journal of vascular surgery*, 48(3):535–545, 2008.

[38] Juan C Parodi, JC Palmaz, and HD Barone. Transfemoral intraluminal graft implantation for abdominal aortic aneurysms. *Annals of vascular surgery*, 5(6):491–499, 1991.

[39] Duncan Drury, JA Michaels, Lisa Jones, and Lynda Ayiku. Systematic review of recent evidence for the safety and efficacy of elective endovascular repair in the management of infrarenal abdominal aortic aneurysm. *British Journal of Surgery*, 92(8):937–946, 2005.

[40] Timothy AM Chuter. Branched and fenestrated stent grafts for endovascular repair of thoracic aortic aneurysms. *Journal of vascular surgery*, 43(2):A111–A115, 2006.

[41] A Millon, A Deelchand, P Feugier, JM Chevalier, JP Favre, University Association for Research in Vascular Surgery (AURC, et al. Conversion to open repair after endovascular aneurysm repair: causes and results. a french multicentric study. *European Journal of Vascular and Endovascular Surgery*, 38(4):429–434, 2009.

[42] Joseph J Ricotta and Gustavo S Oderich. Fenestrated and branched stent grafts. *Perspectives in vascular surgery and endovascular therapy*, 20(2):174–187, 2008.

[43] Kevin J Bruen, Robert J Feezor, Michael J Daniels, Adam W Beck, and W Anthony Lee. Endovascular chimney technique versus open repair of juxtarenal and suprarenal aneurysms. *Journal of vascular surgery*, 53(4):895–905, 2011.

[44] M Boult, W Babidge, G Maddern, M Barnes, and R Fitridge. Predictors of success following endovascular aneurysm repair: mid-term results. *European journal of vascular and endovascular surgery*, 31(2):123–129, 2006.

[45] Michael Wilderman and Luis A Sanchez. Fenestrated grafts or debranching procedures for complex abdominal aortic aneurysms. *Perspectives in vascular surgery and endovascular therapy*, 21(1):13–18, 2009.

[46] Donald T Baril, Ronald A Kahn, Sharif H Ellozy, Alfio Carroccio, and Michael L Marin. Endovascular abdominal aortic aneurysm repair: emerging developments and anesthetic considerations. *Journal of cardiothoracic and vascular anesthesia*, 21(5):730–742, 2007.

[47] ELG Verhoeven, IFJ Tielliu, BE Muhs, WTGJ Bos, CJ Zeebregts, TR Prins, BI Oranen, and JJAM van den Dungen*. Fenestrated and branched stent-grafting: a 5-years experience. *Acta chirurgica Belgica*, 106(3):317–322, 2006.

[48] Dominique B Buck, Joost A Van Herwaarden, Marc L Schermerhorn, and Frans L Moll. Endovascular treatment of abdominal aortic aneurysms. *Nature Reviews Cardiology*, 11(2):112–123, 2014.

[49] Chris N Bakoyiannis, Konstantinos P Economopoulos, Sotirios Georgopoulos, Chris Klonaris, Maria Shialarou, Marina Kafeza, and Efstathios Papalambros. Fenestrated and branched endografts for the treatment of thoracoabdominal aortic aneurysms: a systematic review. *Journal of Endovascular Therapy*, 17(2):201–209, 2010.

[50] Hila Ben Gur, Moses Brand, Gábor Kósa, and Saar Golan. Computational fluid dynamics of blood flow in the abdominal aorta post "chimney" endovascular aneurysm repair (chevar). In *Aortic Aneurysm*. InTech, 2017.

[51] Thomas Larzon and P Skoog. One hundred percent of ruptured aortic abdominal aneurysms can be treated endovascularly if adjunct techniques are used such as chimneys, periscopes and embolization. *The Journal of cardiovascular surgery*, 55(2):169–178, 2014.

[52] Konstantinos P Donas, Felice Pecoraro, Giovanni Torsello, Mario Lachat, Martin Austermann, Dieter Mayer, Giuseppe Panuccio, and Zoran Rancic. Use of covered chimney stents for pararenal aortic pathologies is safe and feasible with excellent patency and low incidence of endoleaks. *Journal of vascular surgery*, 55(3):659–665, 2012.

[53] Raphael Coscas, Hicham Kobeiter, Pascal Desgranges, and Jean-Pierre Becquemin. Technical aspects, current indications, and results of chimney grafts for juxtarenal aortic aneurysms. *Journal of vascular surgery*, 53(6):1520–1527, 2011.

[54] Jason T Lee, Joshua I Greenberg, and Ronald L Dalman. Early experience with the snorkel technique for juxtarenal aneurysms. *Journal of vascular surgery*, 55(4):935–946, 2012.

[55] Jip L Tolenaar, Jasper W Van Keulen, Santi Trimarchi, Bart E Muhs, Frans L Moll, and Joost A Van Herwaarden. The chimney graft, a systematic review. *Annals of vascular surgery*, 26(7):1030–1038, 2012.

[56] Tomas Ohrlander, Björn Sonesson, Krasnodar Ivancev, Timothy Resch, Nuno Dias, and Martin Malina. The chimney graft: a technique for preserving or rescuing aortic branch vessels in stent-graft sealing zones. *Journal of Endovascular Therapy*, 15(4):427–432, 2008.

[57] Konstantinos P Donas, Jason T Lee, Mario Lachat, Giovanni Torsello, Frank J Veith, et al. Collected world experience about the performance of the snorkel/chimney endovascular technique in the treatment of complex aortic pathologies: the pericles registry. *Annals of surgery*, 262(3):546–553, 2015.

[58] Hiroshi Banno, Frédéric Cochennec, Jean Marzelle, and Jean-Pierre Becquemin. Comparison of fenestrated endovascular aneurysm repair and chimney graft techniques for pararenal aortic aneurysm. *Journal of vascular surgery*, 60(1):31–39, 2014.

[59] Jason T Lee, George K Lee, Venita Chandra, and Ronald L Dalman. Comparison of fenestrated endografts and the snorkel/chimney technique. *Journal of vascular surgery*, 60(4):849–857, 2014.

[60] Brant W Ullery, George K Lee, and Jason T Lee. Shuttering of the superior mesenteric artery during fenestrated evar. *Journal of Vascular Surgery*, 59(2):558, 2014.

[61] Thomas Larzon and P Skoog. One hundred percent of ruptured aortic abdominal aneurysms can be treated endovascularly if adjunct techniques are used such as chimneys, periscopes and embolization. *The Journal of cardiovascular surgery*, 55(2):169–178, 2014.

[62] Jorg L de Bruin, Kak K Yeung, Wouter W Niepoth, Rutger J Lely, Qingfeng Cheung, Anesh de Vries, and Jan D Blankensteijn. Geometric study of various chimney graft configurations in an in vitro juxtarenal aneurysm model. *Journal of Endovascular Therapy*, 20(2):184–190, 2013.

[63] Konstantinos G Moulakakis, Spyridon N Mylonas, Ilias Dalainas, George S Sfyroeras, Fotis Markatis, Thomas Kotsis, John Kakisis, and Christos D Liapis. The chimney-

graft technique for preserving supra-aortic branches: a review. *Annals of cardiothoracic surgery*, 2(3):339, 2013.

[64] Getting started with abaqus: Interactive edition. http://abaqus.software.polimi.it/v6.12/pdf_books/get_started.pdf.

[65] Matthew DBS Tam, Stephen D Laycock, James RI Brown, and Matthew Jakeways. 3d printing of an aortic aneurysm to facilitate decision making and device selection for endovascular aneurysm repair in complex neck anatomy. *Journal of Endovascular Therapy*, 20(6):863–867, 2013.

[66] Using 3D printed models for planning and guidance during endovascular intervention. https://3dmedicalconference.com/uncategorized/using-3d-printed-models-for-planning-and-guidance-during-endovascular-intervention-video/.

[67] http://www.who.int/cardiovascular_diseases/en.

[68] C Kleinstreuer, Z Li, CA Basciano, S Seelecke, and MA Farber. Computational mechanics of nitinol stent grafts. *Journal of biomechanics*, 41(11):2370–2378, 2008.

[69] Ferdinando Auricchio, Michele Conti, Stefania Marconi, Alessandro Reali, Jip L Tolenaar, and Santi Trimarchi. Patient-specific aortic endografting simulation: From diagnosis to prediction. *Computers in biology and medicine*, 43(4):386–394, 2013.

[70] Ferdinando Auricchio, Michele Conti, Matthieu De Beule, Gianluca De Santis, and Benedict Verhegghe. Carotid artery stenting simulation: from patient-specific images to finite element analysis. *Medical engineering & physics*, 33(3):281–289, 2011.

[71] Matthieu De Beule. *Finite element stent design*. PhD thesis, Ghent University, 2008.

[72] G Mestres, JP Uribe, C García-Madrid, E Miret, X Alomar, M Burrell, and V Riambau. The best conditions for parallel stenting during evar: an in vitro study. *European Journal of Vascular and Endovascular Surgery*, 44(5):468–473, 2012.

[73] Konstantinos P Donas, Frank J Criado, Giovanni Torsello, Frank J Veith, David J Minion, and PERICLES Registry Collaborators. Classification of chimney evar–related endoleaks: insights from the pericles registry. *Journal of Endovascular Therapy*, 24(1):72–74, 2017.

[74] ImageJ. Image Processing and Analysis in Java., date = , url = https://imagej.nih.gov/ij/docs/intro.html.

[75] Gustavo S Oderich and Joseph J Ricotta. Modified fenestrated stent grafts: device design, modifications, implantation, and current applications. *Perspectives in vascular surgery and endovascular therapy*, 21(3):157–167, 2009.

[76] Stéphan Haulon, Sébastien Amiot, Pierre-Edouard Magnan, Jean-Pierre Becquemin, Patrick Lermusiaux, Mohamad Koussa, Michel Batt, Jean-Pierre Favre, Association Universitaire de Recherche en Chirurgie Vasculaire (AURC, et al. An analysis of the french multicentre experience of fenestrated aortic endografts: medium-term outcomes. *Annals of surgery*, 251(2):357–362, 2010.

[77] 3D Printing Makes Alternative Treatment for Abdominal Aortic Aneurysms Possible. https://www.iths.org/blog/news/3d-printing-makes-alternative-treatment-for-abdominal-aortic-aneurysms-possible/.

[78] TA Resch, NV Dias, J Sobocinski, B Sonesson, B Roeder, and S Haulon. Development of off-the-shelf stent grafts for juxtarenal abdominal aortic aneurysms. *European Journal of Vascular and Endovascular Surgery*, 43(6):655–660, 2012.

[79] William J Quiñones-Baldrich, Andrew Holden, Renato Mertens, Matt M Thompson, Alan P Sawchuk, Jean-Pierre Becquemin, Matthew Eagleton, and Daniel G Clair. Prospective, multicenter experience with the ventana fenestrated system for juxtarenal and pararenal aortic aneurysm endovascular repair. *Journal of vascular surgery*, 58(1):1–9, 2013.

[80] Marco Leopardi, F Cochennec, C Spartera, and J.-P Becquemin. Home-made fenestrated endograft as urgent treatment of complex aortic aneurysms in high risk patients. 23:134–143, 09 2016.

[81] Benjamin Ware Starnes and Billi Tatum. Early report from an investigator-initiated investigational device exemption clinical trial on physician-modified endovascular grafts. *Journal of vascular surgery*, 58(2):311–317, 2013.

[82] Daniel F Leotta and Benjamin W Starnes. Custom fenestration templates for endovascular repair of juxtarenal aortic aneurysms. *Journal of vascular surgery*, 61(6):1637–1641, 2015.

[83] Sebastian Mafeld, Craig Nesbitt, James McCaslin, Alan Bagnall, Philip Davey, Pentop Bose, and Rob Williams. Three-dimensional (3d) printed endovascular simulation models: a feasibility study. *Annals of translational medicine*, 5(3), 2017.

[84] Giovanni Biglino, Claudio Capelli, Jo Wray, Silvia Schievano, Lindsay-Kay Leaver, Sachin Khambadkone, Alessandro Giardini, Graham Derrick, Alexander Jones, and Andrew M Taylor. 3d-manufactured patient-specific models of congenital heart defects for communication in clinical practice: feasibility and acceptability. *BMJ open*, 5(4):e007165, 2015.

[85] Benjamin Ware Starnes and Billi Tatum. Early report from an investigator-initiated investigational device exemption clinical trial on physician-modified endovascular grafts. *Journal of vascular surgery*, 58(2):311–317, 2013.

[86] Stefania Marconi. *Ricostruzione 3D virtuale e fisica del pancreas con discriminazione semiautomatica tra parenchima sano e tessuto tumorale.* PhD thesis, Ph. D. thesis, Corso di Laurea Specialistica in Ingegneria Biomedica, 2010.

[87] Paul A. Yushkevich, Joseph Piven, Heather Cody Hazlett, Rachel Gimpel Smith, Sean Ho, James C. Gee, and Guido Gerig. "User-Guided 3D Active Contour Segmentation

of Anatomical Structures: Significantly Improved Efficiency and Reliability". *Neuroimage*, 31(3):1116–1128, 2006.

[88] http://www-2.unipv.it/compmech/proto-lab.html.

[89] David Minion. Molded parallel endografts for branch vessel preservation during endovascular aneurysm repair in challenging anatomy. *International Journal of Angiology*, 21(02):081–084, 2012.

[90] Hector WL de Beaufort, Elena Cellitti, Quirina MB de Ruiter, Michele Conti, Santi Trimarchi, Frans L Moll, Constantijn EVB Hazenberg, and Joost A van Herwaarden. Midterm outcomes and evolution of gutter area after endovascular aneurysm repair with the chimney graft procedure. *Journal of Vascular Surgery*, 2017.

[91] C Lally, Fl Dolan, and PJ Prendergast. Cardiovascular stent design and vessel stresses: a finite element analysis. *Journal of biomechanics*, 38(8):1574–1581, 2005.

[92] Daryl L. Logan. "A first course in the finite element method", Cengage Learning(2011).

Ringraziamenti

Eh già!!! Finalmente il grande giorno è toccato anche a me.
Cosa potrei dire per riassumere questi 10 anni di università? Si, lo so... Sono troppi ma meglio tardi che mai!!! Ad essere sincero, non bastano le parole e vorrei ringraziare ogni singola persona che ho conosciuto qui a Pavia e dimostrale la mia gratitudine e il mio affetto che provo in questo momento. Tante persone hanno creduto in me, nelle mie capacità e la mia determinazione; nella mia amicizia e nella mia persona. Siete tanti e vi ringrazio immensamente.
Vorrei ringraziare innanzitutto, coloro che mi hanno aiutato nella realizzazione della tesi e sostenuto in questo percorso. In primo luogo ringrazio il mio relatore, il Dottore Michele Conti per la disponibilità, pazienza e sostegno in questi mesi di lavoro e vorrei complimentarmi con te per il grande lavoro che fai. Ringrazio inoltre, il Professor Ferdinando Auricchio per avermi dato la possibilità di svolgere l'attività di tesi presso il suo dipartimento; é un grande onore avere il suo nome presente nella mia tesi. Un ringraziamento va anche ai ragazzi del laboratorio Protolab, un gruppo fantastico umanamente e professionalmente, e sopratutto a Stefania, che grazie alla sua esperienza e competenza, sono riuscito ad integrare la tecnologia della stampa 3D nel mio lavoro . Vorrei ringraziare anche i miei compagni di "banco" e un speciale ringraziamento va a Stefano che mi ha aiutato e supportato tanto in questo percorso. Ringrazio inoltre Giulia e Franca, le mie compagne di Lab ma anche a voi, Luca e Francesco, i miei amici con cui sono cresciuto qui a Pavia, tra le aule dell'università e i strani posti dove andavamo a studiare. Grazie ragazzi!
E che dire dei miei amici? Sinceramente, senza di voi, senza il vostro sostegno, non sarei

qui a festeggiare. Grazie di tutto, veramente. Non riuscirò mai a ringraziarvi abbastanza, questo traguardo è anche merito vostro. Ringrazio per primi i ragazzi del collegio, chi c'è ancora e chi no. Grazie a voi Letizia ed Olimpia, Emanuele e Lara, Fabio e Federica, Carol e Sofia, Flo e Selene, Mohamed e Karam. Vi voglio bene ragazzi!!! Poi ci siete voi! i ragazzi del Mcdonald. Voglio bene a tutti voi! A Domenico e Diego, ad Antonino e Mattia, a Marco e Giulia, ad Adina e Nicolò, Ma sopratutto a te, Matteo, che ti ho lasciato per ultimo perché ti vorrei dedicare un paio di righe, anche se ti mancherei di rispetto per tutte le belle cose che potrei dirti. Tu ci sei stato ovunque e sempre per me, nel bene e nel male e non mi hai mai abbandonato. Ti ringrazio immensamente amico mio e ti voglio un mondo di bene!

Ora tocca a te HABIBI mio! Giulia, tu sei una delle persone più belle che abbia mai conosciuto nella mia vita, Con la tua voce e la tua risata, mi hai reso sereno e tranquillo che mi hai fatto tornare bambino di nuovo. Sei più emozionata tu all'idea che io mi debba laureare. Fai e spero che continui a fare parte della mia vita e di sostenermi e supportare il mio carattere come hai sempre fatto. TI AMO!

Ho lasciato questo ultimo ringraziamento a tutti voi che siete le persone più preziose della mia vita. Ai Miei cugini (Houda, Bob, Hadi, Ahmed) che adoro e voglio un mondo di bene e alle loro fidanzate che fanno parte ormai della nostra famiglia (Clara, Solene). Un particolare ringraziamento va ai miei carissimi fratelli Moudi e Bill e alla sua bellissima fidanzata Paola, che nonostante i loro impegni hanno trovato del tempo da dedicare ad aiutarmi nella realizzazione di questo lavoro e a corregere il mio modesto inglese. Ringrazio finalmente Voi tre! Mia sorellina, Mamma e Papà. Cosa vi posso dire? Vi amo e vi ringrazio immensamente per ogni cosa che avete fatto per me, per il supporto morale che nonostante sia difficile per voi questa distanza siete sempre stati vicini in ogni secondo della mia giornata, sopratutto tu Momy che sei una amica per me.

GRAZIE A TUTTI VOI!!!

Ali Chehab